University of Alberta

# Wear-Corrosion Synergy of Tungsten in $K_3[Fe(CN)_6]$ Slurry for Chemical-Mechanical Planarization

by

Saheed Bamidele Akonko ©

A thesis submitted to the Faculty of Graduate Studies and Research in partial fulfillment of the requirements for the degree of Master of Science

in

Materials Engineering

Department of Chemical and Materials Engineering

Edmonton, Alberta

Fall 2005

Library and Archives Canada

Published Heritage Branch

395 Wellington Street
Ottawa ON K1A 0N4
Canada

Bibliothèque et Archives Canada

Direction du Patrimoine de l'édition

395, rue Wellington
Ottawa ON K1A 0N4
Canada

0-494-09111-8

*Your file Votre référence*
*ISBN:*
*Our file Notre reference*
*ISBN:*

NOTICE:
The author has granted a non-exclusive license allowing Library and Archives Canada to reproduce, publish, archive, preserve, conserve, communicate to the public by telecommunication or on the Internet, loan, distribute and sell theses worldwide, for commercial or non-commercial purposes, in microform, paper, electronic and/or any other formats.

The author retains copyright ownership and moral rights in this thesis. Neither the thesis nor substantial extracts from it may be printed or otherwise reproduced without the author's permission.

AVIS:
L'auteur a accordé une licence non exclusive permettant à la Bibliothèque et Archives Canada de reproduire, publier, archiver, sauvegarder, conserver, transmettre au public par télécommunication ou par l'Internet, prêter, distribuer et vendre des thèses partout dans le monde, à des fins commerciales ou autres, sur support microforme, papier, électronique et/ou autres formats.

L'auteur conserve la propriété du droit d'auteur et des droits moraux qui protège cette thèse. Ni la thèse ni des extraits substantiels de celle-ci ne doivent être imprimés ou autrement reproduits sans son autorisation.

---

In compliance with the Canadian Privacy Act some supporting forms may have been removed from this thesis.

While these forms may be included in the document page count, their removal does not represent any loss of content from the thesis.

Conformément à la loi canadienne sur la protection de la vie privée, quelques formulaires secondaires ont été enlevés de cette thèse.

Bien que ces formulaires aient inclus dans la pagination, il n'y aura aucun contenu manquant.

Canada

## ABSTRACT

Tungsten has found many applications in multilevel metallization due to its refractory properties and good resistance to electromigration. For these applications, tungsten must be planarized using, e.g., chemical-mechanical planarization (CMP). In order to develop an effective CMP process for tungsten planarization, research was conducted to investigate the wear-corrosion synergy of tungsten in $K_3[Fe(CN)_6]$ slurry as a function of slurry pH and applied normal wearing load.

It was demonstrated that the passive film formed on tungsten in this slurry played a major role in the removal of tungsten. The resistance of the passive film to both corrosion and mechanical damages was found to decrease with an increase in slurry pH, thus resulting in higher removal rates. However, a high removal rate may not necessarily produce planar surfaces. The relatively low removal rate at low pH was accompanied with better surface finish. It was found that a higher removal rate with better surface finish could be achieved by applying an anodic potential during the CMP process.

# Acknowledgement

I would like to thank Dr. Dongyang Li for guidance and assistance during this work.

And I also want to thank Natural Sciences and Engineering Research Council of Canada (NSERC), U.S. Department of Energy (DOE), and Intel Corp. for their financial technical support support.

Finally, I would like to express my appreciation to Dr. Margaret Ziomek-Moroz at U.S. Department of Energy, who co-supervised this work, for her support and guidance.

**LIST OF CONTENTS**

1 INTRODUCTION

1.1 Multilevel Metallization.....1

1.2 Planarization Techniques for Multilevel Metallization.....4

1.2.1 Thermal Flow of Borophosphosilicate Glass (BPSG).....5

1.2.2 Spin-on-Glass.....6

1.2.3 Sacrificial Photoresist.....8

1.2.4 Chemical-Mechanical Planarization (CMP).....9

1.3 CMP Variables.....13

1.3.1 CMP Slurry – abrasive, slurry chemistry.....13

1.3.2 Polishing pad.....15

1.4 Wear-Corrosion Synergy in CMP.....19

1.5 Application of Tungsten in Multilevel Metallization.....21

1.5.1 Mechanisms for Tungsten Removal During CMP.....26

1.6 CMP Trends and Future Applications.....29

2 ELECTROCHEMICAL BEHAVIOR OF TUNGSTEN IN $K_3[Fe(CN)_6]$ SLURRY

2.1 Experimental Details.....30

2.1.1 Sample, slurry and polishing pad.....30

2.1.2 Electrochemical tests and surface film characterization.....33

2.2 Polarization Behavior of Tungsten in $K_3[Fe(CN)_6]$ slurry .....36

2.3 Surface morphology of tungsten after immersion in $K_3[Fe(CN)_6]$ slurries with different pH values.....37

2.4 X-ray photoelectron spectroscopy (XPS) analyses of the surface oxides.....47

2.5 Mechanical properties of the surface oxides formed at different pH levels.....49

2.5.1 Nanoindentation Tests.....49

2.5.2 Resistance of surface oxide to scratch.....52

3 WEAR-CORROSION SYNERGY OF TUNGSTEN IN THE $K_3[Fe(CN)_6]$ SLURRY

3.1 Corrosion Rate without Wear, $C_O$.....59

3.2 Total Wear Rate, T.....67

3.3 Pure Wear Rate, $W_O$.....70

3.4 Corrosion Rate in the presence of, $C_W$.....73

3.5 Calculation of Wear-Corrosion Synergy.....75

3.5.1 Wear Rate in the Presence of Corrosion, $W_C$.....76

3.5.2 Increase in wear caused by corrosion, S'.....78

3.5.3 Increase in corrosion caused by wear, S".....79

3.5.4 The material loss caused by wear-corrosion synergy, S.....80

3.5.5 Corrosion augmentation factor, $C_W/C_O$.....81

3.5.6 Wear augmentation factor, $W_C/W_O$.....82

4 THE SRFACE MORPHOLOGY OF POLISHED TUNGSTEN AFTER CMP UNDER DIFFERENT CONDITIONS

4.1 Surface Morphology of polished tungsten under OCP.....84

4.2 Electrochemical polishing under an applied potential.....101

5 SUMMARY AND FUTURE WORK

5.1 Summary.....109

5.2 Possible Future Work.....111

REFERENCES.....112

APPENDIX.....125

LIST OF TABLES

Table 1.1. Specific gravity and compressibility for four different pads [19].....16

Table 1.2. Physical/Metallurgical Requirements for Metals/Conductors used in MLM [6].....22

Table 1.3. Properties of Low resistivity Metals essential in Building MLM [16,75].....24

Table 2.1. Approximate Composition of the $K_3Fe(CN)_6$ slurry.....31

Table 2.2 XPS analysis: atomic compositions of tungsten in different oxidation states after one hour of immersion in slurry with different pH values.....41

Table 2.3 Maximum displacements under load of 40 μN.....45

Table 2.4. The critical failure loads of the passive film formed after one hour of immersion in the slurry at different pH. .....51

Table 3.1. Open-circuit potential ($E_{corr}$), Corrosion-current Density ($I_{corr}$), and the corresponding pure Corrosion rate ($C_O$) of the bulk tungsten in the $K_3[Fe(CN)_6]$ slurry at different pH.....58

Table 3.2. Corrosion-current Density ($I_{corr}$) obtained form extrapolation of Tafel curves for the tungsten during wear in the $K_3[Fe(CN)_6]$ slurry at different pH and applied normal load.....68

Table I. Total wear rate, T (mm/yr), of tungsten in the $K_3[Fe(CN)_6]$ slurry under open circuit potential as a function of slurry pH and normal load.....125

Table II. Pure wear rate, $W_O$ (mm/yr) of bulk tungsten in the $K_3[Fe(CN)_6]$ slurry under a cathodic potential of –0.5 V as a function of slurry pH and normal load.....125

Table III. The total wear rate (mm/yr) of tungsten under electrochemical potential of +1 V in the $K_3[Fe(CN)_6]$ slurry as function of slurry pH and normal load.....126

LIST OF FIGURES

Figure 1-1. Schematic illustration of a two-layer multilevel metallization scheme.....3

Figure 1-2. Loss in planarity due to SOG shrinkage [7].....7

Figure 1-3. Schematic of CMP process.....11

Figure 1-4. Metal CMP.....12

Figure 1-5. Removal rate as a function of time with and without pad conditioning [55]..18

Figure 1-6. Relationship between removal rate and surface finish resulting from chemical etching, mechanical polishing and CMP [63]. .....20

Figure 1-7. Schematic cross-section of a submicron CMOS technology, which employs tungsten for gates, source and drain straps, via plugs, and local interconnection line [72].....23

Figure 1-8. Showing step coverage obtained with (a) PVD Al deposition and (b) CVD tungsten deposition [19].....25

Figure 2-1. The polyurethane polishing pad a- with XY grooving, b – close view on one of the felt.....32

Figure 2-2. Hypothetical Potentiodynamic curve for a passive metal.....35

Figure 2-3. Polarization curves of tungsten in the $K_3[Fe(CN)_6]$ slurry as a function of pH.....36

Figure 2-4. SEM images of surface films formed on tungsten after immersion in the $K_3[Fe(CN)_6]$ slurry for one hour at different slurry pH.....40

Figure 2-5. AFM images of surface morphologies of tungsten after immersion in $K_3[Fe(CN)_6]$ slurries with different pH values for one hour.....46

Figure 2-6. Nanoindentation results from oxide films formed at different slurry pH after immersion in the slurry for 1 hr.....51

Figure 2-7. Changes in the electrical contact resistance (ECR) of passive films formed at different slurry pH levels (after immersion in the slurries for one hr) during micro scratching.....56

Figure 3-1. Typical Tafel curve, showing various parameters that can be obtained [97].....60

Figure 3-2. Tafel curves for bulk tungsten in the $K_3[Fe(CN)_6]$ slurry: a – pH 4, b – pH 5, c – pH 6, d – pH 7, e – pH 9, f – pH 11.....64

Figure 3-3. Corrosion rate of the tungsten in the $K_3[Fe(CN)_6]$ slurry as a function of pH.....65

Figure 3-4. Pourbaix diagram of tungsten [98].....66

Figure 3-5. Schematic of the experimental set up used to determine the total wear rate, T .....68

Figure 3-6. Total wear rate, T, of bulk tungsten in the $K_3[Fe(CN)_6]$ slurry under open circuit potential as function of slurry pH and normal load.....69

Figure 3-7. Schematic of the tribo-corrosion system.....71

Figure 3-8. Pure wear rate, $W_O$ of bulk tungsten in the $K_3[Fe(CN)_6]$ slurry under a cathodic potential of -0.5 V as function of slurry pH and normal load.....72

Figure 3-9. Corrosion rate of the tungsten in the presence of wear in the $K_3[Fe(CN)_6]$ slurry as a function of pH and applied normal load.....74

Figure 3-10. Wear rate of the tungsten in the presence of corrosion in the $K_3[Fe(CN)_6]$ slurry as a function of pH and applied normal load.....77

Figure 3-11. Increase wear rate of tungsten due to corrosion in the $K_3[Fe(CN)_6]$ slurry as a function of pH and applied normal load.....78

Figure 3-12. Increase corrosion rate due to wear of tungsten in the $K_3[Fe(CN)_6]$ slurry as a function of pH and applied normal load.....80

Figure 3-13. Material loss that resulted from the wear-corrosion synergy during corrosive wear of the tungsten in the $K_3[Fe(CN)_6]$ slurry as a function of pH and applied normal load.....81

Figure 3-14. Changes in $C_W/C_O$ against slurry pH and applied load.....82

Figure 3-15. The wear augmentation factor as a function of slurry pH and applied load.83

Figure 4-1. SEM micrographs of surface morphology after corrosive wear under OCP at different slurry pH levels under a normal load of 1 N.....87

Figure 4-2. SEM micrographs of surface morphology after corrosive wear under OCP at different slurry pH levels under a normal load of 3 N.....90

Figure 4-3. SEM micrographs of surface morphology after corrosive wear under OCP at different slurry pH levels under a normal load of 5 N.....93

Figure 4-4. SEM micrographs of surface morphology after corrosive wear under OCP at different slurry pH levels under a normal load of 7 N.....96

Figure 4-5. AFM images of surface morphology after corrosive wear under OCP at different slurry pH levels under a normal load of 7 N.....100

Figure 4-6. The total wear rate of tungsten under electrochemical potential of +1 V in the $K_3[Fe(CN)_6]$ slurry as function of slurry pH and normal load.....102

Figure 4-7. SEM micrographs of surfaces after corrosive polishing at different slurry pH levels under a potential of +1 V and a normal wearing load of 5 N.....105

Figure 4-8. SEM micrographs of surfaces after corrosive polishing at different slurry pH under a potential of +1 V and a normal wearing load of 7 N.....108

## 1.0 Introduction

Multilevel metallization (MLM) is essential for building interconnection between the active and passive components of an integrated circuit (IC). The chemical-mechanical planarization (CMP) has become an effective process for achieving global planarization in building multilevel integrated circuits. In this chapter, a brief description of MLM is presented and various planarization techniques with their merits and demerits are discussed. Details about the CMP process are also given in this chapter, including its variables and the roles of wear and corrosion in achieving material removal for global planarization. Finally, the use of tungsten in MLM due to its inherent electrical, physical/metallurgical and process/chemical properties is discussed.

## 1.1 Multilevel Metallization

The miniaturization of devices and circuits aimed at effective power consumption, higher device packing density, higher speed, lower cost, and faster signal propagation [1-6], has led to complex and densely packed discrete elements on a single chip. A reliable and efficient way of connecting the elements is therefore of importance in achieving high packing densities and quality interconnectivity, which will not negatively affect the performance of the device. This could be easily realized through multilevel metallization by which non-conducting dielectrics are used to isolate numerous layers of patterned conductors. Electrical contacts are made between conductors on the different layers through vias in the dielectric. With such a layout, only bulk silicon is assumed to have

active devices that are interconnected by multilevel metallization [7]. The chip size and performance of very large scale integration [VLSI] circuits are determined by the multilevel metallization scheme, since the RC delay is proportional to the resistivity, the length of the conductor line, and the dielectric constant of the dielectric material as expressed in equation (1.1)

$$RC = \rho\varepsilon\frac{l^2}{td} \tag{1.1}$$

where R and C are the capacitance and resistance of the metal line. ρ, l, and d are the resistivity, length and thickness of the metal line respectively. And ε, t are the permittivity and thickness of the insulator.

The advantages of multilevel metallization include design flexibility allowing external circuitry to be connected to the terminals of the discrete device, input-output terminals of the IC, and shorter interconnect line through proper routing [4]. Figure 1-1 shows a cross-sectional view of a two-layer multilevel metallization interconnection scheme. Brief descriptions of various components in the structure are given below:

i. Contact: This layer includes contact opening used to provide ohmic contact from the first layer of metal to the silicon device or component as indicated in figure 1-1. It is composed of various silicides, salicides, and doped polysilicon. Contacts are differentiated by their purposes, e.g. base contact, source or drain contact, resistor contact, etc. [8]

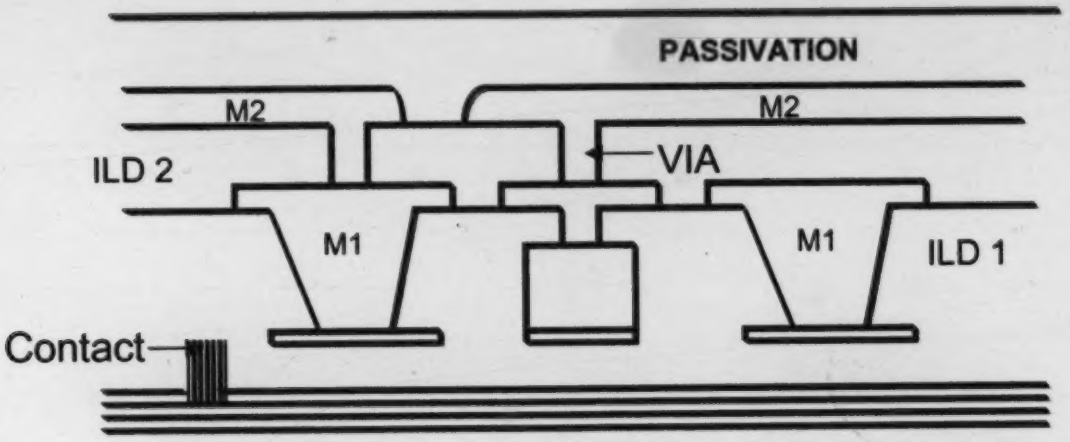


Figure 1-1. Schematic illustration of a two-layer multilevel metallization scheme

ii. Interlevel dielectric and Passivation: The interlevel dielectrics are insulators, for example $SiO_2$, Si, $Si_3N_4$ [7]; they help insulate metal layers within the layer and from each other or the underlying silicon. They are designated ILD1, ILD2 in figure 1-1. There is usually a final layer of dielectric referred to as 'passivating' layer or 'passivation', which provides physical and chemical protection to the underlying metal and device structure during final assembly, and operating processes. It generally consists of one or more layers of dielectric capable of preventing diffusion of moisture and corrosive ions to metal surfaces.

iii. Interconnects: They are designated M1, M2 in figure 1-1. These are metals used to achieve ohmic contact at different layers; which can be made possible by direct or indirect routing from the silicon device. They are required to have low electrical

resistivity and high resistance to electromigration that could result from high current densities. Presently, several metals (Al, Cu, W) are used as interconnects.

iv. Vias: These metallic conductors in the holes between dielectric layers are used to provide connection between layers of interconnect.

## 1.2 Planarization Techniques for Multilevel metallization

Multilevel metallization is needed to effectively connect the active components of integrated circuits. However, the additional levels of interconnections may lead to irregularities in surface topography. In order to obtain a good step coverage and fine line resolution required for a continuous and reliable metallization scheme, an effective planarization process is necessary.

In order to obtain planarized surfaces, step heights resulting from deposition of thin films and dielectrics used in multilevel metallization need to be removed, so that additional levels can be placed on flat surfaces. Several techniques have been developed and used in the semiconductor industry to achieve planarization; these have been briefly discussed in this section.

### 1.2.1 Thermal Flow of Borophosphosilicate Glass (BPSG)

Borophosphosilicate glass (BPSG) has been used as interlayer dielectric between the first metal level, as well as a passivation layer [8-12]. Surface smoothing is achieved by chemical vapor deposition (CVD) deposition of a BPSG film onto the interconnect line, followed by annealing step causing the film to soften and flow. The molten BPSG is then left on the interconnect, resulting in a smooth surface. This technique helps to reduce surface roughness and produces tapered sidewall of contact holes. The tapered sidewall permits continuity and maintenance of film thickness of subsequently deposited conductor lines [13-15], and also eliminates electrical defects and reduces electromigration.

The planarization behavior of a BPSG film is affected by a few parameters such as composition of film, step coverage and thickness of deposited film. The boron content helps to lower the glass transition temperature as well as its viscosity [9, 11, 16] so that the molten film can flow over or into topographic features such as gap in response to the driving force of its own surface tension. The film stress has also been reported [11] to decrease with increasing boron content, which makes BPSG a reliable top passivation layer. The phosphorus content, on the other hand, helps to stabilize the chemical structure of the glass and also provides trapping sites for mobile alkali metal ions such as sodium, thus minimizing impurity penetration [16-18]. The thickness of the film relative to the step height to be filled determines the ease at which the molten BPSG flow to fill it up. A film that is thick relative to the step height can readily flow in the vicinity of the step edge while the step offers substantial resistance to the flow of a thin molten film.

There are some disadvantages of using the thermal flow BPSG films for planarization, they are:

(a) The need for high flow temperature, usually over 750°C, may result in unintentional diffusion of dopants [16]. The high flow temperature also means that the technique may only be suitable for refractory metals and cannot be used after deposition of relatively low melting metals such as Al (660°C) [4,8,19].

(b) The boron and phosphorus contents are hygroscopic, readily reacting with moisture in ambient atmosphere. This could lead to the formation of phosphoric and boric acid micro-crystals on the surface of the dielectric and result in corrosion of the metal line as well as an increased defect density [9, 20-24].

### 1.2.2 Spin-on-Glass

Spin-on-glass (SOG) planarization is achieved by spin-coating a layer of a SOG material (silicate, polysiloxane) while in liquid state [25-29]. The SOG is a liquid mixture driven across the wafer surface by centrifugal forces and then by capillary forces over steps, thus filling gaps and consequently producing a smooth surface. Baking and curing are needed in the late stage of the process. The baking typically in temperature range of 125-200°C helps to expel most of the remaining solvents and initiate the hydrolysis of its silica constituents. Curing process initiates condensation polymerization (i.e. cross linking), resulting in a solid film made up of Si-O backbones with organic and silanol

side chains [8]. SOG intermetal dielectrics are usually made up of two layers of CVD oxide, the first layer, "CVD-1", is deposited directly on the underlying metal line while the second layer, "CVD-2", provides good adhesion between the interlevel and overlying metal line. The use of SOG has been successfully implemented in double-level metal devices [25 -28].

In addition, the SOG planarization can also be used in pre-metal planarization between polycide and first level of metal as an alternative for the conventional BPSG flow process [29]. This process could also be employed in planarization of the final passivation dielectric as well as for gap filling, since it can flow into relatively small gaps. The use of SOG offers simple process control, high planarization effect, low cost, and mass productivity [28,30]. A material with low stress level, simple curing process, long shelf life and good thermal stability is essential for a reliable SOG planarization process [31].

Major setbacks in the use of this planarization technique include:

(a) Shrinkage of SOG as a result of solvent loss, hydrolysis, and cross linking reactions during the baking and curing processes. This produces large tensile stresses in the film and so SOG films usually have low resistance to cracking [8, 32]. This is schematically illustrated in Figure 1.2.

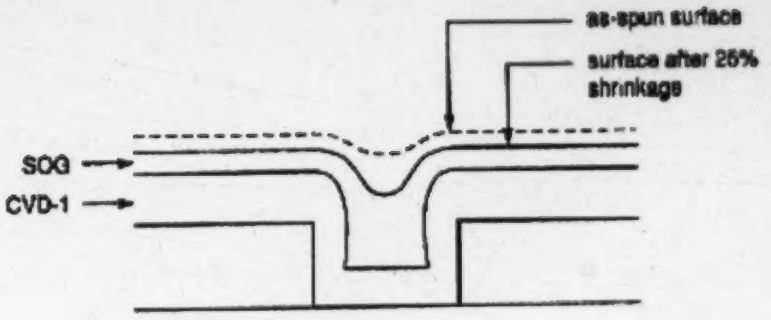


Figure 1-2. Loss in planarity due to SOG shrinkage [8]

(b) The presence of water in the cured SOG film which may outgas during subsequent processes; corrosion of exposed metal line is also a great concern when using this technique [8, 19].

(c) This technique can only be used to achieve local planarity; the shrinkage of SOG film during curing often lead to loss of planarity as shown in Fig 1.2.

### 1.2.3 Sacrificial Photoresist

This planarization technique is similar to that used for SOG materials. This technique involves initial deposition of a CVD oxide, usually $SiO_2$, onto the interconnects that are to be planarized. A spin coating of a photoresist is then made on the oxide; this resist is then baked and its smooth surface topography replicated on the underlying CVD oxide by means of a non-selective etchback process, so that the etching rates of the resist and CVD oxide are equal [19, 33]. The planarity of the photoresist resist can not be

effectively transferred if the equal etch rate condition is not met. A second layer of CVD oxide may be needed in order to achieve the desired thickness for the planarized dielectric.

Limitations to the use of the technique are:

(a) In order to be able to transfer the planarity of the resist on the CVD oxide, the etching rates of the two materials must be equal. However, it is difficult to maintain equal etching rates for the resist and CVD oxide.

(b) Similar to the case of SOG films, the photoresist also shrinks when baked and thus can only be used to achieve local planarization [34].

### 1.2.4 Chemical-Mechanical Planarization

This is the most widely accepted planarization technique for achieving global planarization. Surface planarization is achieved by continuously moving a wafer across a polymeric pad under pressure in the presence of corrosive slurry. This process combines (1) chemical reactions between the surface and the slurry and (2) mechanical interaction between the chemically modified surface and the pad as well as sub-micron abrasives contained in the slurry. A major difference between CMP and other planarization techniques is that in CMP, the planarity is achieved due to the extreme flatness of the polishing platen on which a pad is mounted, while in other techniques planarizing layers are used so that their planarity is pattern dependent [19]. Chemical-mechanical

planarization (CMP) has been used to planarize metals, alloys, dielectrics, plastics and ceramics using the synergistic interaction of corrosion and wear. This process results in global planarization (smoothing and planning), which is required for building a reliable multilevel integrated circuit (IC). A schematic cross section of a pad-slurry-wafer is illustrated in Figure 1-3.

The CMP process involves continuously moving the wafer to be planarized relative to a porous polymer pad attached to a platen fed with a slurry composed of chemicals and submicron-sized particles under controlled downward force.

The wafer and pad rotates with angular velocities of $\omega_s$ and $\omega_p$, respectively. The wafer is pressed downward against the pad while the slurry is provided between the wafer and pad. The mechanical polishing by the submicron-sized abrasive plus the chemical attack can make metals and dielectrics planarized.

The polish rate caused by CMP is usually expressed using the Preston equation which is an empirical formula [35]:

$$\text{Polish Rate} = \frac{\Delta H}{\Delta t} = K_p P \frac{\Delta s}{\Delta t} \tag{1.2}$$

where $\Delta H$ is the change in the height of the surface, $\Delta t$ is the elapsed time, P is the pressure, $\Delta s/\Delta t$ is the linear velocity of the pad relative to the work wafer, and $K_p$ is the Preston coefficient.

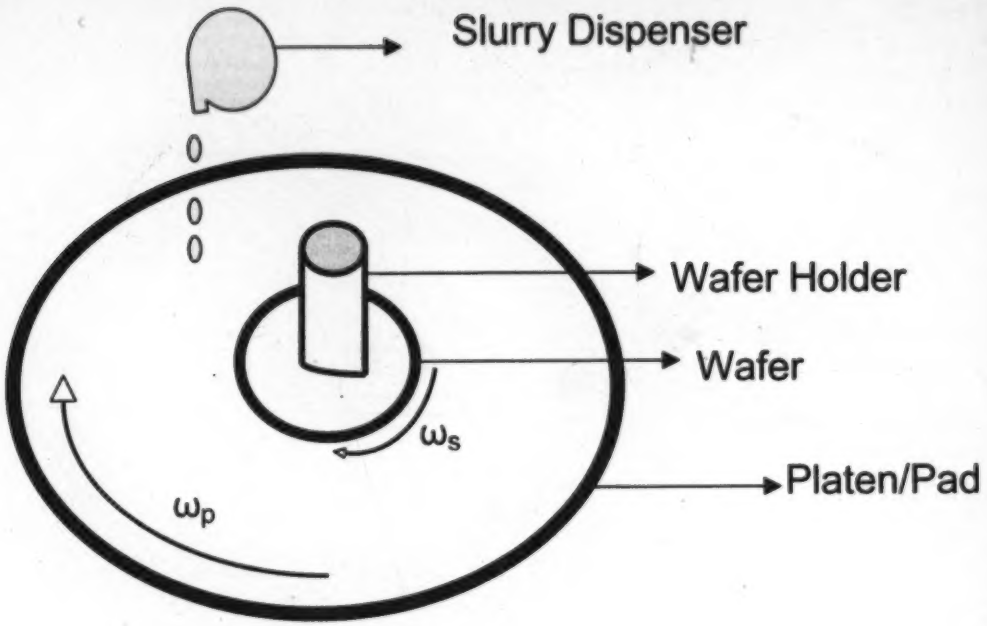


Figure 1-3. Schematic of a CMP process

Although CMP has been widely used, it is not well understood. A consummate understanding of CMP requires interdisciplinary knowledge that includes particle technology, corrosion, tribology and tribo-chemical processes, wet and surface chemistry, fluid flow and mechanical properties of polymer [19]. Figure 1-4 illustrates a metal CMP process.

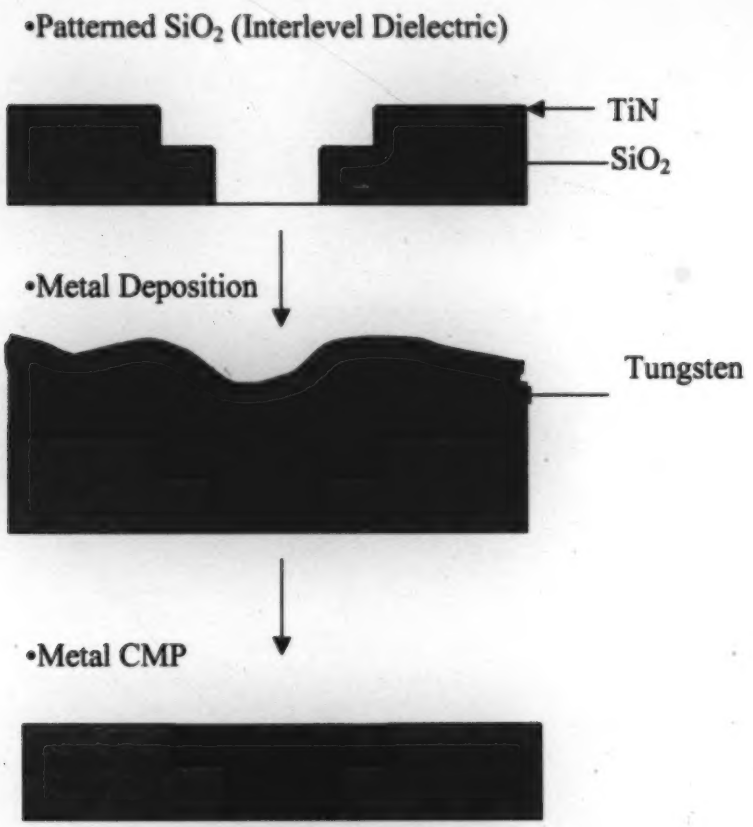


Figure 1-4. Metal CMP

## 1.3 CMP Variables

With the stringent requirements of planar geometries essential for building multilevel metallization schemes, there is a need to fully understand CMP and carefully select CMP parameters for optimum planarization.

### 1.3.1 CMP Slurry

CMP slurry needs to be tailored to suit the material being polished as well to be compatible with other components in a CMP process. The constituents of a CMP slurry interact with one another and with other components of a CMP process. The basic constituents of CMP slurry will be described in this section.

i. Abrasive

The abrasive particles in slurry are needed for mechanical interaction for the CMP process [19, 36], which abrade the chemically modified surface.

Slurry abrasives must have certain surface charges to prevent coagulation as well as adequate impact strength, and suitable chemical properties to prevent dissolution in the slurry [37-38]. Other properties of abrasive that may affect polish rate and planarity include the type of abrasive, size, shape, hardness and concentration.

Literature data indicate that a clear relationship has not yet been established between the abrasive particle size and polish rate. The polish rate has been found to change with the abrasive particle size, but the results are quite different [36, 38-39]. The concentration of abrasive in the slurry also plays an important role in determining the polish rate; a higher concentration or a larger number of particles result in more mechanical attack to the surface and thus lead to a larger polish rate [38-40]. However, a further increase in the concentration of the abrasive could saturate the material removal rate, since such increase in concentration of particles may not increase the number of active abrasives in the contact area between the wafer and the pad [41]. For CMP, silica ($SiO_2$) is widely used for oxide polishing while alumina ($Al_2O_3$) and silica are often used for metal polishing.

ii. Slurry Chemistry

The chemical components of CMP slurry include solution, pH, buffering agents, oxidizers and complexing agents.

The solution provides the chemical agents (pH adjusters, oxidizers, catalysts, inhibitors etc.), and the electrostatic or steric balance needed to stabilize the abrasive suspension and lubrication between the wafer and pad. The solution also helps to transport waste materials and to control temperature [37]. The pH level determines the surface chemical condition during CMP. For some metals such as W, low pH slurry is required to form a passive film softer than the tungsten substrate, which is therefore

easily abraded [42]. The pH level also affects the dissolution rate of the modified surface and the solubility of the reaction products. The slurry pH level also affects the stability of the pad material and abrasive particles.

Buffering agents are needed to preserve the slurry pH level during use and storage. During a CMP process, certain reactions may consume or produce more $H^+$ than is usually required. This may lead to change in the local pH level of the wafer-pad contact area. On the other hand, the slurry pH may decrease after exposure in air [43] due to the dissolution of atmospheric $CO_2$ [44]. Oxidizers help to improve the oxidation behavior of a metal, resulting in dissolution of the metal or formation of a surface film that could increase the removal rate [19,42-46]. Whether or not an oxidizer is needed depends on the material being polished. Oxidizers may not be necessary for metal such as Al [46] that is easily passivated. Complexing agents may increase the solubility of the surface film or that of reaction products [19] and thus help keep a balance between the mechanical removal rate and the dissolution of waste products in the slurry. This eliminates redeposition of waste products on the surface of the material being polished [47]. For example, glycine has been reported to enhance the removal rate of Cu at alkaline pH due to the formation of a highly soluble copper-glycine complex [48].

### 1.3.2 Polishing Pad

The polishing pad is one of the most essential components for CMP [19]. Sufficient knowledge of the structure and properties of a pad is needed to determine the

polish rate and planarization [19]. CMP polishing pads are made from polymers with adequate mechanical and chemical properties to withstand the rigors of polishing. They are composed of either a matrix of cast polyurethane foam with filler material to control the hardness or polyurethane impregnated with felts. Polyurethane is made from the reaction of di- or poly- functional isocyanates with polyols [38, 49]. The choice of polyurethane is based on the fact that the pad can be tailored for desired mechanical properties [38].

Mechanical properties of interest include the resistance to tearing and wear, modulus, hardness, compressibility, and specific gravity [19, 47, 49]. Specific gravities and compressibility values of four different polishing pads are listed in Table 1.1. The specific gravity helps to determine the porosity of a pad; the lower the specific gravity, the higher the porosity. The pad porosity is an essential property in determining the rate at which slurry and reaction products are transported through the pores of the pad [50]. The hardness and compressibility can be used to determine the ease at which a pad will bend and conform to the wafer surface for material removal in low regions. Table 1.1. Specific gravities and compressibility values of four different pads [19].

| Pad* | Specific Gravity | Compressibility |
|---|---|---|
| Suba IV | 0.3 | 16% |
| Suba 500 | 0.34 | 12% |
| IC-60 | 0.7 | N/A |
| IC-1000 | 0.6-0.8 | 5% |

* Pads were manufactured and named by Rodel Corp.

The planarization capability of a polishing pad can be described by its shear modulus of elasticity. A pad with large shear modulus will not be able to conform to the wafer surface; both elastic and viscoelastic deformations are experienced by the pad during polishing. For a pad to remove the materials in high areas it is compressed when in contact with high area and the extent of compression is determined by the pad's modulus and the exerted pressure on the high area. As the pad moves, from a high area to a lower area, it expands elastically at a rate determined by its viscoelasticity. The pressure exerted in the low region is a measure of the extent to which the pad expands [19]. Since an effective CMP process should remove materials faster in the high regions than in the lower regions [51-53], there is a need to minimize the extent to which the pad expands in the low area to obtain the desired surface planarity. The roughness of the polishing pad is another important parameter that affects the polishing rate and resultant surface planarity [38, 50]. The polishing rate has been found to increase with pad roughness [50].

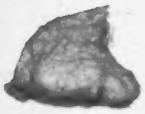

Besides, the polishing pad must be able to withstand the slurry chemistry without degrading, delaminating, blistering or warping [54]. Also, the pad must be adequately hydrophilic, that is, the slurry must wet the surface of the pad and form a liquid film between the wafer and the pad. If the slurry beads on the surface of the pad rather than wetting, it will be easily swept away by the wafer edge, so that there would be insufficient slurry for an effective CMP process [54]. Several methods have been developed to enable less hydrophilic polymers to be used as CMP polishing pads; they include adding wetting agents to the slurry, adding hydrophilic fillers such as silica to normally hydrophobic polymers, or by chemically modifying the hydrophobic polymer to make it more hydrophilic. Pad conditioning is also an essential process during CMP,

which helps to prevent glazing occurring as the surface of the pad undergoes plastic deformation so that the surface becomes smoother. Pad conditioning involves removal of CMP by-products, used slurry, and any form of abrasion of the pad surface. Glazing often leads to a decrease in polish rate [38, 55] as shown in figure 1-5. With conditioning, embedded abrasives on the pad constantly move to the surface of the pad by the friction force between the pad and wafer. The use of hydrophilic polymers can also ensure self-conditioning by aiding the removal of weakened surface layer of the pad.

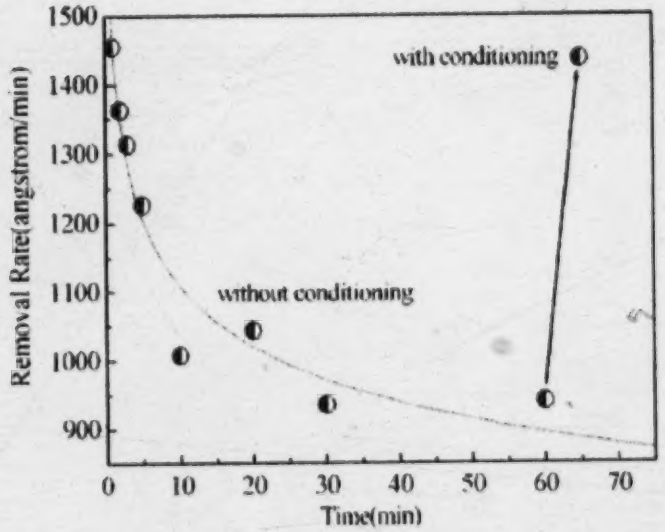


Figure 1-5. Removal rate as a function of time with and without pad conditioning [55].

## 1.4 Wear-Corrosion Synergy in CMP

The interaction of corrosion and wear often results in a significant increase in material loss, compared to those caused by individual processes [56-61]. CMP takes advantage of the interaction between corrosion and wear to achieve global planarization [19, 62-65]. Chemical dissolution or mechanical abrasion alone cannot be used to obtain global planarization required to build multilevel metallization schemes.

Chemical etching or dissolution alone cannot result in global planarization, because most chemical actions proceed in all direction at the same rate [19, 64]. Material removal by chemical etching results from material dissolution in the corrosive solution. This process is however constant with time [63] and therefore will not eliminate topographic features. However, in a CMP process, the chemical etching plus mechanical abrasion can make a surface planarized.

Mechanical abrasion or grinding involves indentation and scratching of a surface by abrasive particles [36]. Abrasion or grinding may planarize a surface to some degree. However, since large-sized particles are usually required to effectively abrade a surface, the resultant surface damage may not be acceptable [66]. The removal rate may therefore be inversely proportional to the surface finish [63]. If chemical reaction is involved, the chemically modified surface is readily abraded in a CMP process. During CMP, the slurry leads to synergistic interaction between the chemical and mechanical actions; this eliminates a scratched surface and nonuniform chemical attack, leading to a smooth surface. For metal CMP, material removal is achieved through removing a continuously growing thin, relatively brittle, non-dissolving, and chemically passivating surface film

by the mechanical action of abrasive particles. In the case of dielectric such as silicon dioxide ($SiO_2$), CMP is achieved by removal of a soft and ductile layer resulting from the interaction of the slurry and the dielectric. Figure 1-6 illustrates the removal rate and surface finish, caused by chemical etching, mechanical polishing, and CMP, respectively.

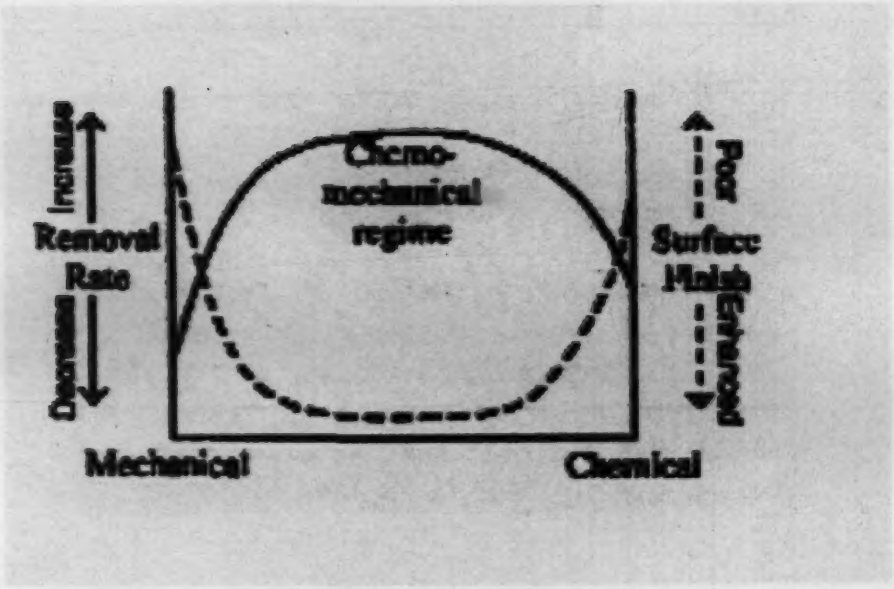


Figure 1-6. Relationship between removal rate and surface finish resulting from chemical etching, mechanical polishing and CMP [63].

## 1.5 Application of Tungsten in Multilevel metallization

With increasing dimension and complex array of components, there is a demand to improve the interconnectivity system, so that it would not become a limiting factor to the overall performance of the device. Materials used in multilevel metallization are classified into two groups: conductors and insulators; they can be further classified into two sets: low (e.g. Al and Al-based alloys) and high (e.g. doped poly-Si, refractory metal silicides, W) process temperature materials based on the temperature they can withstand during and after material processing [7]. The required properties of the materials used in multilevel metallization include electrical, physical/metallurgical and process/chemical properties [7]. Since no material can satisfy all the requirements, the choice of material used at any level is determined by the most essential criteria at that level. Some of the physical/metallurgical properties of materials used in MLM are presented in Table 1.2.

Because of the stringent requirements on the properties of the materials used in MLM, there is a need to use new materials and develop new processes for integrating them into multilevel integrated circuits. Tungsten is one of the newly selected materials. The basic requirements for a conductor used in interconnect metallization are low resistivity and good resistance to electromigration [1, 51, 66-71]. Since it has such desired properties, tungsten and its alloys have been used in several applications such diffusion barriers, gate contacts, vias, multilevel interconnects, source/drain shunt straps and etch-stop windows [72-75]. Figure 1-7 shows a cross-section of a submicron complimentary oxide semiconductor (CMOS) in which W is used as gates, source and drain shunt straps, via plugs, and local interconnect line.

Table 1.2. Physical/Metallurgical Requirements for Metals/Conductors used in MLM [7

| | Al | Cu | W | TiW | $WSi_2$ | PtSi |
|---|---|---|---|---|---|---|
| Low stress Film | Fair | Fair | Fair | Fair | Fair | Fair |
| No Hillock formation | Fair | Fair | Good | Fair | Good | |
| Good Adhesion | Good | Good | Poor | Good | Fair | |
| Good Barrier Property | Poor | Poor | Good | Good | Fair | Poor |
| Reliable Shallow Junct-ion contact | Poor | Poor | Good | Poor | Good | Good |

Because of its refractory properties together with a relatively low resistivity and acceptable electromigration resistance, W is an attractive conductor in MLM. Low resistivity helps to reduce interconnect delay in an IC. This is a measure of the RC (product of total resistance and capacitance) time delay, which is the time for a voltage input transferred form one end of a wire to the other end to reach 63 % of its original value. Although there are several metals with lower resistivity than tungsten, they however do not meet other requirements for use in MLM.

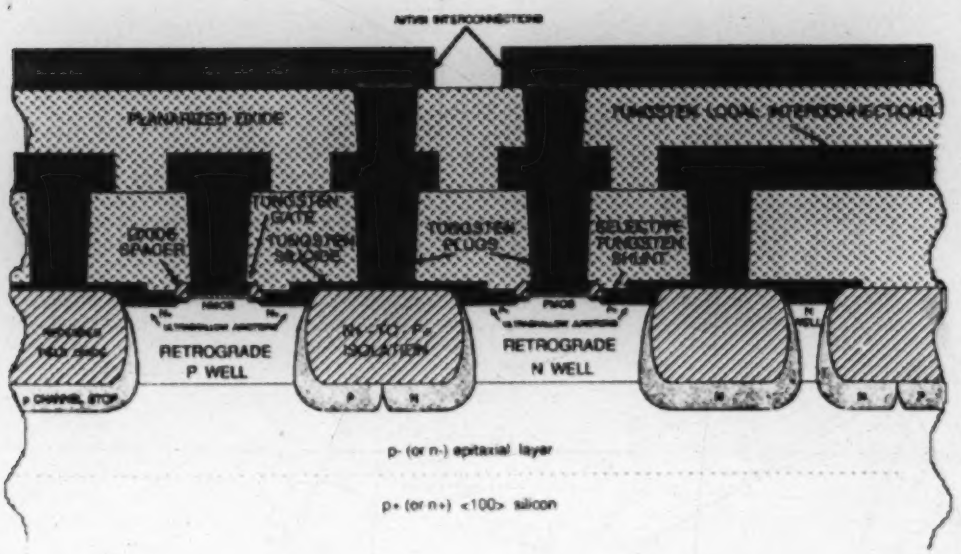


Figure 1-7. Schematic cross-section of a submicron CMOS technology which employs tungsten for gates, source and drain straps, via plugs, and local interconnection line [72].

Table 1.3 presents some low resistivity metals. Silver with the best resistivity is not suitable because it has deep levels in the silicon band gap [76], diffuses very fast in $SiO_2$ [77] and is susceptible to electromigration due to its low melting point [75]. Tungsten matches silicon in terms of thermal expansion, which leads to low stress and hillock free layers associated with low temperature metal such as Al [78], which is also an added advantage for using W in MLM. A common problem encountered in metallization scheme is the formation of non-conformal coatings for contacts or vias and the associated electromigration failure. A conformal coating covers all surfaces with a uniform depth while non-conformal coating deposits more on higher surfaces than on the bottom and/or side surfaces.

Table 1.3. Properties of Low resistivity Metals essential in Building MLM [16,75]

| | Ag | Al | Al Alloy | Au | Cu | W |
|---|---|---|---|---|---|---|
| Resistivity (μΩ-cm) | 1.59 | 2.66 | ~3.5 | 2.35 | 1.67 | 5.65 |
| Electromigration Resistance | Poor | Poor | Fair-Poor | Very Good | Good | Very Good |
| Corrosion Resistance | Poor | Good | Good | Good | Excellent | Poor |
| Adhesion to $SiO_2$ | Poor | Good | Good | Poor | Poor | Poor |
| Si Deep Levels | Yes | No | No | Yes | Yes | No |

A conformal coating of tungsten can be made by CVD due to its refractory properties; a suitable CVD process has not yet been developed for Al due to its relatively low melting temperature. This eliminates the formation of keyholes and gaps with acceptable step coverage [19]. Figure 1-8 illustrates a non-conformal tungsten film deposited using PVD (figure 1-8a) and a conformal Al film deposited using CVD (figure 1-8b). The deposited tungsten has a better step coverage which is the ratio of the thinnest point to the thickest point in the coating.

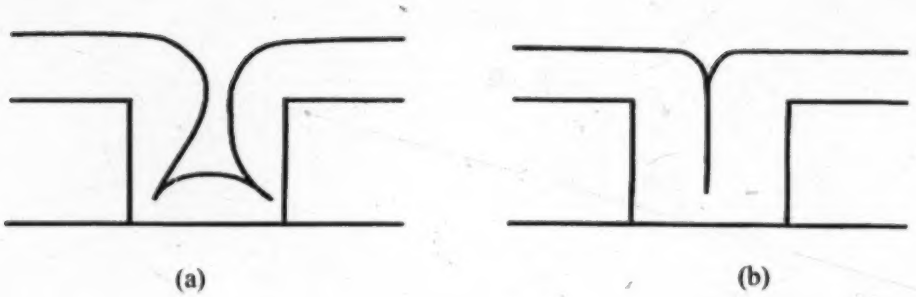


Figure 1-8. Step coverage of (a) Al film deposited by PVD and (b) tungsten deposited by CVD [19].

The thin points in the conformal coating are initiation sites for electromigration. These thin-films can withstand high current densities, however, due to the continuing miniaturization of very large scale integrated (VLSI) circuits, thin-film metallic conductors, vias (contacts) and interconnects are subjected to higher current densities that may lead to electromigration. This is due to momentum transfer from the electrons, which move in the applied electric field, to the ions which make up the lattice of the thin-film metallic material. Electromigration failure can lead to disconnection of interconnects and vias/contacts, thus reducing the circuit lifetime to an unacceptable level. Tungsten has high resistance to electromigration. In addition, tungsten-filled vias have been found to be more planar than aluminum-filled vias [19].

A major limitation to the use of W is its poor adhesion to $SiO_2$, a widely used dielectric material. This however can be improved by using adhesion promoters such as TiN.

### 1.5.1 The Mechanism for Tungsten Removal During CMP

Due to its high hardness, it is difficult to planarize tungsten. A chemically modified tungsten surface is therefore required to facilitate the material removal by CMP. Studies have been carried out to explain the mechanism involved in tungsten removal during CMP. This section summarizes the studies on the mechanism responsible for removal of W during CMP.

A passivation-abrasion-repassivation mechanism [79] has been proposed for tungsten removal by CMP. During the process, the interaction among an etchant, passivating and abrasive agents occurs. In order to achieve planarization of W, the slurry must be tailored to passivate the W surface forming $WO_3$ oxide. For this reason, the slurry's pH should be kept in the passivating range [80]. The use of an oxidizer such as $H_2O_2$, $K_3Fe(CN)_6$ and weak base complexing agents may help extend the passivating range of W [80]. When exposed to the slurry, the W surface was reported to be passivated through the reaction expressed by equation (1.3) [19]:

$$W + 6Fe(CN)_6^{3-} + 3H_2O \rightarrow WO_3 + 6Fe(CN)_6^{4-} + 6H^+ \qquad (1.3)$$

$WO_3$ is softer than the W substrate; it can be readily abraded, resulting in high removal rate. Once formed, $WO_3$ prevents further oxidation and dissolution of the underlying W. This self-limiting property with its dense and nonporous nature helps protect the low regions from the slurry [19]. It has been reported that the passive film formed on tungsten is a duplex layer of $WO_3/WO_2$ [82, 83].

In the meantime, repassivation occurs. A repetitive process of passivation-abrasion-repassivation results in effective planarization. Several other studies [39, 62,84] support this mechanism. However, the claim that the surface passive layer plays a major role has also received criticism. Attempts were made to compare the oxidation rate to the removal rate. If CMP of W is achieved primarily due to oxide formation, its abrasion and repassivation, then the oxidation rate should be comparable to the polish/removal rate. It was reported that the oxidation rate during polishing was lower than measured polishing rate or removal rate during commercial CMP processes [84]. An equal polish rate has been reported at open circuit potential (OCP) and cathodic potential of –0.5V relative to OCP [85]. Also, atomic force microscopy (AFM) images of polished tungsten substrates indicate that transgranular fracture assisted by intergranular corrosion could be responsible for material removal observed during CMP of W [84]. Further studies are certainly necessary in order to clarify the mechanism responsible for CMP of tungsten.

## 1.6 CMP – Trend and Future Applications

Multilevel metallization has become indispensable for increasingly complex, dense and miniaturized integrated circuits, which consist of both active and passive components. The performance of IC has now been dominated by the MLM scheme [86], which has led to a growing need to use new materials and to develope new processes to integrate these materials. The manufacturing issues related to MLM can be divided into two categories: materials and technologies [87]. Metallurgical, physical and electrical properties of conductors and insulators are considered for specific material requirements while efficient technologies are required to process the materials in the integrated circuits. Resolving some of these issues has led to the use of low resistivity materials such as Cu and W [88], and low κ-materials [89]; both are needed to reduce RC delay. The use and integration of these materials into MLM schemes have also given rise to issues such as poor step coverage, electromigration, and resistivity. There are also concerns about the difficulty and cost in the process implementation as well as selecting a suitable planarization technique.

CMP has become a widely accepted planarization technique for achieving global planarization needed to effectively build multilevel IC. Since the introduction of CMP, research and development have been aimed at improving related tools, processes and consumables. Owing to the need to use new materials in MLM, CMP has been used in planarizing more materials in addition to $SiO_2$, Cu, and W. These materials include aluminum and Al-alloys, diffusion barriers/adhesion promoters, ceramics, high dielectric

materials used for increasing capacitance, high $T_c$-superconductor used for zero resistance interconnections, and optoelectronic materials.

Major advance to CMP has come in the area of consumables, notably the slurry. Slurries containing nano-sized particles and novel particles such as ceria, coated and nanoporous particles have been developed. A significant breakthrough is the development of abrasive-free slurries for planarizing soft metals like Cu [90]. In this case, the chemistry of the slurry is tailored to chemically modify the surface of a material being polished for easy removal by a polymer pad. The absence of abrasive particles helps to reduce surface defects such as micro-scratches.

A major challenge in CMP is that the process is very complex and different for each material being planarized. There is therefore a need to better understand the CMP processes for individual materials used in MLM, particularly the electrochemical and mechanical aspects of the CMP processes.

Due to its high resistance to electromigration, tungsten is suitable for various applications in MLM. It is therefore necessary to have sufficient understanding of tungsten CMP. The objective of this work is to investigate the synergy of wear and corrosion in tungsten removal during CMP in $K_3Fe(CN)_6$ slurries for MLM applications. The possibility of obtaining higher removal rate with appropriate planarization from CMP under anodic potential was also investigated.

# 2.0 Electrochemical Behavior of Tungsten in the $K_3[Fe(CN)_6]$ Slurry

## 2.1 Experimental Details

### 2.1.1 Sample, Slurry and Polishing Pad

The tungsten samples were provided by U.S. Department of Energy, Albany research center. Intel Corp. provided the polishing pads and slurry used in the work. The poly-crystalline tungsten samples (10mm x 10mm x 5mm) were made from bulk tungsten material containing Na (0.12 wt%), Si (0.17 wt%), K (0.07 wt%), Li (0.01 wt%), Cu (0.008 wt%), Ca (0.006 wt%), and V (0.0075 wt%).

The slurry was prepared with de-ionized water containing silica (amorphous, fumed and crystalline free) as the abrasive, potassium ferricyanide $K_3Fe(CN)_6$ as the oxidant and acetic acid as the pH buffer. The pH value of the as-received slurry was 4.0. The composition of the slurry is given in Table 2.1. In order to preserve the chemistry of the slurry, pH adjustment was made using potassium hydroxide pellets purchased from Fisher Chemicals Inc. The pH measurements were carried out using a three calibration point pH meter made by OAKTON Inc.

Table 2.1. Approximate Composition of the $K_3Fe(CN)_6$ slurry.

| | |
|---|---|
| Silica(Amorphous, Fumed, Crystalline Free) | 9.2% |
| Potassium Ferricyanide | 5.6% |
| Acetic Acid | 2.8% |
| De – ionized Water | 82.1% |

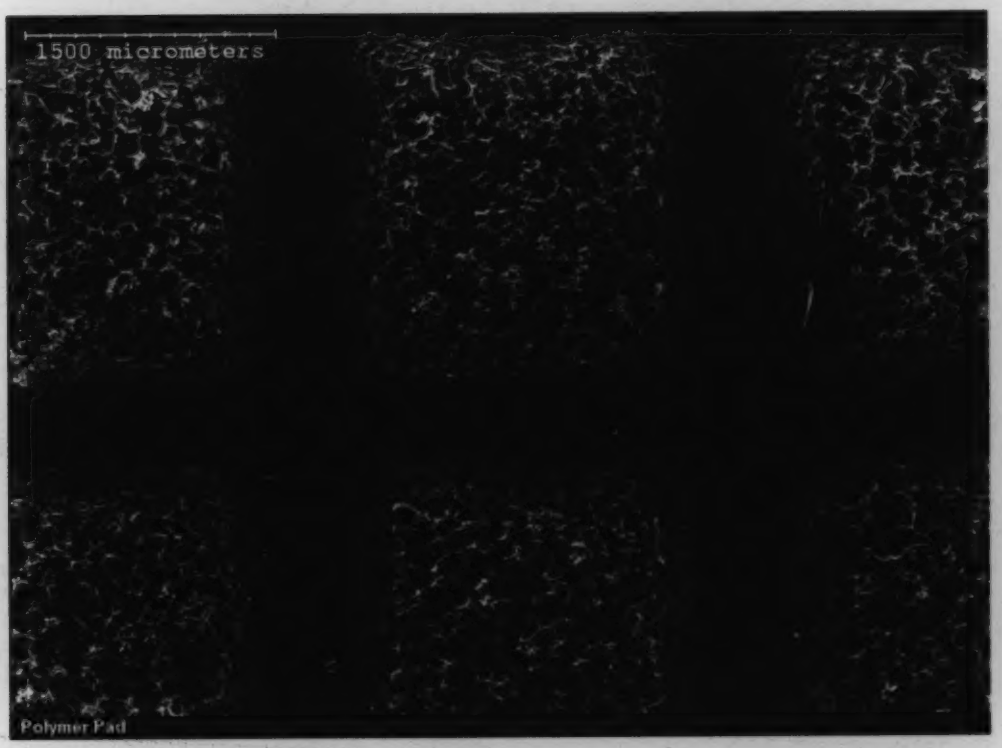


(a)

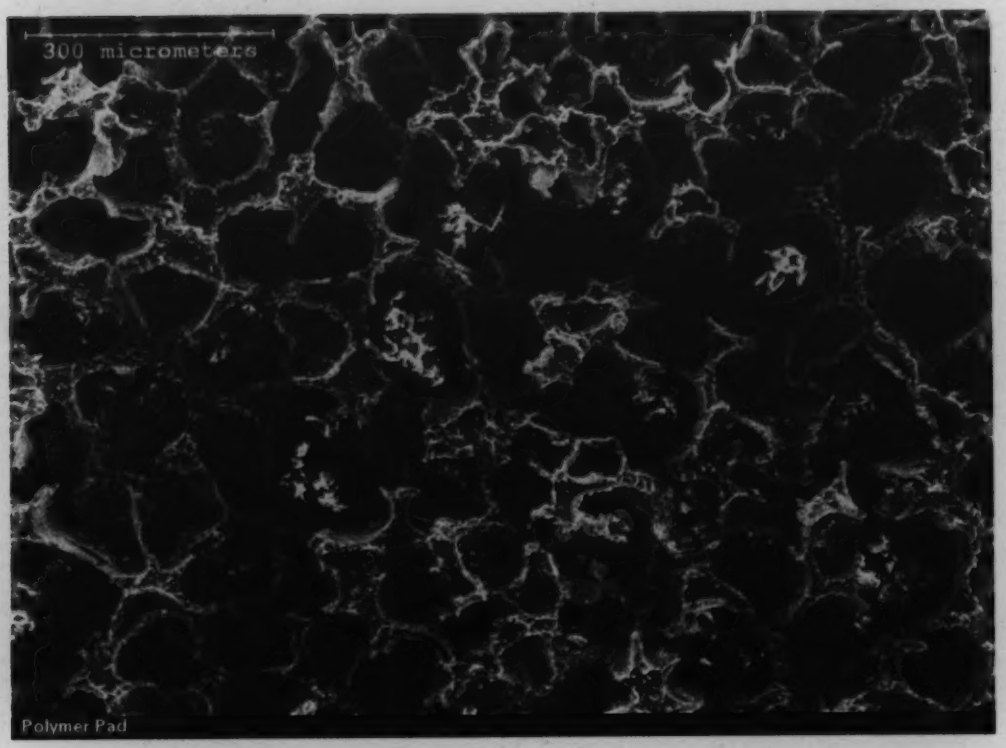


(b)

Figure 2-1. (a)The polyurethane polishing pad with XY grooving, (b) a close-up view of one of the felt

The polishing pad was made from polyurethane with XY grooving as shown in figure 2-1. The pad was chemically stable in the slurry showing no visible degradation after use.

Tungsten samples with dimensions of 10mm x 10mm x 5mm were mounted in epoxy and connected with copper wire through which electrochemical potential could be applied for *in situ* monitoring of changes in the electrochemical behavior of tungsten during electrochemical and tribo-corrosion tests. The electrical contact resistances of surface films formed on these samples under different pH conditions were also

investigated. For each test, a sample surface was polished with SiC abrasive papers and finally finished with a diamond (6 μm) paste. Cavities between at the sample/epoxy interface were covered with an epoxy/hardener to eliminate any interference of the interface during electrochemical tests. Prior to each test, the tungsten sample was immersed/rinsed in a 5 M KOH solution for 45 seconds and then rinsed thoroughly with distilled water. This was done to remove possible air-formed surface layer when exposed to air.

### 2.1.2 Electrochemical tests and Surface film Characterization

Several polarization methods are used in the laboratory to investigate the corrosion mechanism, corrosion rate, passivity and pitting susceptibility of materials to corrosion under specific electrochemical conditions. Potentiodynamic polarization tests generate polarization curves. It involves changing the potential of the working electrode and *in situ* monitoring of the corresponding changes in current with time or the applied potential. The potentiodynamic polarization test can characterize the behavior of a material under both cathodic and anodic potentials. A hypothetical potentiodynamic curve for a passive metal is shown in figure 2.2, it refers to a metal showing active-passive behavior. Useful information such as corrosion potential ($E_{corr}$), range of passive potential, and passive current ($i_p$) can be determined from the potentiodynamic curve. The decrease in current from point A to B resulted from the formation of a protective passive film. The higher the corrosion potential ($E_{corr}$) of a metal in a specific medium, the more resistant is the metal to corrosion in the medium.

In this work, the electrochemical behavior of tungsten in the $K_3[Fe(CN)_6]$ slurry was evaluated. A GAMRY PC4/750 electrochemical measuring system was used for the electrochemical polarization tests. A platinum wire- counter electrode and a saturated calomel reference electrode were used in a three-electrode working system. Potentiodynamic polarization curves were generated at a scan rate of 0.33 mV/s in the potential region of –0.5 $V_{OCP}$ and approximately +2.0 $V_{OCP}$ for different slurry pH. All polarization tests were repeated at least thrice and the results were repeatable.

Scanning electron microscopy (SEM), atomic force microscopy (AFM) and X-ray photoelectron spectroscopy (XPS) were used to analyze surface morphologies and chemical compositions of the surface oxide formed at different slurry pH values respectively. Mechanical properties of the passive films formed after immersion in the $K_3[Fe(CN)_6]$ slurry for one hour were evaluated using nanoindentation and micro-scratch tests.

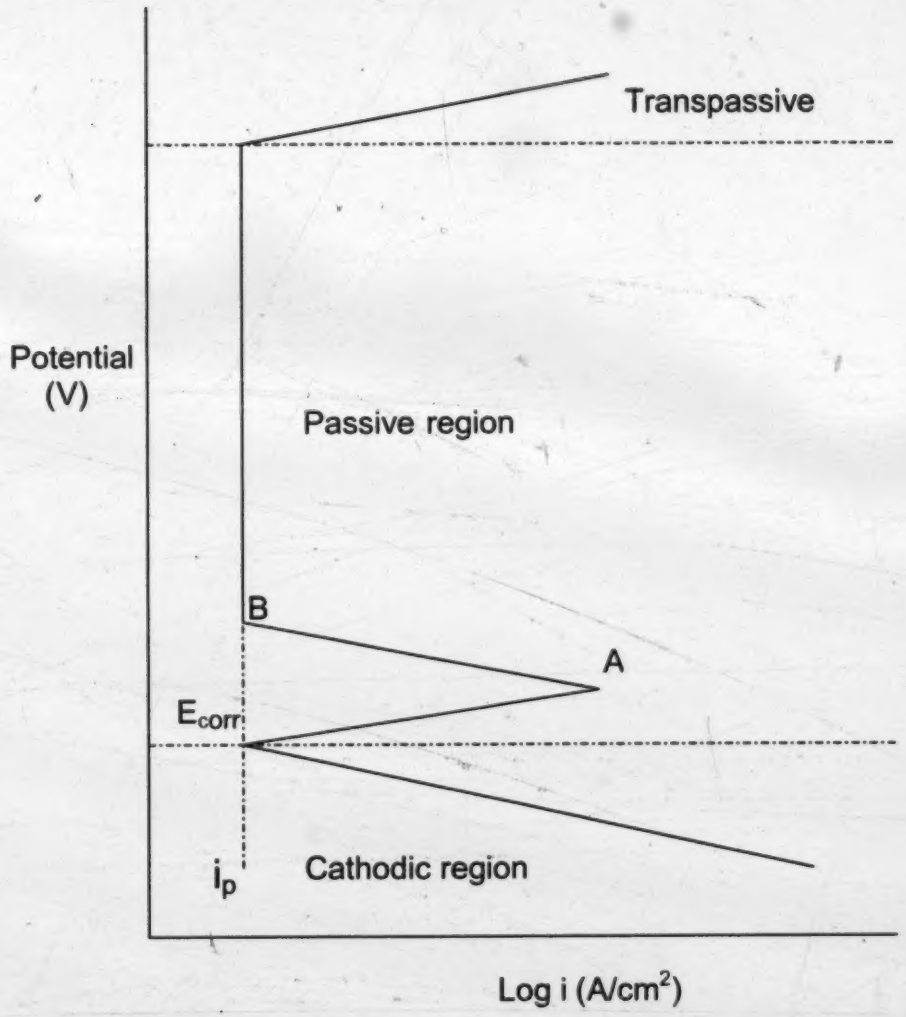


Figure 2-2. Hypothetical Potentiodynamic curve for a passive metal

## 2.2 Polarization Behavior of Tungsten in the $K_3[Fe(CN)_6]$ Slurry

Figure 2-3 shows the polarization behavior of tungsten in the $K_3[Fe(CN)_6]$ slurry as a function of pH. $K_3[Fe(CN)_6]$ is an oxidant which allows passivation beyond the pH range specified by the Pourbaix diagram [80]. As shown, the corrosion potential, $E_{corr}$, of the tungsten decreases with an increase in slurry pH value. The lowest passive current density under any applied potential was observed in the slurry of pH 4 ($\sim 10^{-5.5}$); the low passive current was an indication that a protective layer was formed which offered protection from corrosion. The protective role of the passive film was thus expected to decrease with an increase in pH.

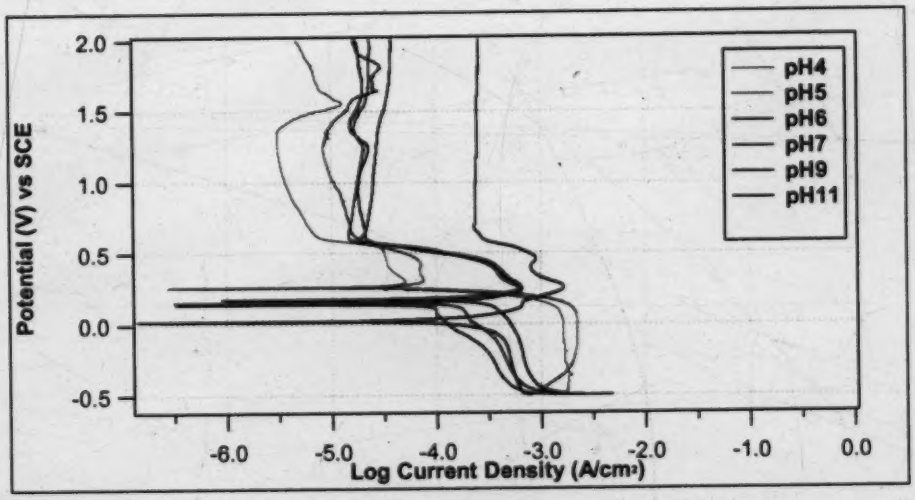


Figure 2-3. Polarization curves of tungsten in the $K_3[Fe(CN)_6]$ slurry as a function of pH

## 2.3 Surface morphology of tungsten after immersion in $K_3[Fe(CN)_6]$ slurries with different pH values

In order to better understand the polarization behavior of tungsten at different pH level, the surface morphology of tungsten samples immersed in the $K_3[Fe(CN)_6]$ slurries with different pH values for one hour were examined using the SEM and AFM. The observed SEM and AFM surface morphologies are shown in figures 2-4 & 2-5 respectively. The surface at relatively high slurry pH values (6~ 11) appeared to be "spongy". The surfaces morphologies at high pH values indicates strong etching reaction occurred, which was highly discontinuous and led to a porous surface. However, at lower pH (i.e. 4 and 5) level, the surface was less porous, continuous, and more compact. The morphology observation is consistent with the polarization test. At lower pH levels, tungsten showed better passivation behavior, accompanied with more protective passive films. They may offer better resistance to corrosion, reducing pitting and morphological inhomogeneity.

In conclusion, $K_3[Fe(CN)_6]$ slurry was able to passivate tungsten over the range of pH in this study. However, the degree of protection offered by the respective passive film against corrosion decreased with an increase in pH level.

6 micrometers
pH 4
PH4 OCP(SE

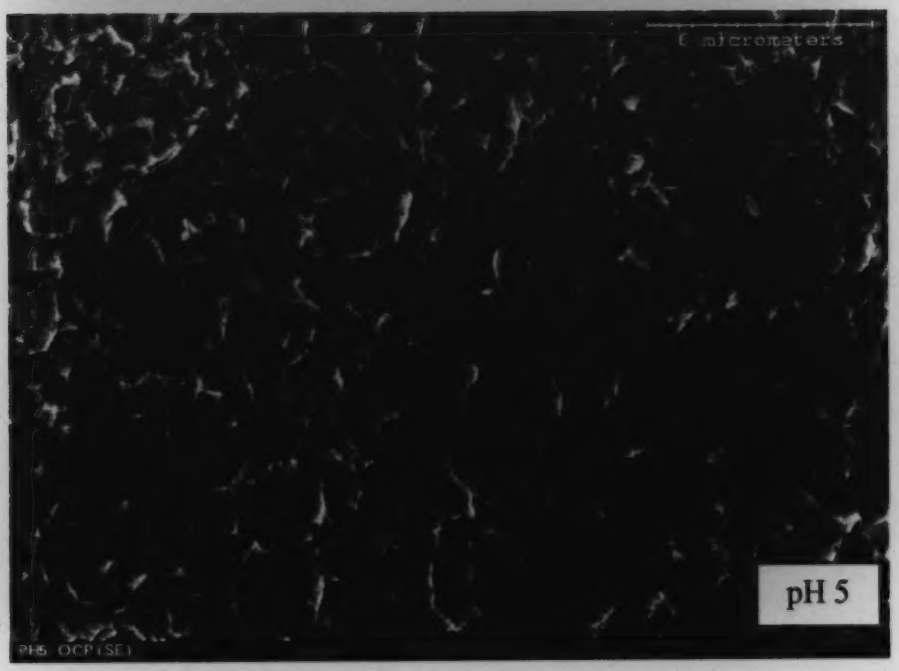
6 micrometers
pH 5
PH5 OCP(SE)

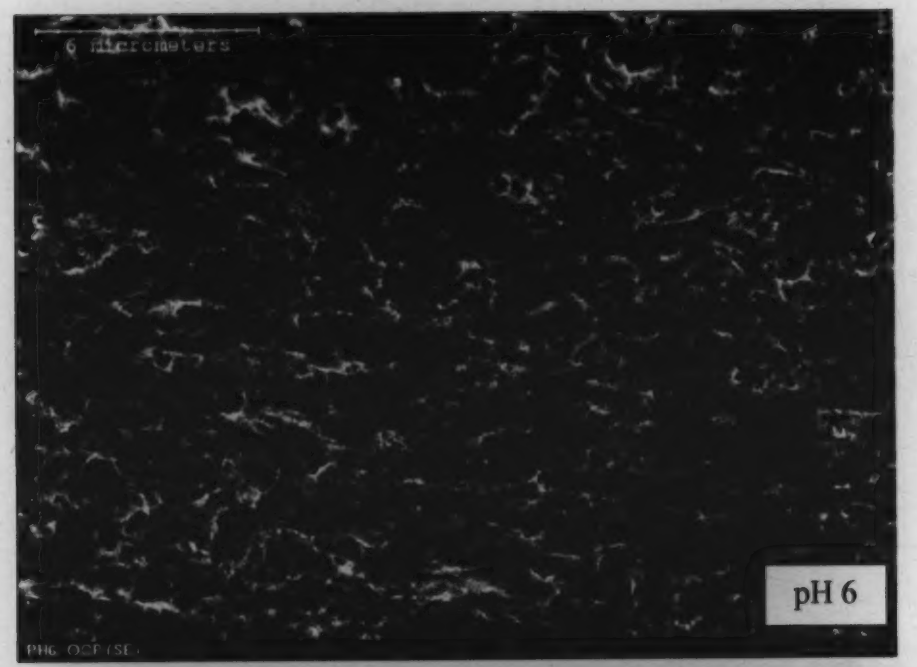
6 micrometers
pH 6
PH6 OCP(SE)

6 micrometers
pH 7
PH7 OCP(SE)

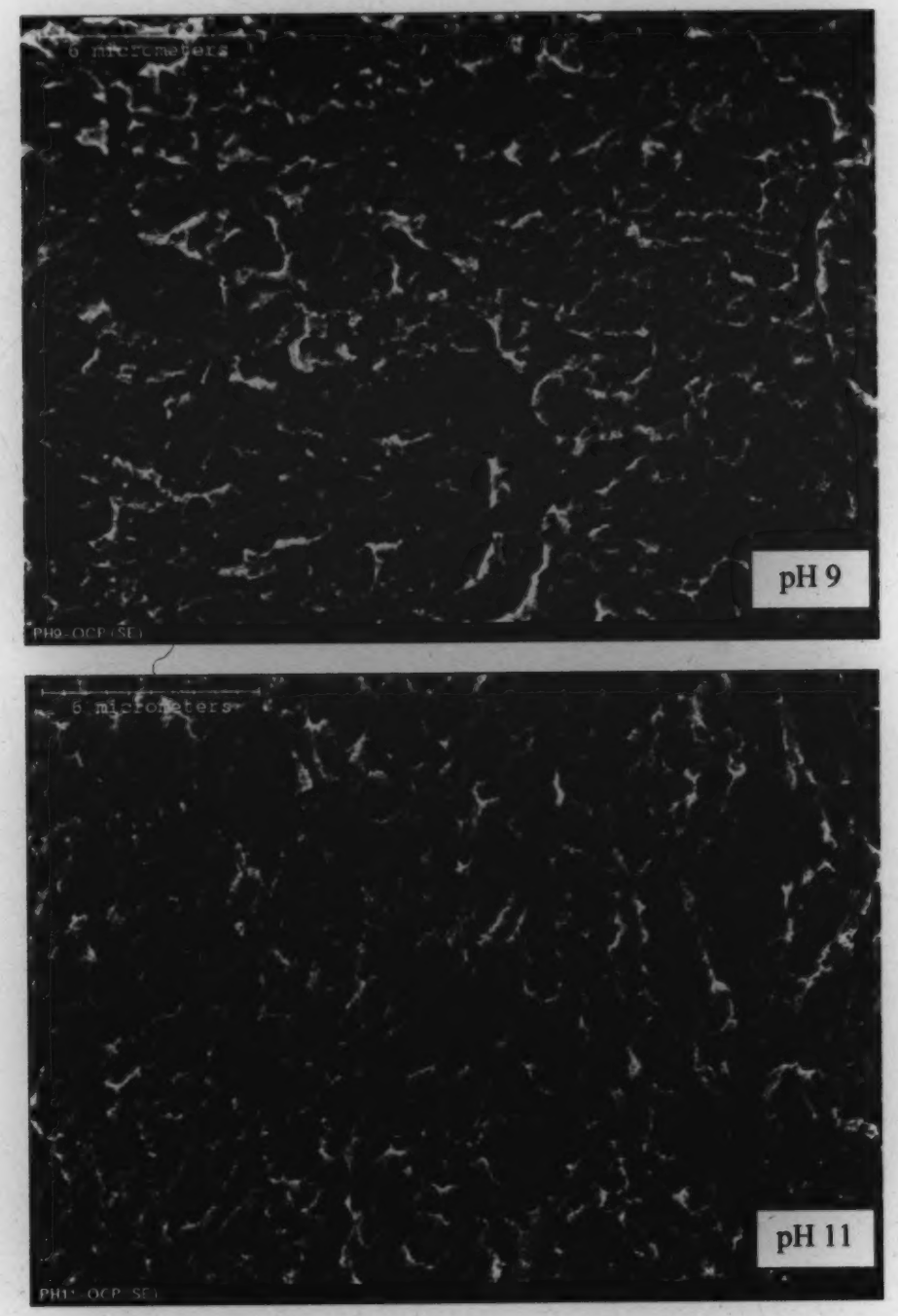


Figure 2-4. SEM images of surface morphologies of tungsten after immersion in $K_3[Fe(CN)_6]$ slurries with different pH values for one hour.

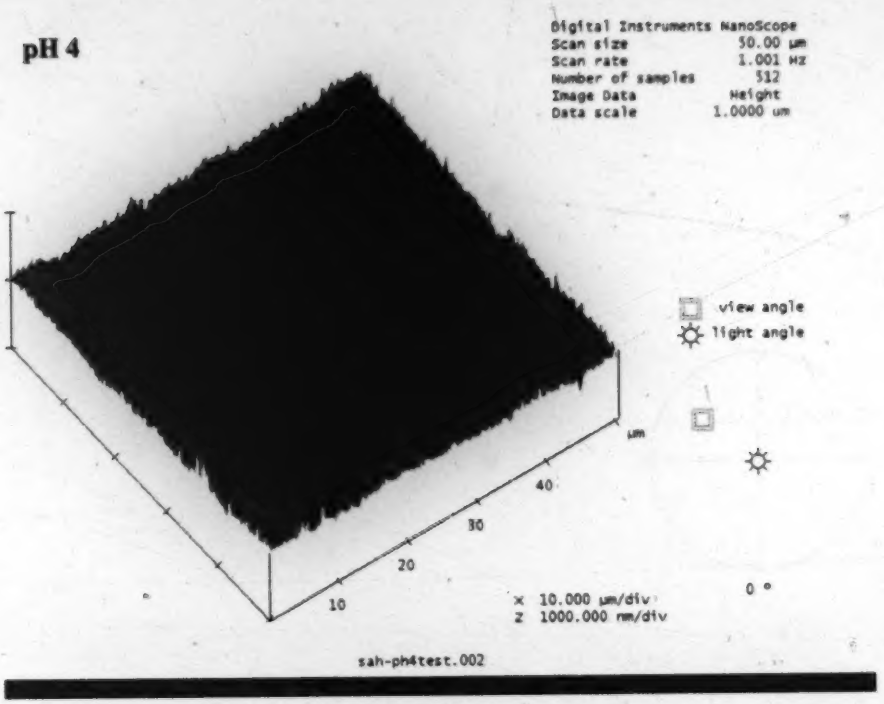
pH 4
Digital Instruments NanoScope
Scan size 50.00 µm
Scan rate 1.001 Hz
Number of samples 512
Image Data Height
Data scale 1.0000 um
view angle
light angle
µm
10
20
30
40
x 10.000 µm/div
z 1000.000 nm/div
0 °
sah-ph4test.002

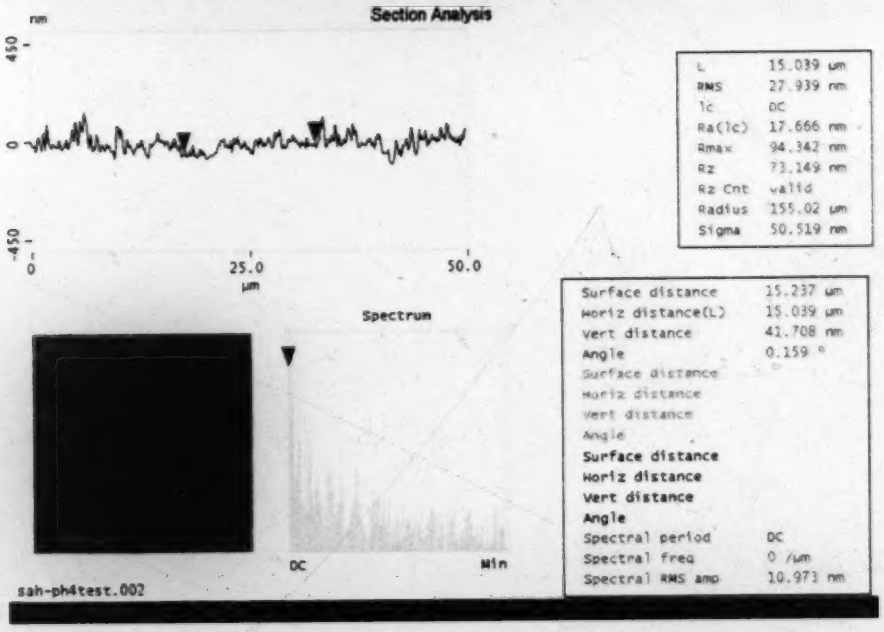
Section Analysis
nm
450
0
-450
0
25.0
µm
50.0
L 15.039 µm
RMS 27.939 nm
lc DC
Ra(lc) 17.666 nm
Rmax 94.342 nm
Rz 73.149 nm
Rz Cnt valid
Radius 155.02 µm
Sigma 50.519 nm
Spectrum
DC
Min
Surface distance 15.237 µm
Horiz distance(L) 15.039 µm
Vert distance 41.708 nm
Angle 0.159 °
Surface distance
Horiz distance
Vert distance
Angle
Surface distance
Horiz distance
Vert distance
Angle
Spectral period DC
Spectral freq 0 /µm
Spectral RMS amp 10.973 nm
sah-ph4test.002

**pH 5**

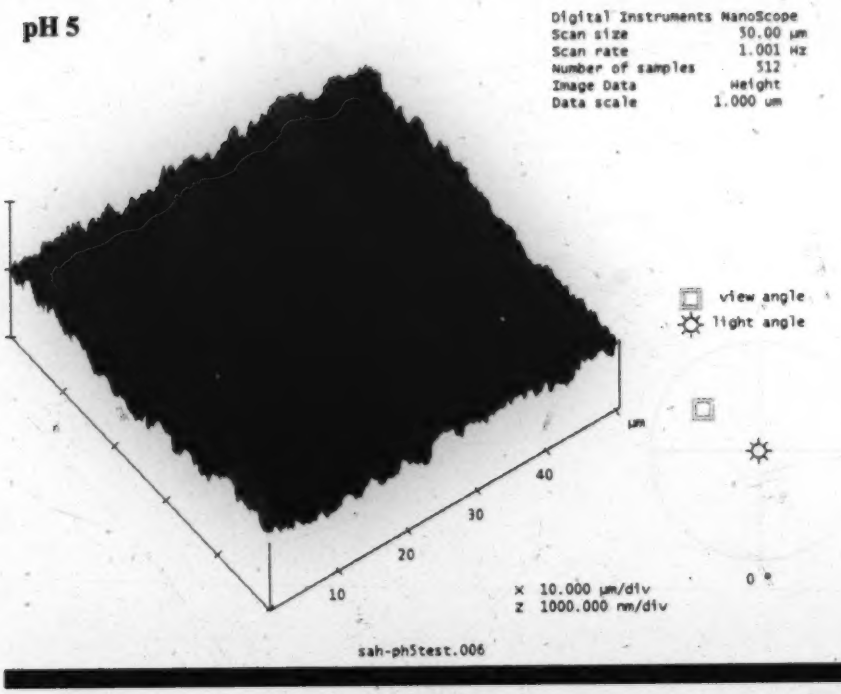
Digital Instruments NanoScope
Scan size 50.00 µm
Scan rate 1.001 Hz
Number of samples 512
Image Data Height
Data scale 1.000 um
view angle
light angle
µm
10
20
30
40
0 °
x 10.000 µm/div
z 1000.000 nm/div
sah-ph5test.006

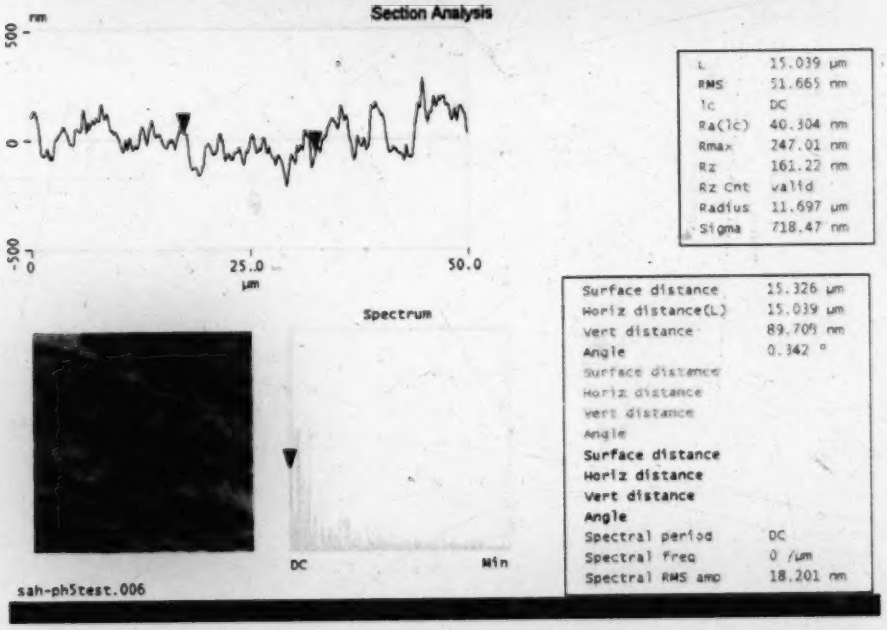
Section Analysis
nm
500
0
-500
0
25.0
µm
50.0
L 15.039 µm
RMS 51.665 nm
lc DC
Ra(lc) 40.304 nm
Rmax 247.01 nm
Rz 161.22 nm
Rz Cnt valid
Radius 11.697 µm
Sigma 718.47 nm
Spectrum
DC
Min
Surface distance 15.326 µm
Horiz distance(L) 15.039 µm
Vert distance 89.709 nm
Angle 0.342 °
Surface distance
Horiz distance
Vert distance
Angle
Surface distance
Horiz distance
Vert distance
Angle
Spectral period DC
Spectral freq 0 /µm
Spectral RMS amp 18.201 nm
sah-ph5test.006

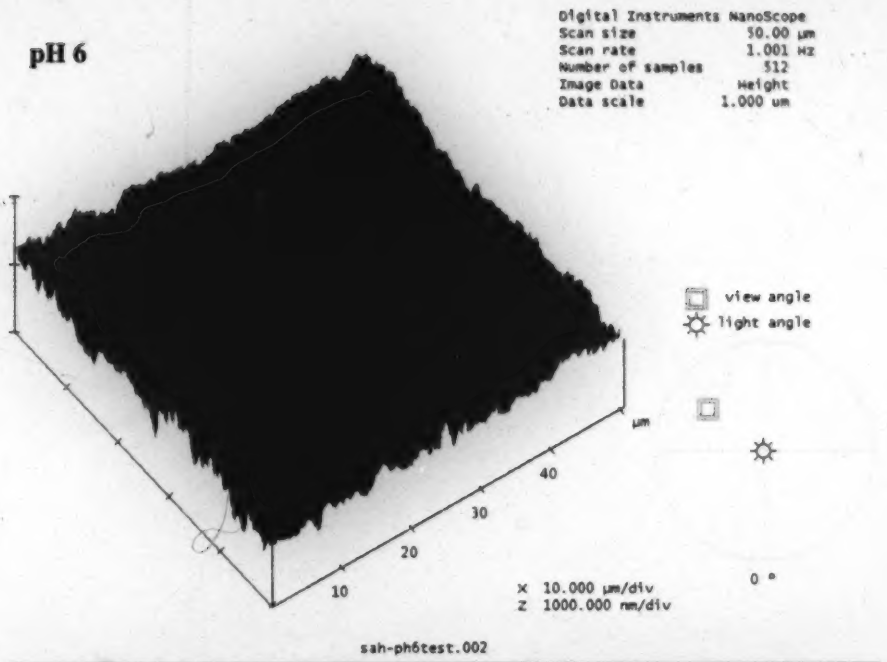
pH 6
Digital Instruments NanoScope
Scan size 50.00 µm
Scan rate 1.001 Hz
Number of samples 512
Image Data Height
Data scale 1.000 um
view angle
light angle
µm
10
20
30
40
0 °
x 10.000 µm/div
z 1000.000 nm/div
sah-ph6test.002

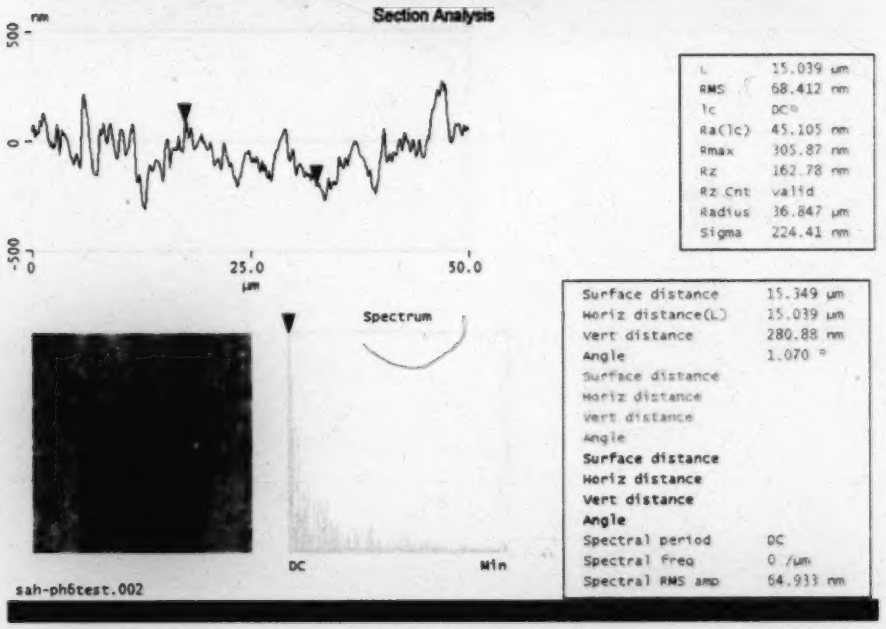
Section Analysis
nm
500
0
-500
0
25.0
50.0
µm
L 15.039 µm
RMS 68.412 nm
lc DC
Ra(lc) 45.105 nm
Rmax 305.87 nm
Rz 162.78 nm
Rz Cnt valid
Radius 36.847 µm
Sigma 224.41 nm
Spectrum
DC
Min
Surface distance 15.349 µm
Horiz distance(L) 15.039 µm
Vert distance 280.88 nm
Angle 1.070 °
Surface distance
Horiz distance
Vert distance
Angle
Surface distance
Horiz distance
Vert distance
Angle
Spectral period DC
Spectral freq 0 /µm
Spectral RMS amp 64.933 nm
sah-ph6test.002

**pH 7**

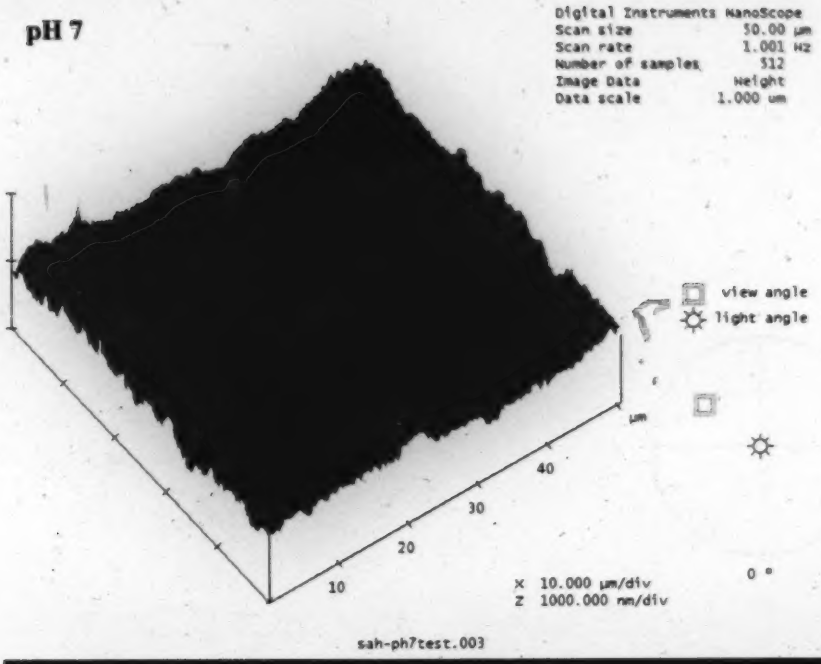
Digital Instruments NanoScope
Scan size 50.00 µm
Scan rate 1.001 Hz
Number of samples 512
Image Data Height
Data scale 1.000 um
view angle
light angle
µm
10
20
30
40
0 °
X 10.000 µm/div
Z 1000.000 nm/div
sah-ph7test.003

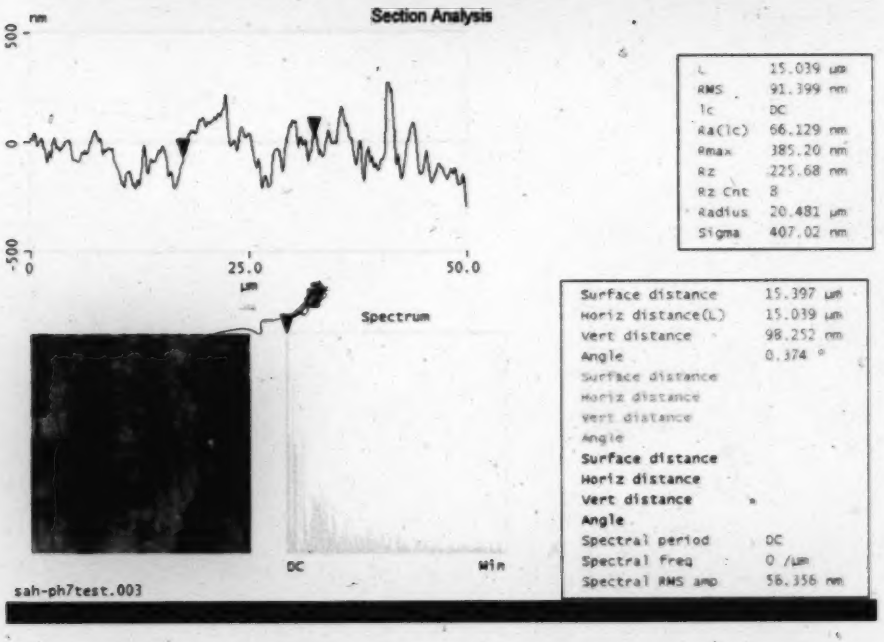
Section Analysis
nm
500
0
-500
0
25.0
50.0
µm
Spectrum
DC
Nin
sah-ph7test.003
L 15.039 µm
RMS 91.399 nm
lc DC
Ra(lc) 66.129 nm
Rmax 385.20 nm
Rz 225.68 nm
Rz Cnt 8
Radius 20.481 µm
Sigma 407.02 nm
Surface distance 15.397 µm
Horiz distance(L) 15.039 µm
Vert distance 98.252 nm
Angle 0.374 °
Surface distance
Horiz distance
Vert distance
Angle
Surface distance
Horiz distance
Vert distance
Angle
Spectral period DC
Spectral freq 0 /µm
Spectral RMS amp 56.356 nm

**pH 9**

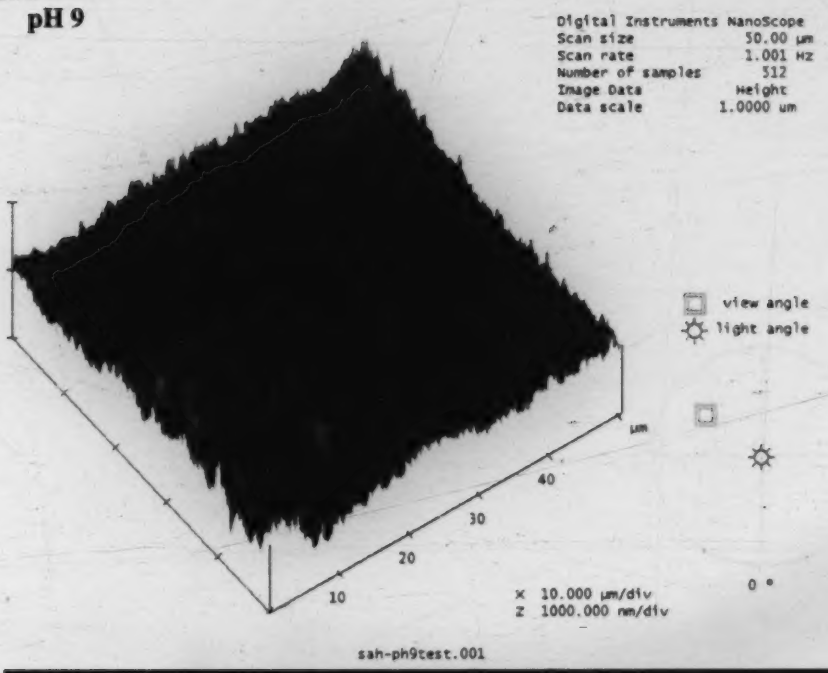
Digital Instruments NanoScope
Scan size 50.00 µm
Scan rate 1.001 Hz
Number of samples 512
Image Data Height
Data scale 1.0000 µm
view angle
light angle
µm
10
20
30
40
0 °
x 10.000 µm/div
z 1000.000 nm/div
sah-ph9test.001

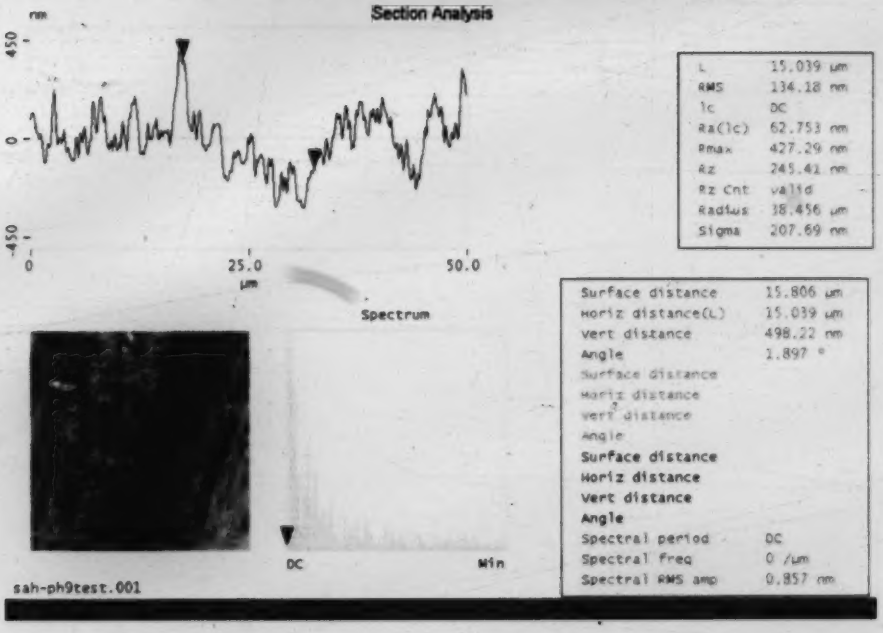
Section Analysis
nm
450
0
-450
0
25.0
50.0
µm
L 15.039 µm
RMS 134.18 nm
lc DC
Ra(lc) 62.753 nm
Rmax 427.29 nm
Rz 245.41 nm
Rz Cnt valid
Radius 38.456 µm
Sigma 207.69 nm
Spectrum
DC
Min
Surface distance 15.806 µm
Horiz distance(L) 15.039 µm
Vert distance 498.22 nm
Angle 1.897 °
Surface distance
Horiz distance
Vert distance
Angle
Surface distance
Horiz distance
Vert distance
Angle
Spectral period DC
Spectral freq 0 /µm
Spectral RMS amp 0.857 nm
sah-ph9test.001

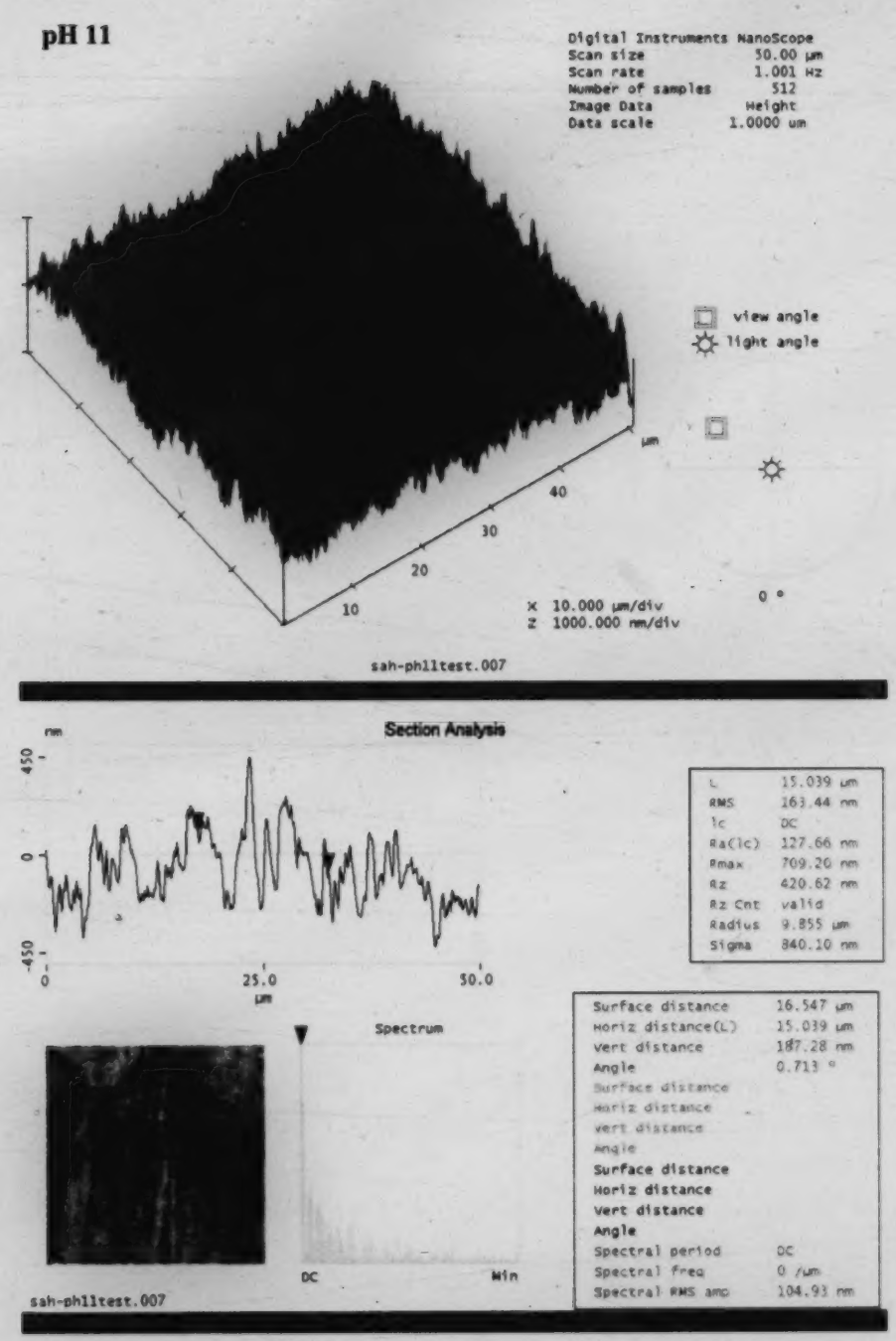


Figure 2-5. AFM images of surface morphologies of tungsten after immersion in $K_3[Fe(CN)_6]$ slurries with different pH values for one hour.

## 2.4 X-ray Photoelectron Spectroscopy (XPS) Analyses

XPS analyses were carried out to obtain information on the surface oxide formed at different slurry pH values. The XPS analyses were made using an Axis 165 Kratos XPS spectrometer with an Al (mono) X-ray source, and the electron pass energy was 20 eV. The surface films formed at different slurry pH levels after immersion in the $K_3[Fe(CN)_6]$ slurries with different pH values for one hour were analyzed. Observed peaks came from the tungsten 4f ($4f_{7/2}$ and $4f_{5/2}$) core level spectra. Table 2.2 shows fractions of the characteristic peaks of oxide films.

Table 2-2 XPS analysis: atomic compositions of tungsten in different oxidation states after one hour of immersion in slurry with different pH values

| Peak \ pH | 4 | 5 | 6 |
|---|---|---|---|
| W 4f-7/2(at %) | 7.84 | 35.68 | 41.52 |
| W 4f-5/2(at %) | 5.92 | 25.05 | 30.84 |
| W03 4f-7/2(at %) | 45.77 | 13.37 | 5.76 |
| W03 4f-5/2(at %) | 34.73 | 10.41 | 4.54 |
| W02 4f-7/2(at %) | 3.42 | 9.13 | 10.73 |
| W02 4f-5/2(at %) | 2.31 | 6.02 | 6.60 |

The XPS analysis indicated that the oxide films on tungsten mainly contained $WO_3$ phase at all pH values considered in this study (see Table 2.2). Although, thermodynamically, $WO_3$ should be stable only below pH 2 [80], the $K_3[Fe(CN)_6]$ oxidant in the slurry may be responsible for the existence of $WO_3$ at all pH values. $WO_3$ has been reported to be mainly beneficial to the passivation capability of tungsten [91].

As shown, higher pH values led to lower contents of $WO_3$. This could be one of the reasons why the passive film became less protective at higher pH values. However, XPS analyses showed the presence of another oxide phase, $WO_2$, especially at higher pH values. $WO_2$ has been reported to be less beneficial to the corrosion resistance of tungsten. Therefore, the more the amount of $WO_2$ in the duplex layer of $WO_3/WO_2$, the lower the resistance of the surface oxide to corrosion [92].

In Table 2.2, information on passive films formed in slurries with pH higher than 6 was not presented. The reason is that it was difficult to obtain distinct peaks from tungsten for slurries with pH higher than 6. This was due to the overlapped binding energies of W 4f and K 3s peaks. The higher potassium content was as a result of the KOH used in adjusting the pH value of the slurry. However, based on the larger passive steady-state current densities at higher pH values (see figure 2.3) and the SEM morphology observation (see figure 2.4), it may be concluded that the surface oxides formed at higher slurry pH (7 – 11) may contain more $WO_2$ but less $WO_3$ phase and other tungsten oxides.

## 2.5 Mechanical Properties of Surface oxides films formed at different pH levels

The passive film on tungsten plays an important role in resisting corrosion and wear; its mechanical properties strongly influence the chemical-mechanical planarization of tungsten. It is thus essential to evaluate the mechanical properties of passive films on tungsten formed in slurries with different pH values. In this study, the mechanical properties of the surface oxides formed on tungsten were evaluated using nanoindentation and micro-scratch techniques.

### 2.5.1 Nanoindentation tests

The Nanoindentation technique can be used to evaluate the mechanical behavior of a passive film. During the test, an indenter tip is pressed to penetrate into the film under an applied load. This is an efficient technique for evaluating mechanical properties of a thin surface film since the indentation can be performed under light loads. The hardness of a passive film can be evaluated from the Load-Displacement curve obtained during indentation; under a fixed load, the penetration depth reflects the hardness of the film.

In this study, a Triboscope (Hysitron Inc., USA) equipped with a four-sided pyramidal shaped diamond nanoindenter under atomic force microscope was used to evaluate the mechanical properties of passive films formed after immersion in the $K_3[Fe(CN)_6]$ slurry for one hour at different pH values. Resolutions of the force and displacement of the instrument were 0.1 μN and 0.2 nm respectively. The Load-

Displacement curves obtained under a maximum load of 40 μN are presented in Figure 2.6.

It was observed that the hardness of the passive films decreased with an increase in the slurry pH value; this is reflected by the increase in maximum indentation depth as presented in Table 2.3. This observation may be attributed to the fact that the surface films were becoming porous, discontinuous and less compact with an increase in slurry pH. The films formed at lower pH are thus expected to offer better protection from mechanical damage. Most significantly, the passive films are softer than the tungsten substrate. And thus the formation of surface oxide will facilitate tungsten removal during a tribo-corrosion process.

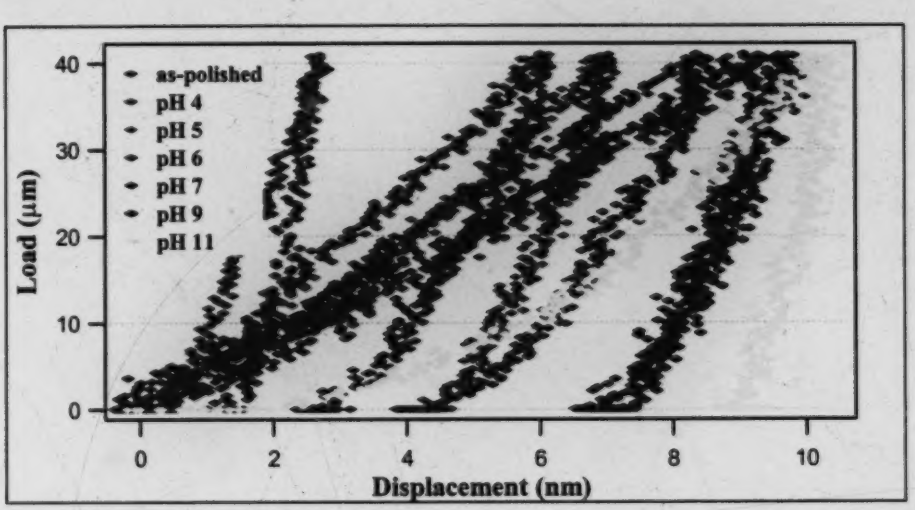


Figure 2-6. Nanoindentation results from oxide films formed at different slurry pH after immersion in the slurry for 1 hr.

Table 2.3. Maximum displacements under load of 40 μN

| Slurry pH | Maximum indentation depth under a load of 40 μN (nm) |
|---|---|
| 4 | 6.02 |
| 5 | 7.05 |
| 6 | 8.37 |
| 7 | 9.07 |
| 9 | 9.73 |
| 11 | 9.98 |

It should be noted that the indentation depth is an approximate indication of the hardness of a surface thin film, since the measurement could be affected by the substrate. However, looking at the roughness of the passive film (see Figure 2-5), e.g. Rmax=94.3 for pH 4 and Rmax=709.20 for pH 11, one may expect that the oxide scale could be in the range of $10^2$ or larger, since the roughness only represents the fluctuation in thickness of a passive film formed on a substrate. Based on common sense, the thickness of the film should be larger than the fluctuation in thickness. Therefore results obtained from a small load of 40 μN and a maximum indentation depth less than 10 nm may largely reflect hardness of the surface films.

### 2.5.2 Resistance of Surface Film to Scratch

The degree of protection offered by a passive film is also dependent on its adherence to the metal substrate [92]. Poor film-substrate adhesion may result in easy removal of the film by mechanical force as well as little or no resistance to corrosion attack. The adherence of a film to its substrate can be evaluated using a scratch test commonly used in assessing a coating's adherence [93].

In this study, a universal micro-tribometer (Center for Tribology, USA) was used to evaluate the bond strength between the tungsten substrate and its surface films formed at different slurry pH levels. The passive films were scratched using a tungsten carbide tip under a continuously increasing normal load from 0.5 N to 10 N. The scratch tests

were performed at a scratch speed of 0.03 mm/s over a distance of 3 mm. The film was then expected to fail at a critical load at which interfacial debonding would occur between the film and the substrate. Results of the micro-scratch tests are presented in Figure 2-7; the metal-film interfacial debonding was determined by a drop in the electrical contact resistance (ECR) under a critical load, which is a measure of the resistance to scratch. The negative force reflects the downwardly applied normal load. As shown passive films formed at low slurry pH (pH 4 and 5) offered relatively high resistance to mechanical scratching, while those formed at higher pH levels (pH 6-11) offered little or no resistance to mechanical damage. As a matter of fact, the electrical contact resistance for passive films formed at pH 7 – 11 dropped as soon as they came in contact with the tungsten carbide tip. These results show that the metal-film bonding and the resistance to mechanical scratch decrease with an increase in pH. The critical loads needed to remove the passive films from the tungsten substrate are presented in Table 2.4. Because the oxides formed at high slurry pH can be easily damaged, the removal rate during tribo-corrosion process may thus be expected to be higher in slurries having high pH values. This observation is similar to results obtained for copper in slurries containing $H_2O_2$ for pH greater than 6 [94].

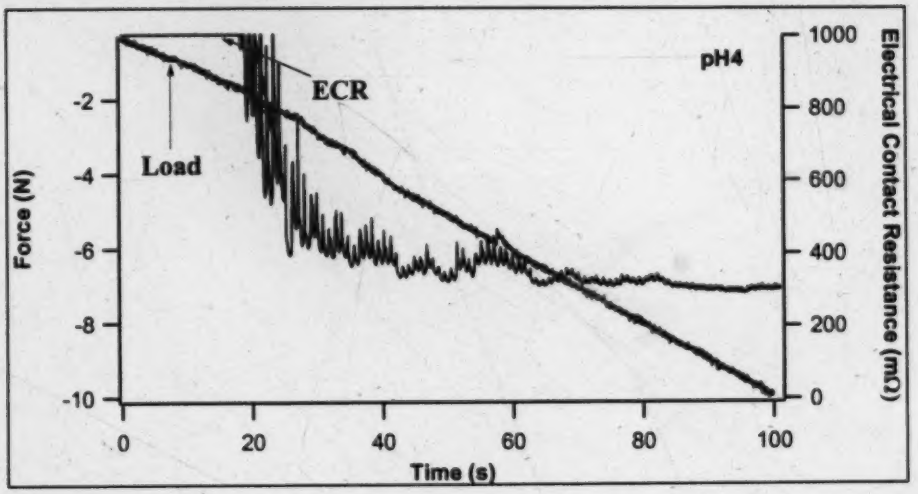
pH4
ECR
Load
Force (N)
Time (s)
Electrical Contact Resistance (mΩ)
-2
-4
-6
-8
-10
0
20
40
60
80
100
1000
800
600
400
200
0

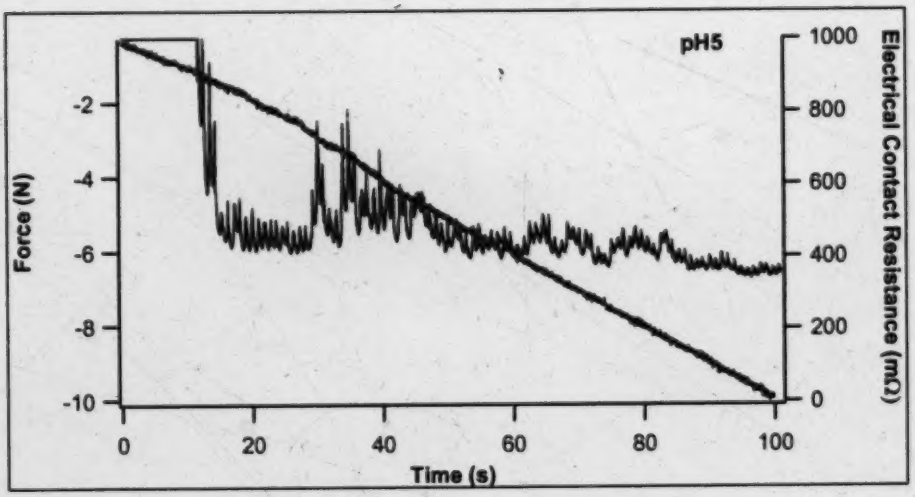
pH5
Force (N)
Time (s)
Electrical Contact Resistance (mΩ)
-2
-4
-6
-8
-10
0
20
40
60
80
100
1000
800
600
400
200
0

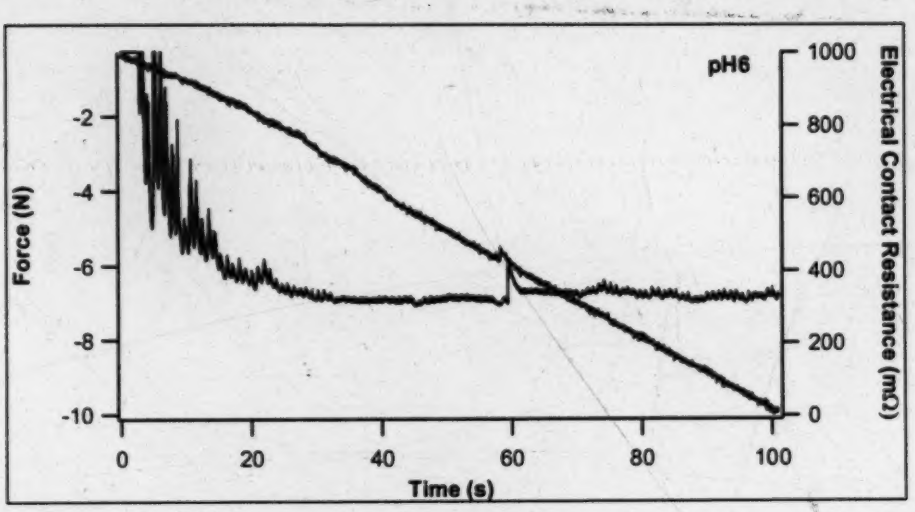
pH6
Force (N)
-2
-4
-6
-8
-10
0
20
40
60
80
100
Time (s)
1000
800
600
400
200
0
Electrical Contact Resistance (mΩ)

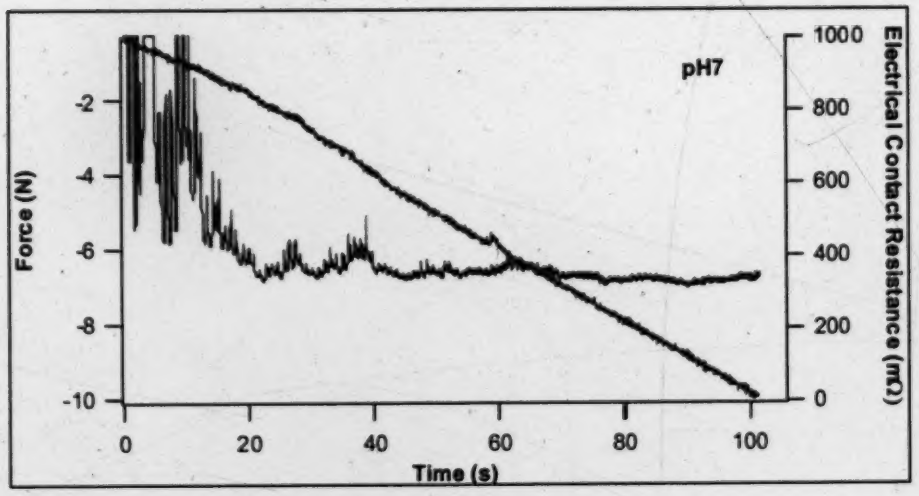
pH7
Force (N)
-2
-4
-6
-8
-10
0
20
40
60
80
100
Time (s)
1000
800
600
400
200
0
Electrical Contact Resistance (mΩ)

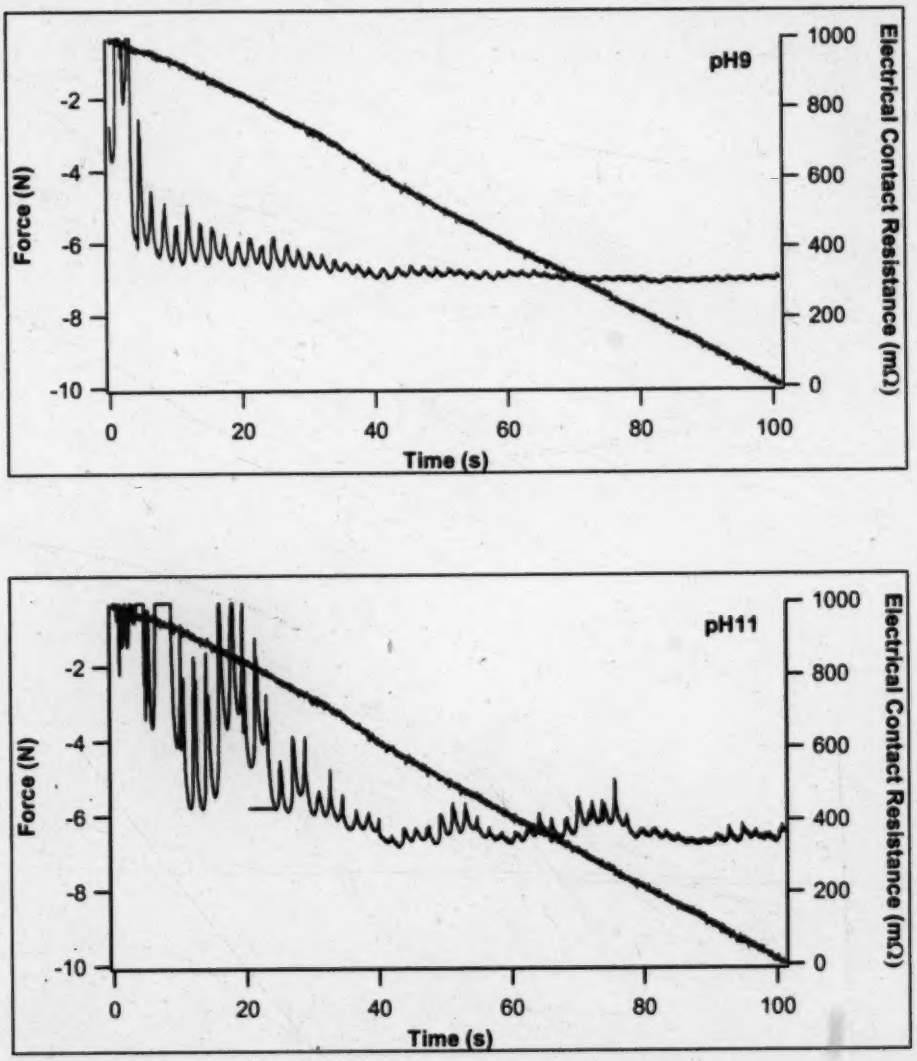


Figure 2-7. Changes in the electrical contact resistance (ECR) of passive films formed at different slurry pH levels (after immersion in the slurries for one hr) during micro scratching.

Table 2-4. The critical failure loads of the passive film formed after one hour of immersion in slurries having different pH values.

| Slurry pH | Critical Failure load (N) |
|---|---|
| 4 | 1.71 |
| 5 | 1.21 |
| 6 | 0.60 |
| 7 | 0.53 |
| 9 | 0.51 |
| 11 | 0.51 |

## 3.0 Wear-Corrosion Synergy of Tungsten in the $K_3[Fe(CN)_6]$ Slurry

In a corrosive wear process, corrosion enhances wear and wear on the other hand leads to increase in corrosion rate. The wear-corrosion synergy often results in considerable increase in material loss, compared to those caused by the individual processes. The synergistic interaction of wear and corrosion plays an important role in material removal during a chemical-mechanical planarization process.

Wear-corrosion synergy can be calculated using equation 3.1 [95]:

$$T = W_O + C_O + S \tag{3.1}$$

where S is the material loss rate caused by the synergism of wear and corrosion, T is the total material loss rate caused by corrosion wear, $C_O$ is the material loss rate caused by corrosion in the absence of wear, and $W_O$ is the material loss rate in the absence of corrosion. The synergistic component (S) includes two parts: increase of mechanical wear due to corrosion, S', and the increase of corrosion due to mechanical wear, S",

$$S = S' + S'' \tag{3.2}$$

therefore equation (3.1) can be expressed as

$$T = W_O + C_W + S' \tag{3.3}$$

hence $$S'' = C_W - C_O \tag{3.4}$$

and $$W_C = T - C_W \tag{3.5}$$

where $C_W$ and $W_C$ are the corrosion rate in the presence of wear and wear rate in the presence of corrosion respectively.

In this chapter, the total loss rate (T), pure corrosion rate ($C_O$), pure wear rate ($W_O$), and corrosion rate accelerated by wear ($C_W$) were determined experimentally. S, $S'$, $S''$, and $W_C$ were then calculated using the equations above. Two dimensionless factors, corrosion augmentation factor ($C_W/C_O$) and wear augmentation factor ($W_C/W_O$) are then obtained to describe the degree of synergism. Error bars are given in all figures that present the experimental results.

## 3.1 Corrosion rate without wear – $C_O$

The pure corrosion rate can be determined by extrapolation of the Tafel line for the anodic and cathodic reaction to the corrosion potential [96]. The corrosion current may be obtained form the point of intersection of the Tafel lines. A typical Tafel curve is shown in figure 3-1. Several important electrochemical parameters can be obtained from the extrapolation of such a curve. These parameters include open circuit potential and corrosion current density.

In this study, Tafel curves for tungsten were generated for different slurry pH at a scan rate of 0.33 mV/s. The Tafel curves of tungsten for different slurry pH values are presented in figure 3-2. The corrosion current density can be obtained from the intersection of the extrapolated lines in the cathodic and anodic regions of the Tafel

curve, which can be used to calculate the corrosion rate using Faraday's equation as expressed in equation (3.6) [95].

$$C_o = \frac{K(\frac{mm-g}{\mu A-cm-yr}) * i_{corr}(\mu A/cm^2) * EQ}{\rho(g/cm^3)} \quad (3.6)$$

K= 3.27 X $10^{-3}$ mm g/ μA cm yr
EQ = Equivalent weight (30.64, for Tungsten assuming valence of +6)
ρ= Density (19.3 g/ $cm^3$)

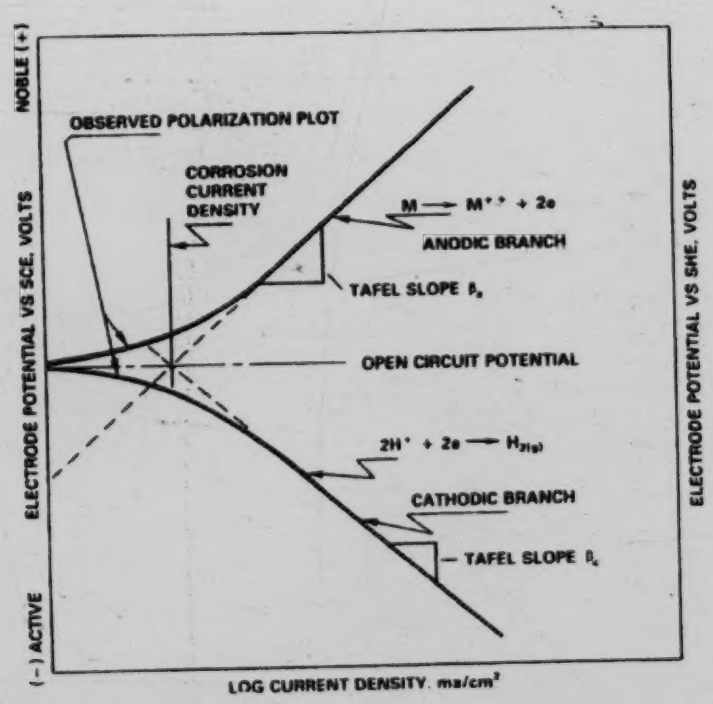


Figure 3-1. Typical Tafel curve, from which several electrochemical parameters can be obtained [97].

The Open-circuit potential ($E_{corr}$), corrosion-current Density ($i_{corr}$), and the corresponding pure Corrosion rate ($C_O$) of the bulk tungsten in the $K_3[Fe(CN)_6]$ slurry at different pH values are presented in Table 3.1.

Table 3.1. Open-circuit potential ($E_{corr}$), Corrosion-current Density ($i_{corr}$), and the corresponding pure Corrosion rate ($C_O$) of the tungsten in the $K_3[Fe(CN)_6]$ slurry at different pH levels.

| Slurry pH | $E_{corr}$ (mV) | $i_{corr}$ ($\mu A/cm^2$) | Corrosion rate, $C_O$, ($mm^3/mm^2$-yr) |
|---|---|---|---|
| 4 | 291.3 | 2.997 | 0.01558 |
| 5 | 268.7 | 6.863 | 0.03563 |
| 6 | 182.9 | 11.42 | 0.134767 |
| 7 | 170.4 | 20.5 | 0.312778 |
| 9 | 168.7 | 38.79 | 0.361006 |
| 11 | 146.5 | 47.48 | 0.39558 |

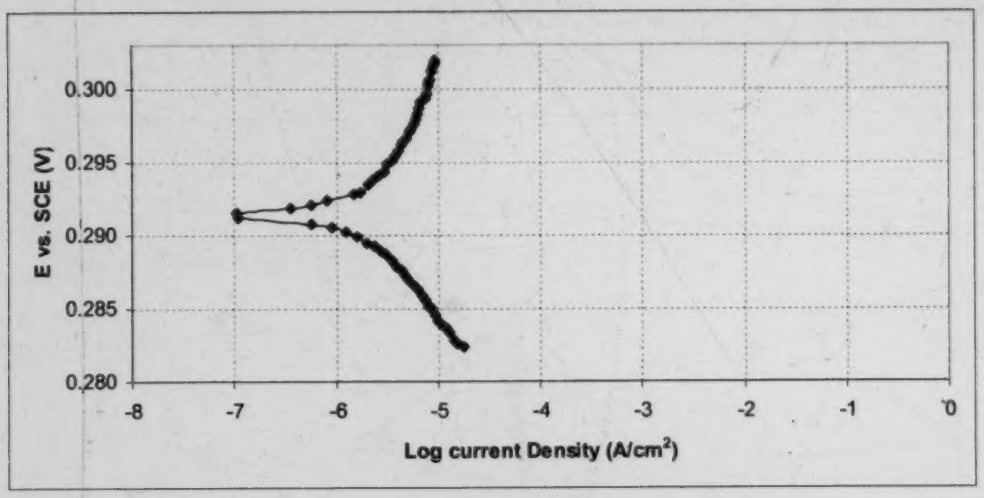
E vs. SCE (V)
0.300
0.295
0.290
0.285
0.280
-8
-7
-6
-5
-4
-3
-2
-1
0
Log current Density (A/cm²)

(a)

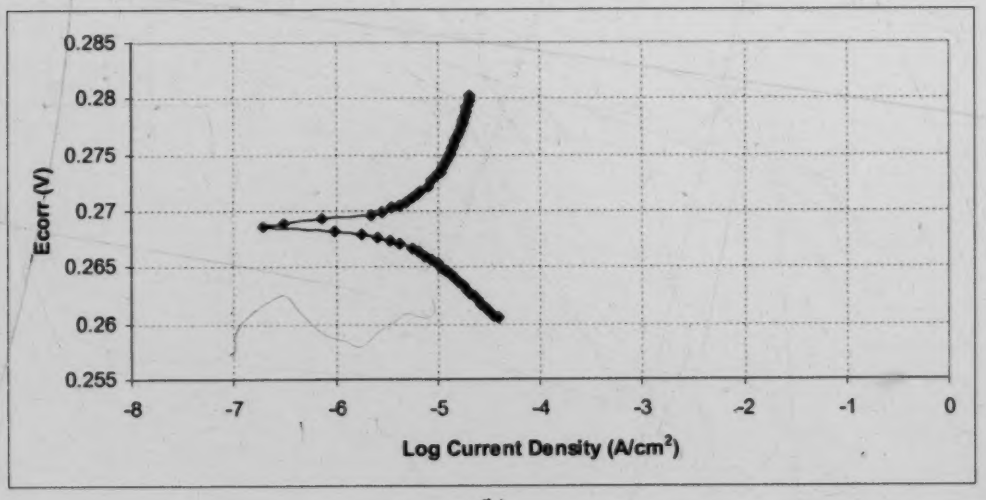
Ecorr (V)
0.285
0.28
0.275
0.27
0.265
0.26
0.255
-8
-7
-6
-5
-4
-3
-2
-1
0
Log Current Density (A/cm²)

(b)

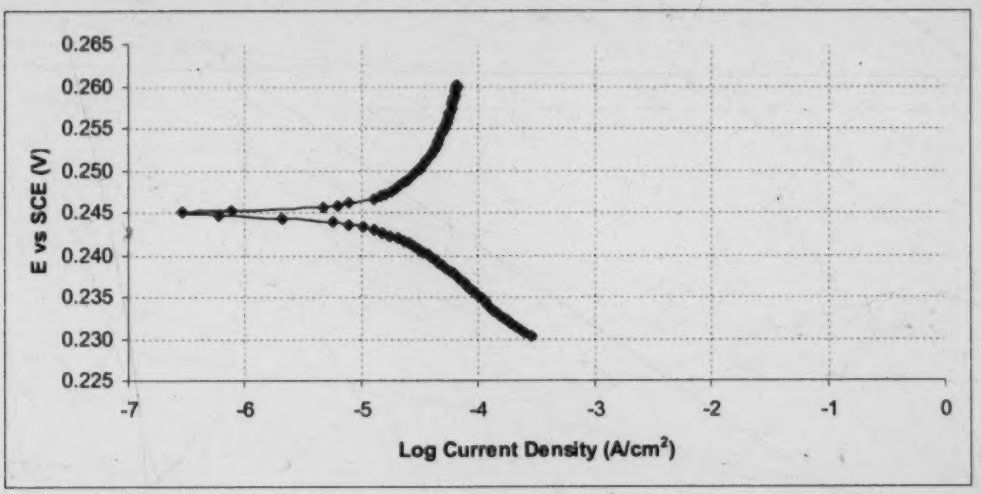
0.265
0.260
0.255
0.250
0.245
0.240
0.235
0.230
0.225
E vs SCE (V)
-7
-6
-5
-4
-3
-2
-1
0
Log Current Density (A/cm²)

(c)

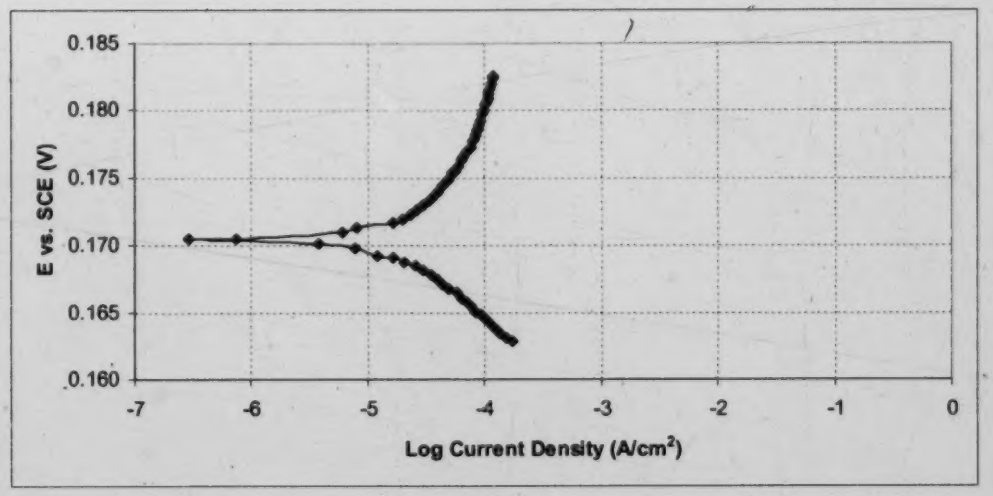
0.185
0.180
0.175
0.170
0.165
0.160
E vs. SCE (V)
-7
-6
-5
-4
-3
-2
-1
0
Log Current Density (A/cm²)

(d)

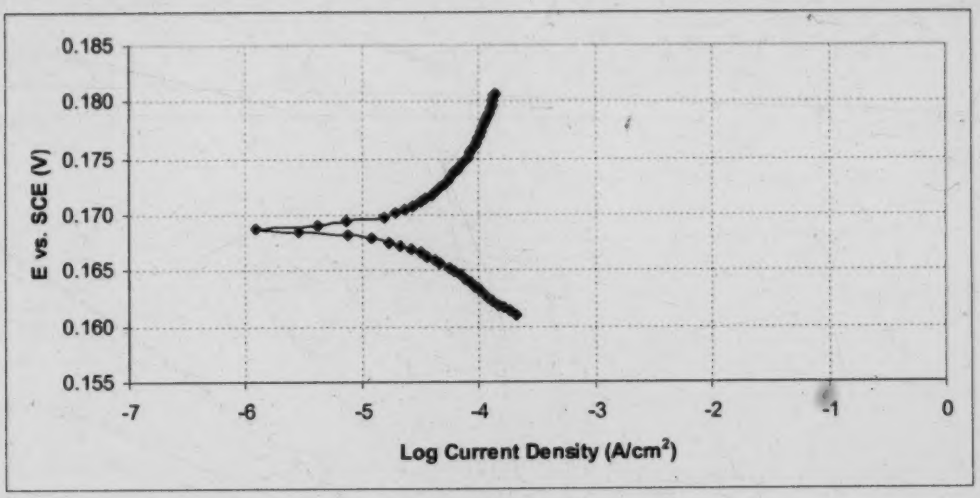


(e)

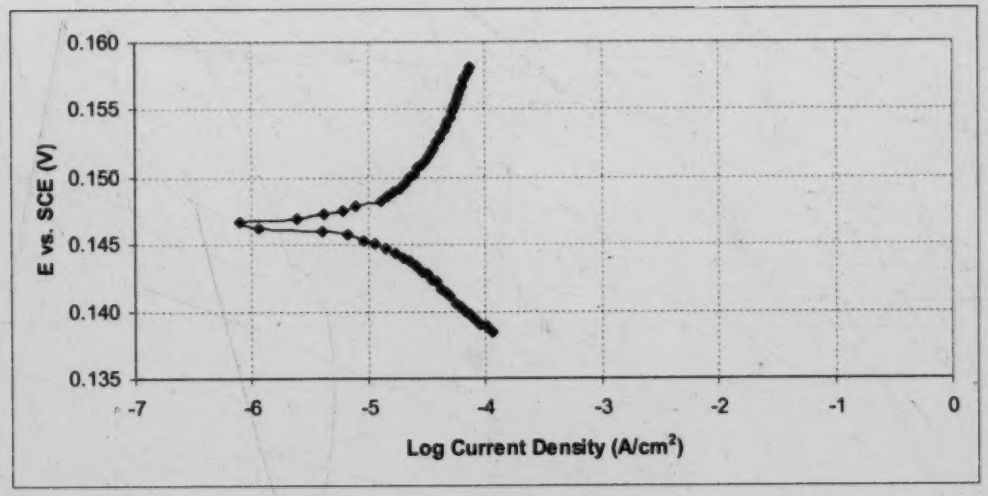


(f)

Figure 3-2. Tafel curves of tungsten in the $K_3[Fe(CN)_6]$ slurry: (a) pH 4, (b) pH 5,(c) pH 6, (d) pH 7, (e) pH 9, (f) pH 11.

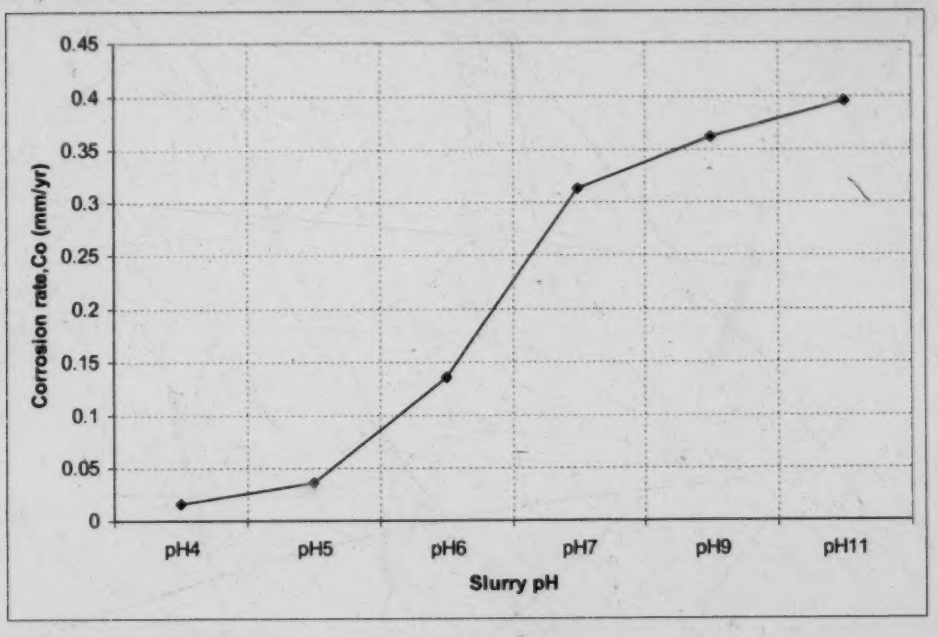


Figure 3-3. Corrosion rate of the tungsten in the $K_3[Fe(CN)_6]$ slurry as a function of pH

From Table 3-1, the open-circuit potential of the tungsten shifts to less noble ranges as the pH increases, corresponding to higher dissolution rates as the slurry was made more alkaline. This result is in agreement with the Pourbaix diagram of tungsten in Figure 3-4. Figure 3-3 illustrates the corrosion rate of tungsten in the slurry as a function of slurry pH. As shown, the corrosion rate increases with an increase in the slurry pH, the rapid increase in corrosion rate at these higher slurry pH values can be attributed to the increased dissolution rate at higher pH values. Higher corrosion rate at higher slurry pH led to rough and porous corroded surfaces as observed from the SEM micrograph of tungsten after immersion in the slurry at these higher pH values (see Figure 2-4). The higher dissolution rates at higher slurry pH levels are consistent with the observed passive current densities (see Figure 2-3). The lower corrosion currents at lower slurry

pH values indicates that the surface oxide layers formed on tungsten at lower pH values offer better protection from chemical dissolution than those formed at higher pH values.

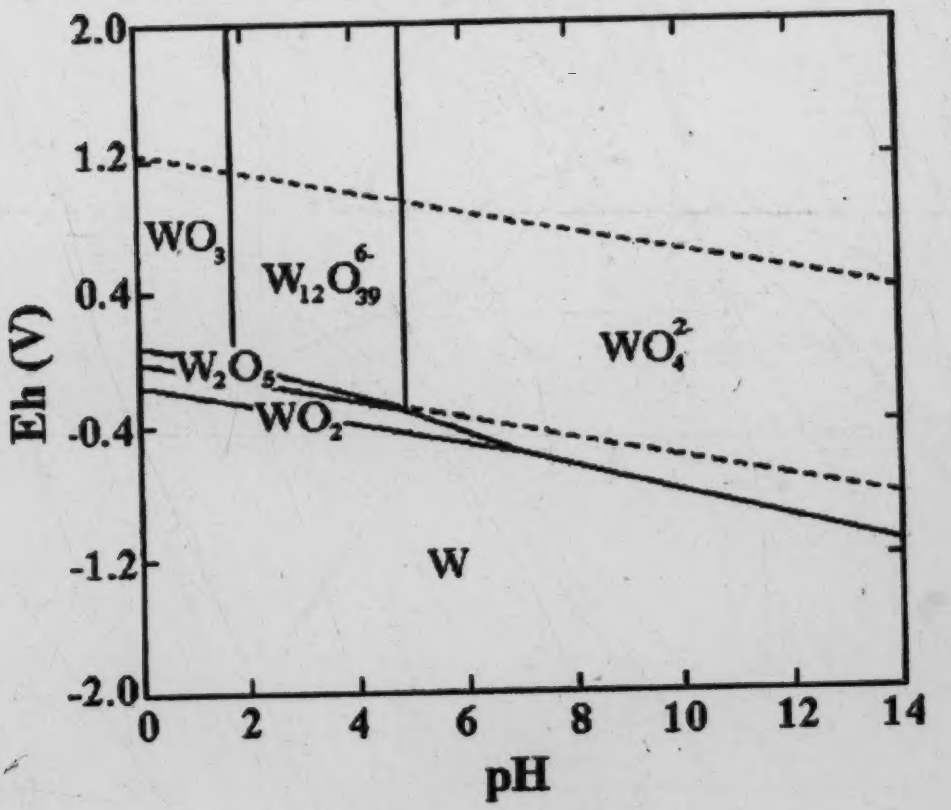


Figure 3-4. Pourbaix diagram of tungsten [98]

## 3.2. Total Wear rate, T

The total wear rate is the wear rate caused by corrosive wear. Using a pin-on-disc tribometer (CSEM, USA), the total wear rate was determined from the weight loss of the tungsten after corrosive wear at open-circuit potential (OCP). For the pin-on-disc test, a polishing pad was used to wear a tungsten sample. The total wear rate was determined by total mass loss of the tungsten sample after corrosive wear under open circuit potential. The experimental set up is shown in Figure 3-5. A polyvinyl chloride (PVC) holder was used to hold a polishing pad of 0.4 x 0.4x 0.1mm , which was used to wear a tungsten sample of 10 x 10 x 5 mm held by a PVC cup which also contained the slurry. For the corrosive wear test, the polishing pad slide on the tungsten sample for 1000 laps at a constant speed of 0.4 cm/s. After each polishing test, the tungsten sample was immediately rinsed in deionized water and dried with argon gas. The sample was then placed in an airtight-vacuumed desiccator and allowed to dry before measuring its weight loss. The total wear rate was calculated using equation (3.7) [95].

$$T = \frac{WL(g) * 24\frac{h}{d} * 365\frac{d}{yr}}{SA(mm^2) * \rho(g/cm^3) * t(h)} \qquad (3.7)$$

where WL is the measured weight loss of the sample, SA is the sample contact area, ρ is the sample density, and t is the test duration.

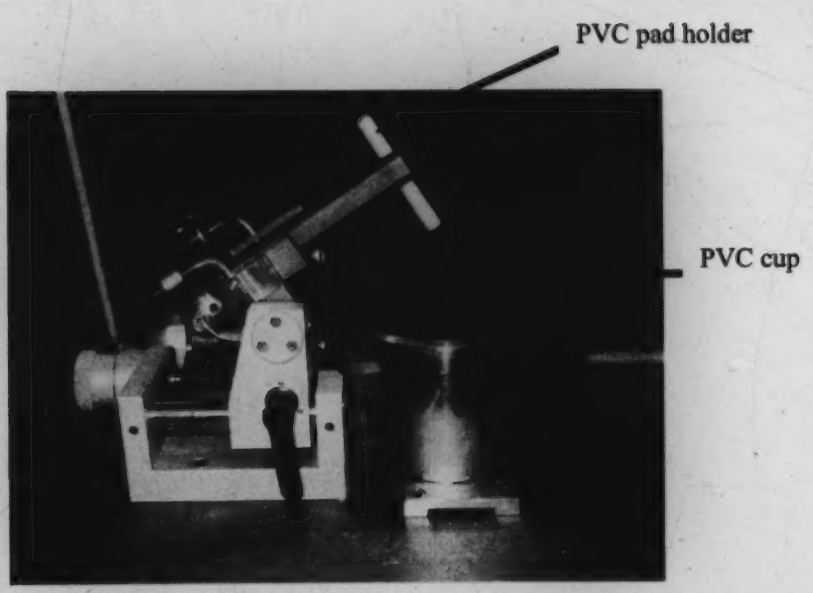


Figure 3-5. Pin-on-disc tribometer used for determining the total wear

The total wear rates of the tungsten samples as a function of slurry pH and applied normal load are present in figure 3-6. Each wear rate was an average of four measurements.

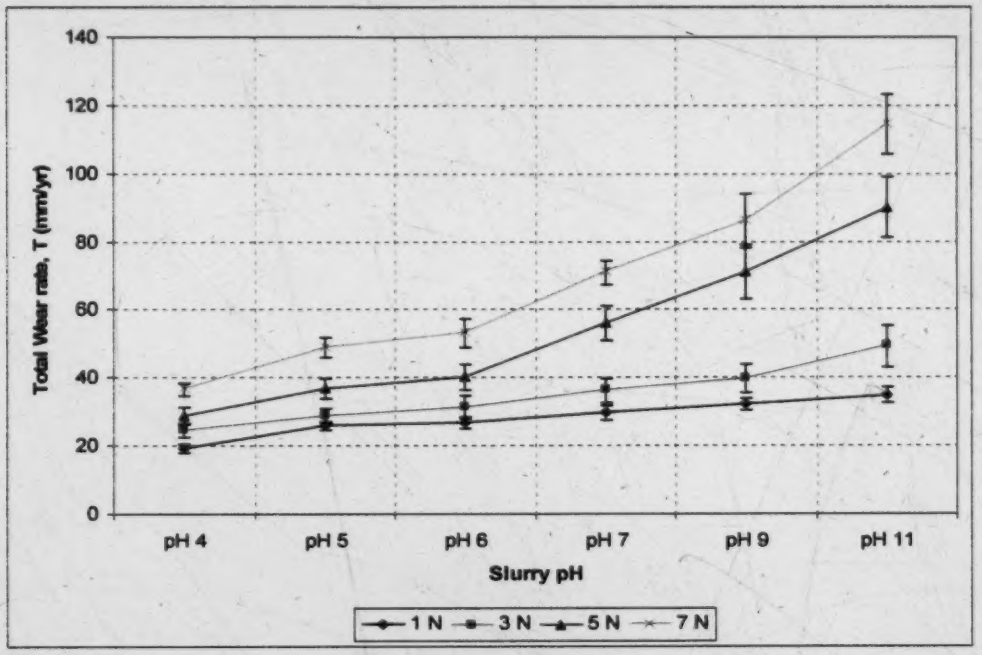


Figure 3-6. Total wear rate, T, of tungsten in the $K_3[Fe(CN)_6]$ slurry under open circuit potential as a function of slurry pH and normal load.

From figure 3-6, the total wear rate was found to increase as either the slurry pH increased or the normal wearing load increased. The higher removal rate at higher slurry pH values could be attributed to enhanced degradation at higher pH values. In addition, the increased fraction of $WO_2$ phase formed at higher slurry pH made the oxide scale softer and less resistant to wear. As a result, the surface oxide was easier to be removed by the abrasives in the slurry and the polishing pad, followed by continuous repassivation-removal cycles of the oxide scale. At low slurry pH (~ pH 4 – 6), the oxide scales were stronger and could offer higher resistance to mechanical wear and corrosion,

thus resulting in lower removal rates. Regarding the effect of wearing load on the total wear rate, higher normal loads could easily remove the surface oxide and thereby increase the removal rate at any pH value.

## 3.3 Pure Wear rate, $W_O$

In order to understand the corrosion-wear synergism during CMP, it is important to evaluate the contribution of pure mechanical wear to the total wear loss. The pure wear rate can be determined experimentally if the corrosive wear is carried out under the condition that the corrosion influence is eliminated or minimized. Cathodic protection is an effective approach to achieve this goal. The basic principle of cathodic protection is the reduction of metal dissolution or oxidation reaction in a corrosive solution by applying a negative potential to suppress the oxidation reaction that occurs on the target surface. The cathodic potential i.e. the applied negative potential, brings the metal closer to an immune state. Cathodic protection has been used in determining the contribution of wear to a corrosive wear process [99-108].

In this study, a constant cathodic potential (potentiostatic condition) of -0.5 $V_{SCE}$ was applied to the working electrode (i.e. the tungsten sample) during the corrosive wear test. Figure 3-7 shows a tribo-electrochemical system used in this study. The set-up consisted of a pin-on-disc tribometer (CSEM) and an electrochemical system (GAMRY). The system permitted wear measurement with *in-situ* monitoring changes in friction and current density during the test. The changes in potential and current density were determined by the GAMRY data acquisition system. The slurry was contained in a non-

conducting cell made of polyvinyl chloride (PVC). A tungsten sample served as the working electrode and a coiled platinum wire served as the counter electrode. A saturated calomel electrode (SCE) was used as the reference electrode. The polishing pad was attached to a PVC holder as described in section 3.2 of this chapter (see figure 3-5). The pure wear rate was determined as a function of slurry pH and normal load. The weight loss of the sample was determined by measuring the weight loss of the sample, which was used to calculate the wear rate using equation (3.8) [95].

$$W_o = \frac{WL(g) * 24\frac{h}{d} * 365\frac{d}{yr}}{SA(mm^2) * \rho(g/mm^3) * t(h)} \tag{3.8}$$

where WL is the measured weight loss of the sample, SA is the sample contact area, ρ is the sample density, and t is the test duration.

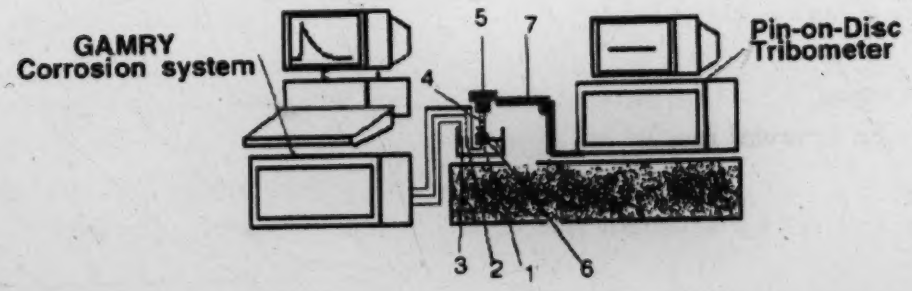


Figure 3-7. Schematic of the tribo-corrosion system: 1. Sample, 2. Counter electrode, 3. Reference electrode, 4. PVC pin holder (with pad attached to the end), 5. Normal load, 6. Polishing pad, 7. Tribometer arm/lever.

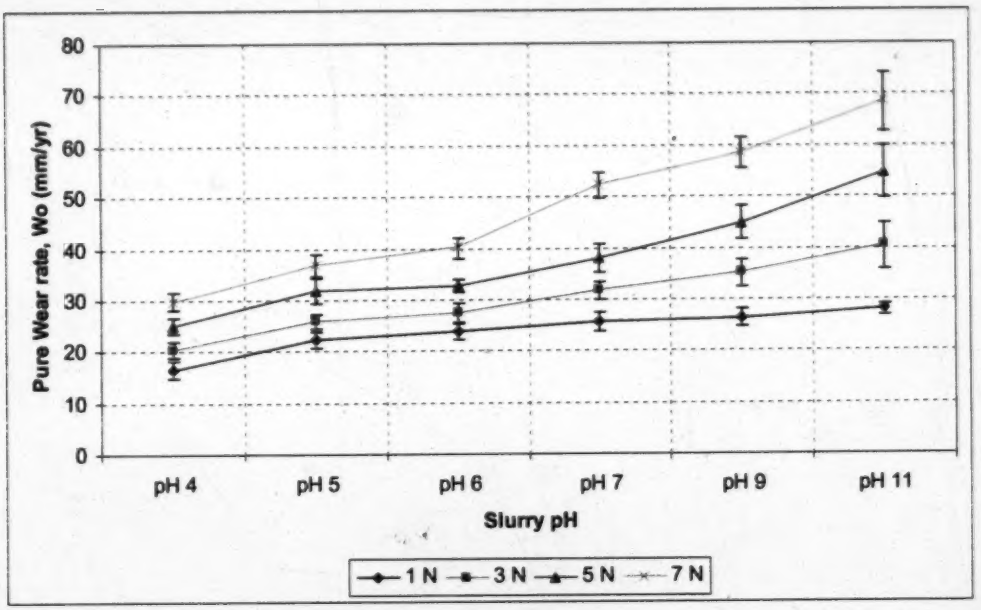


Figure 3-8. Pure wear rate, $W_O$ of bulk tungsten in the $K_3[Fe(CN)_6]$ slurry under a cathodic potential of –0.5 V as a function of slurry pH and normal load.

The pure wear rates as a function of the slurry pH and normal wearing load is presented in figure 3-8. The pure wear rate was an average of five measurements. As shown, the wear rates increased with an increase in slurry pH and normal load. This is similar to the result obtained for total wear rate with wear and corrosion components present. However, the cathodic potential of –0.5 V helped to either reduce or eliminate the corrosion component for the pH and load range used in this study (see Tables I & II of the Appendix). The reduction or elimination of oxidation excludes the formation of oxide that facilitates tungsten removal since the oxides are softer than the tungsten substrate as demonstrated by the nanoindentation tests performed on the oxides (see Figure 2-5). Clearly, the wear rates were reduced compared to those obtained for total

wear rates under OCP. This observation further supports the need of surface oxide to increase the removal rate for effective CMP of tungsten.

## 3.4 Corrosion rate in the presence of wear, $C_W$

The rate of corrosion in the presence of wear was determined using Tafel curves obtained in the presence of wear. The experimental set-up illustrated in Figure 3-7 was used to obtain the Tafel curves. In this study, Tafel curves for different slurry pH values were determined by measuring current density within ± 20 mV of the open circuit corrosion potential in the presence of wear. The corrosion current density obtained from the extrapolation of the Tafel curve was then used to calculate the corrosion rate using equation (3.9) [95]:

$$C_w = \frac{K\left(\frac{mm-g}{\mu A-cm-yr}\right) * i_{corr}(\mu A/cm^2) * EQ}{\rho(g/mm^3)} \qquad (3.9)$$

K= 3.27 X $10^{-3}$ mm g/ μA cm yr

EQ = Equivalent weight (30.64, for Tungsten assuming valence of +6)

ρ= Density (19.3 g/ $cm^3$)

Table 3.2. Corrosion-current Densities ($i_{corr}$) obtained from extrapolation of Tafel curves for the tungsten during wear in the $K_3[Fe(CN)_6]$ slurry at different pH levels and applied normal loads.

| Load (N) / pH | 0 | 1 | 3 | 5 | 7 |
|---|---|---|---|---|---|
| 4 | 2.997 | 32.9 | 49.1 | 57.1 | 60.7 |
| 5 | 6.863 | 45.4 | 55.2 | 59 | 70.7 |
| 6 | 11.42 | 52.7 | 66 | 78.1 | 81.5 |
| 7 | 20.5 | 71.6 | 80.5 | 93 | 100 |
| 9 | 38.79 | 76.42 | 84 | 95 | 105.2 |
| 11 | 47.48 | 81.9 | 88.8 | 101 | 120 |

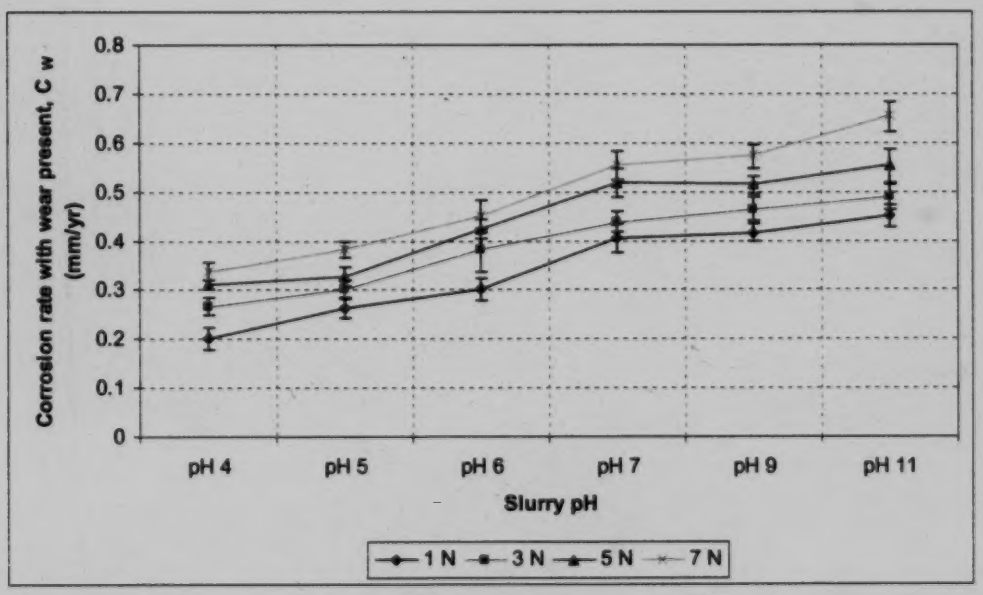


Figure 3-9. Corrosion rates of tungsten in the presence of wear in the $K_3[Fe(CN)_6]$ slurry as a function of pH and applied normal load.

The corrosion rates with wear present are presented in figure 3-9. As shown, the corrosion rates with wear present are always greater than corrosion rates without wear for all slurry pH values and normal wearing loads. By comparing data presented in Tables 3.1 and 3.2, it may be seen that the corrosion current density increased dramatically at low slurry pH even at a very low load of 1 N. For instance, for pH 4 at 1 N, the current density increased from 2.997 (Table 3.1) to 32.9 $\mu A/cm^2$ (Table 3.2). This increase by 10 times in current density can be attributed to the removal of a protective surface oxide scale and introduction of defect in the surface layer caused by wear. However, at high slurry pH, the increase in current density was relatively small. For instance, for pH 11 at 1N, the current density increased from 47.48 (Table 3.1) to 81.9 $\mu A/cm^2$ (Table 3.2). This increase in $i_{corr}$ by less than two times indicates that the oxide scales formed in higher pH levels was less protective and could not lead to an increase in $i_{corr}$ as large as that in the case of lower pH values (see Table 2-4). From Fig. 3-9, one may also see that increasing the normal wearing load led to an increase in dissolution and that the least corrosion rate was observed at pH 4 and the largest at pH 11 for all applied loads.

## 3.5 Calculation of Wear-Corrosion Synergism

The parameters obtained in the preceding sections (sections 3.1 – 3.4) can be used to calculate several other parameters that help to better understand the wear-corrosion synergism. Parameters to be calculated include

$W_C$ – wear rate in the presence of corrosion, to be calculated from $W_C = T - C_W$

$S'$ – increase in mechanical wear losses due to corrosion, calculated from $S' = W_C - W_O$

$S''$ – increase in corrosion losses due to wear, calculated from $S'' = C_W - C_O$

S – loss resulting from the interaction of wear and corrosion, calculated from $S = S' + S''$

Corrosion augmentation factor: $C_W/C_O$

Wear augmentation factor: $W_C/W_O$

### 3.5.1 Wear rate in the presence of corrosion, $W_C$

The wear rate in the presence of corrosion, $W_C$ can be determined from equation (3.10):

$$W_C = T - C_W \tag{3.10}$$

where T is the total wear rate caused by corrosive wear and $C_W$ is the corrosion rate in the presence of wear.

Figure 3-10 presents the calculated $W_C$ as a function of slurry pH and applied load.

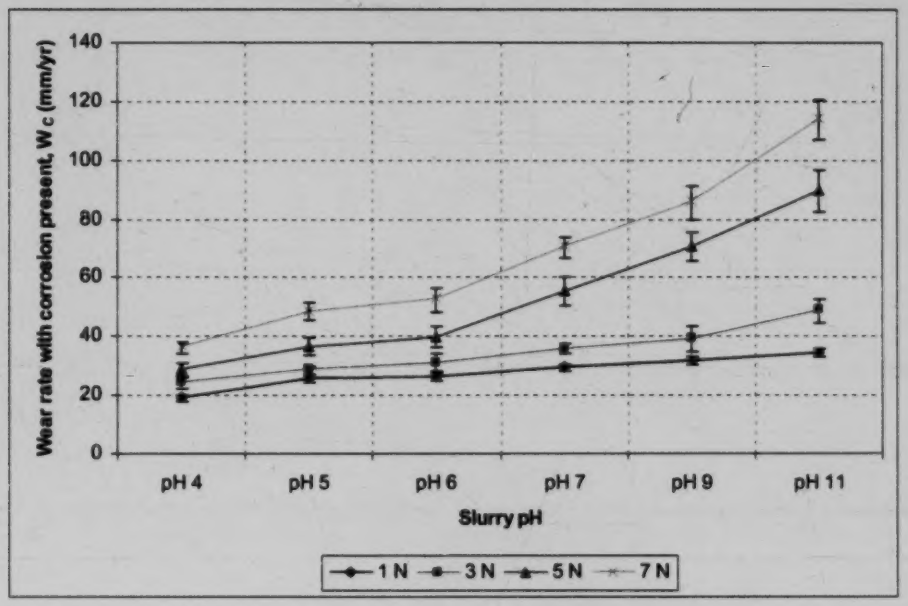


Figure 3-10. The wear rate of the tungsten in the presence of corrosion in the $K_3[Fe(CN)_6]$ slurry as a function of pH and applied normal load.

As shown, $W_C$ increased with an increase in the slurry pH. The high wear rate at higher slurry pH values could be attributed to easier removal of less protective oxide scales formed in the slurries having higher pH values. The passivation – film removal – repassivation process led to higher removal rates at higher pH levels.

### 3.5.2 Increase in wear rate caused by corrosion, S'

The increase in wear loss due to corrosion, S' can be determined using equation (3.11):

$$S' = W_C - W_O \qquad (3.11)$$

where $W_C$ is the wear rate in the presence of corrosion and $W_O$ is the wear rate in the absence of corrosion,i.e. the pure wear rate. Figure 3-11 illustrates the increase in wear rate caused by corrosion.

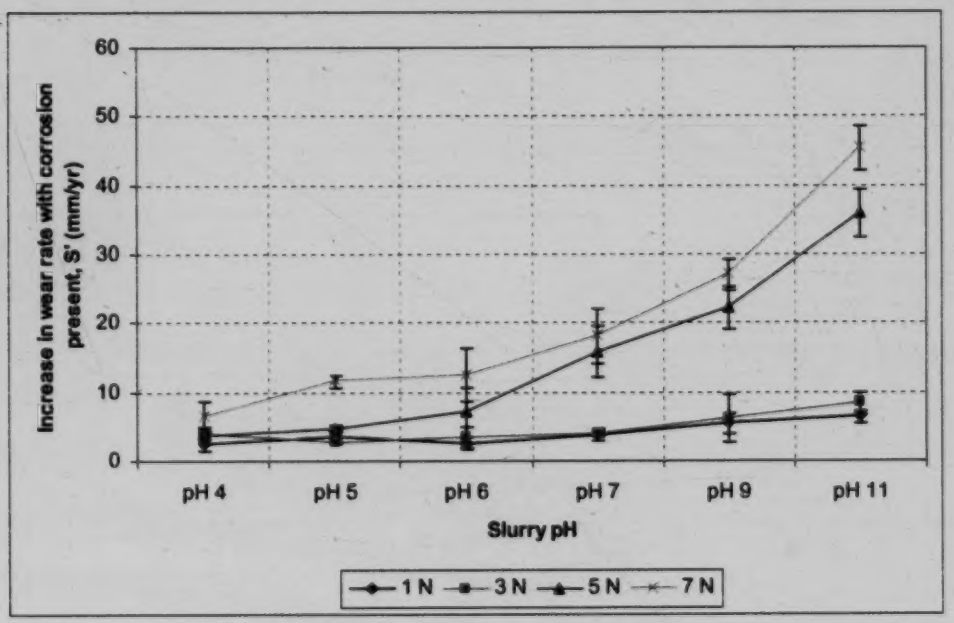


Figure 3-11. The increase in wear rate of tungsten due to corrosion in the $K_3[Fe(CN)_6]$ slurry as a function of pH and applied normal load.

It can be seen that increased corrosion led to extra wear. The extra wear was larger at higher pH levels. As shown, the rate of the extra wear loss was 47 mm/yr at pH

11, while it was ~6 mm/yr at pH 4 under a load of 7 N. By comparing with Fig. 3-8, one may see that the extra wear was quite substantial, indicating that corrosion plays an important role in removing tungsten during the CMP process. Under higher wearing loads, S' was larger because the larger loads helped to abrade off oxidation product from the tungsten surface more effectively and left larger fresh surface exposed to continuous attack.

### 3.5.3 Increase in corrosion rate caused by wear, S"

The increase in corrosion loss caused by wear, S" can be determined using equation (3.12):

$$S'' = C_W - C_O \qquad (3.12)$$

where $C_W$ is the corrosion rate in the presence of wear and $C_O$ is the corrosion rate in the absence of wear.

The rate of extra corrosion loss in the presence of wear is shown in figure 3-12. As shown, S" increased as the pH increased from 4 to 5; this is attributed to the less protective oxide scale at the higher pH level. However, as the slurry pH further increased, S" decreased. This could be explained as follows: at higher pH levels, the surface oxide films became relatively soft, porous and, therefore, non-protective, so that the removal of the non-protective surface film by wear would not necessarily lead to a considerable increase in the corrosion rate.

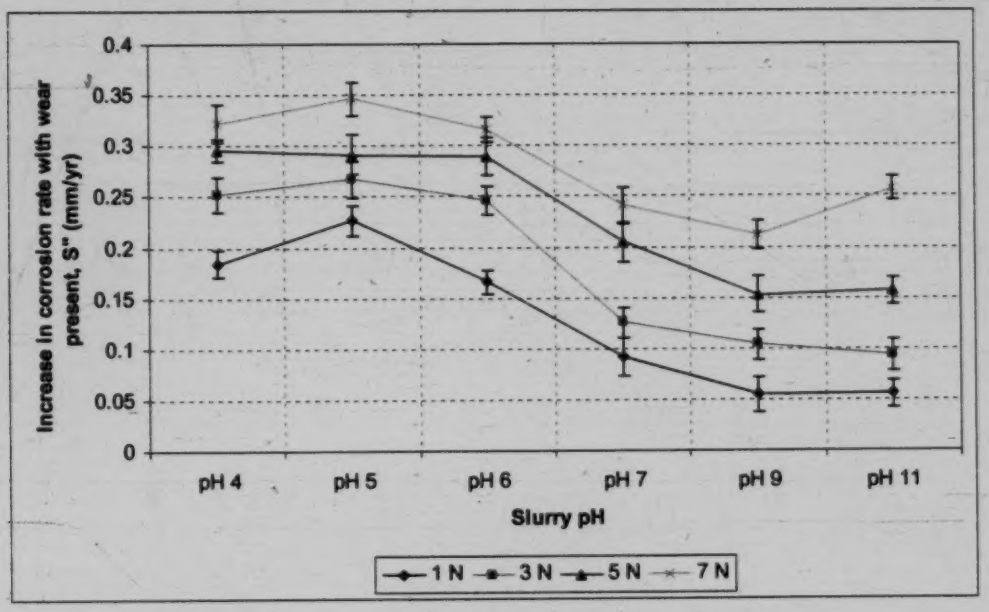


Figure 3-12. The increase in corrosion rate of tungsten due to wear in the $K_3[Fe(CN)_6]$ slurry as a function of pH and applied normal load.

### 3.5.4 The material loss caused by wear-corrosion synergy, S

The material loss resulting from wear-corrosion synergy, S can be determined using equation (3.13):

$$S = S' + S'' \tag{3.13}$$

For the present study, this loss was determined and is presented in figure 3-13. As shown, the contribution of the wear-corrosion synergy increased with increase in either the slurry pH or the applied wearing load. The observations are understandable. Since

higher slurry pH corresponded to more corrosion and higher wearing loads resulted in larger tungsten loss, the synergism of wear and corrosion was enhanced when either the pH level or the wearing load was increased. Higher wearing loads could easily remove any corrosion product form the surface and expose the bare metal for re-oxidation. High slurry pH would result in higher oxidation or dissolution rate.

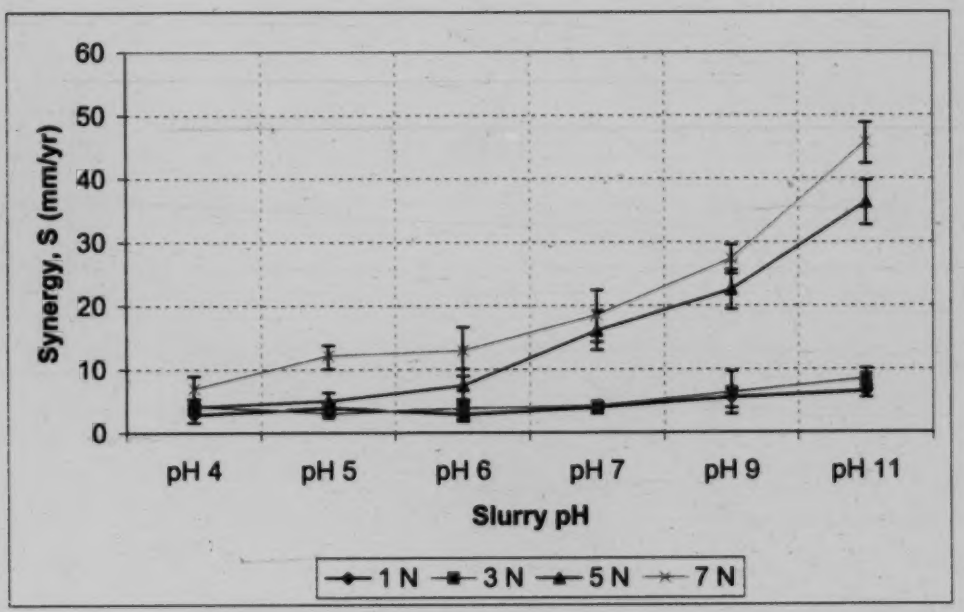


Figure 3-13. Material loss that resulting from the wear-corrosion synergy during corrosive wear of the tungsten in the $K_3[Fe(CN)_6]$ slurry as a function of pH and applied normal load.

### 3.5.5 Corrosion augmentation factor, $C_W/C_O$

The corrosion augmentation factor is the ratio of corrosion rate in the presence of wear to the pure corrosion rate. This factor was determined for the present case and is presented in figure 3-14 as a function of slurry pH and applied load. As shown, the augmentation factor decreased with an increase in slurry pH. This decrease is due to the fact that surface oxides formed at higher pH levels were less protective to corrosion so that the extra corrosion caused by wear at higher pH levels would be small, compared to those observed at lower pH levels, thus leading to a decrease in $C_W/C_O$. Or in other words, as pH increases, the surface oxides could offer little protection from corrosion, so that removal of the surface oxides may not necessarily lead to an increase in corrosion.

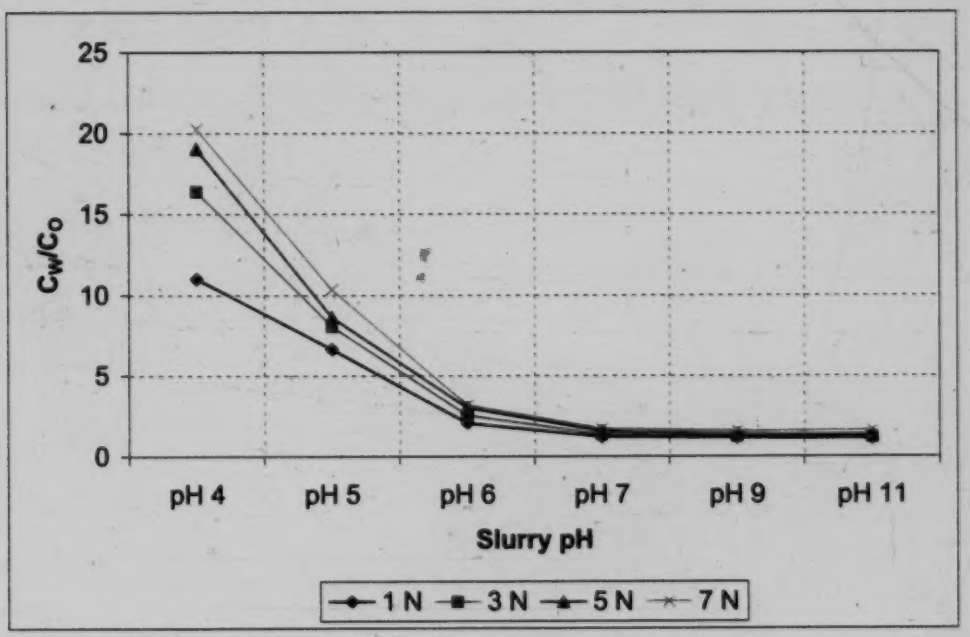


Figure 3-14. Changes in $C_W/C_O$ against slurry pH and applied load.

### 3.5.6 Wear augmentation factor, $W_C/W_O$

The wear augmentation factor is the ratio of wear rate in the presence of corrosion to the pure wear rate. In this study, the wear augmentation factor was determined and is presented in figure 3-15 as a function of slurry pH and wearing load. It was observed that the wear augmentation increased under higher loads (5 N, 7 N) as the pH increased, which was expected. As expected, an increase in the load would lead to an increase in the wear rate. As the pH value increased, the resultant weaker surface oxides were easier to be destroyed and thus an increase in $W_C/W_O$ can be anticipated. However, the $W_C/W_O$ ratio was relatively stable with pH when the load was small as shown in Fig. 3-15

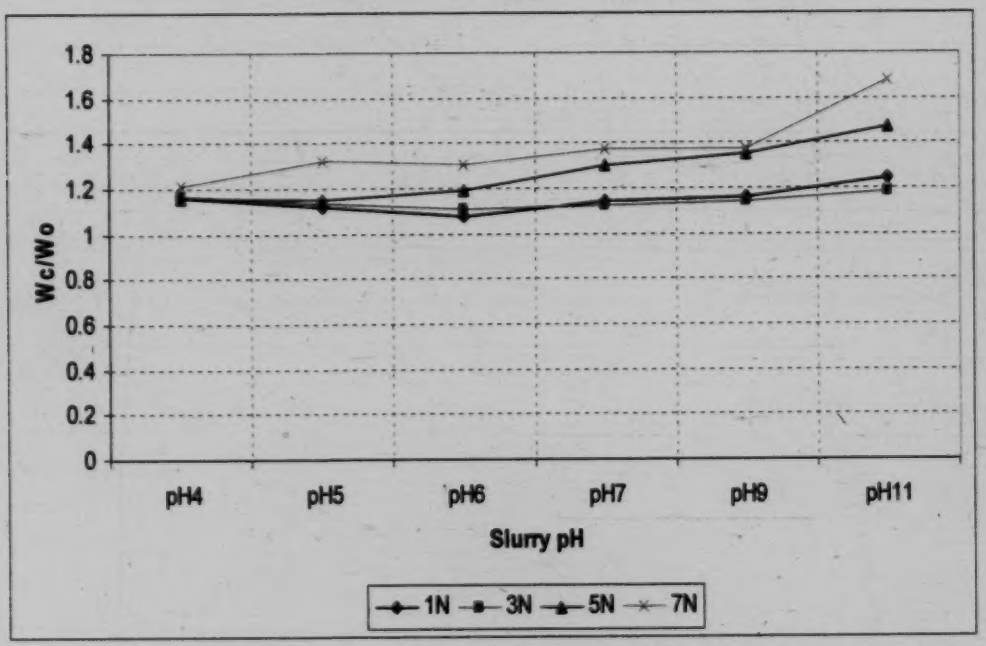


Figure 3-15. The wear augmentation factor as a function of slurry pH and applied load

## 4.0 The surface morphology of tungsten after CMP under different conditions.

In this chapter, surface morphologies of tungsten after polishing at OCP (see section 3.2) are presented. The objective is to study the finished surface quality with respect to the slurry pH values and normal wearing load. Effects of applied electrochemical potential on the removal rate and resultant surface finish were also investigated under a constant passive potential of +1.0 $V_{SCE}$.

## 4.1 Surface morphology of polished surface under OCP

An efficient CMP must be able to generate high quality surface at low cost. In order to achieve this, there is therefore a need to correlate process outputs such as removal rate and surface defects to the ultimate planarized surface. In the previous two chapters, various effects of the CMP process parameters on the material removal have been investigated. This chapter is focused on the morphology of finished surfaces in order to know how the process parameters affect the quality of planarized surface.

In chapter three, it has been demonstrated that the total wear rate increases with increasing slurry pH and applied normal load. However, a high removal rate may not necessarily produce a smooth or globally planarized surface. Figures 4-1, 4-2, 4-3 and 4-4 present SEM micrographs of surface morphologies for different slurry pH values under applied loads of 1 N, 3 N, 5 N, and 7 N, respectively.

6 micrometers
pH 4
PH4 1N OCP(SE)

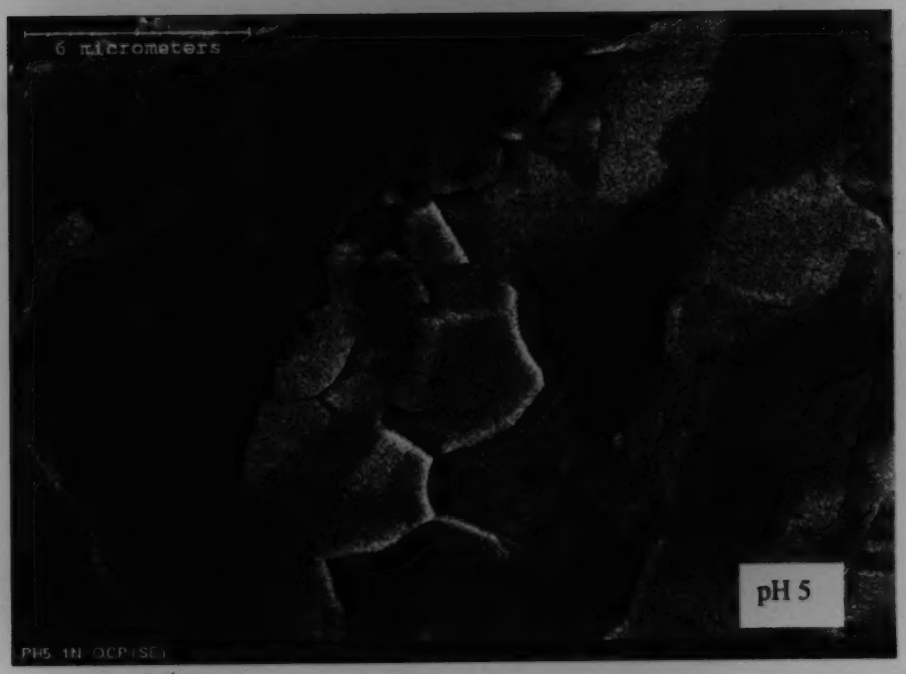
6 micrometers
pH 5
PH5 1N OCP(SE)

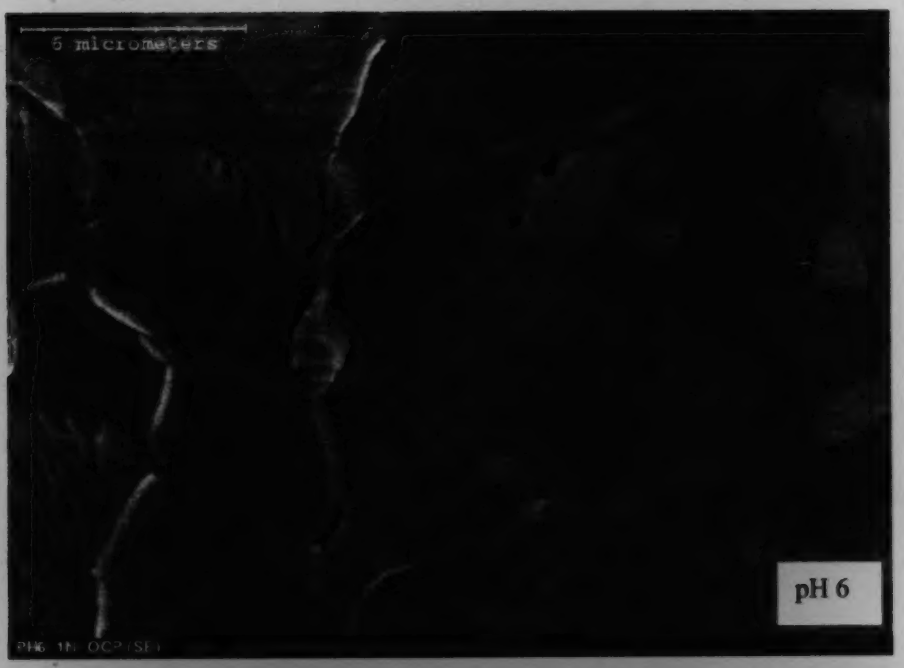
6 micrometers
pH 6

6 micrometers
pH 7

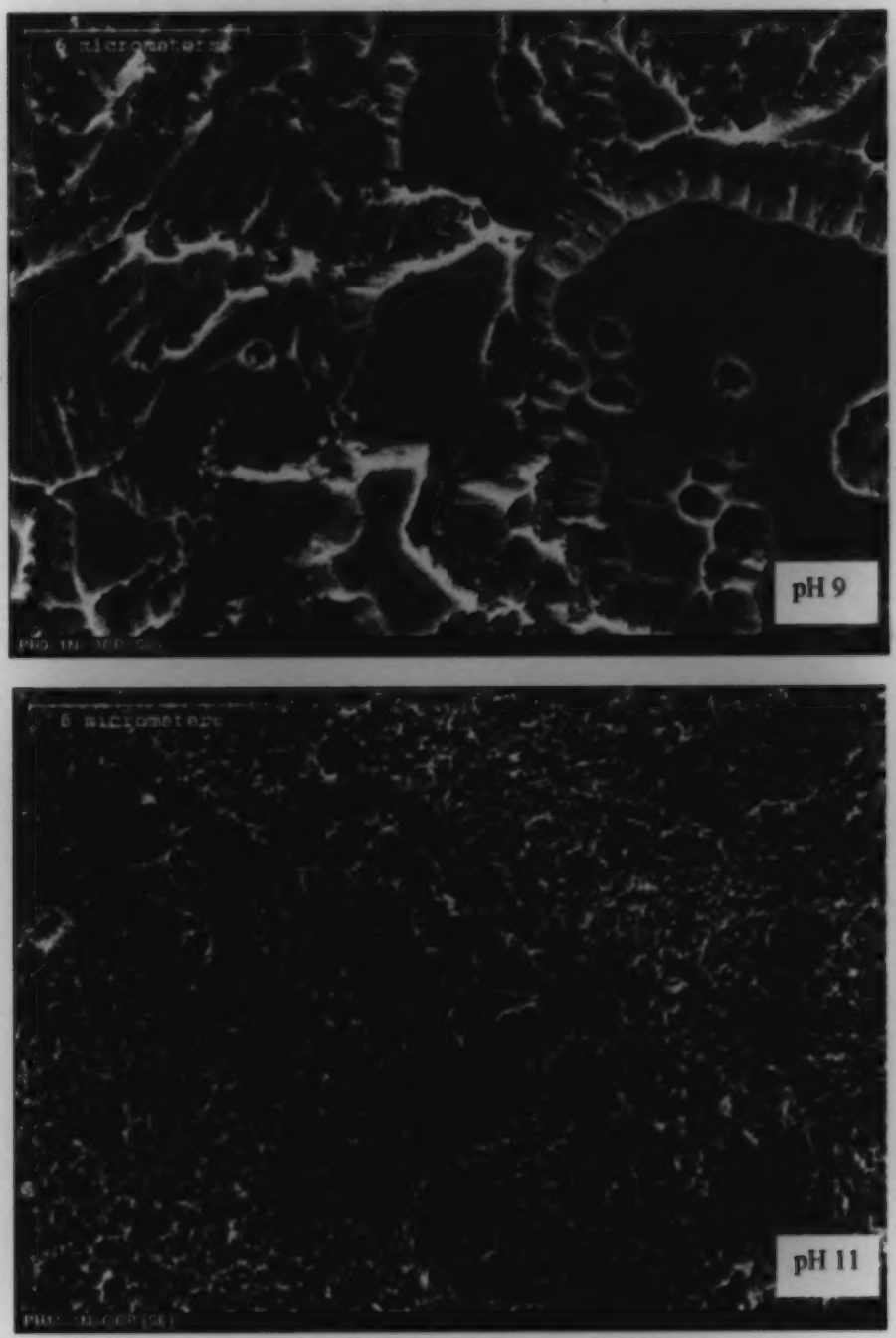


Figure 4-1. SEM micrographs of surface morphology after corrosive wear under OCP at different slurry pH levels under a normal load of 1 N.

6 micrometers
pH 4

6 micrometers
pH 5

6 micrometers
pH 6

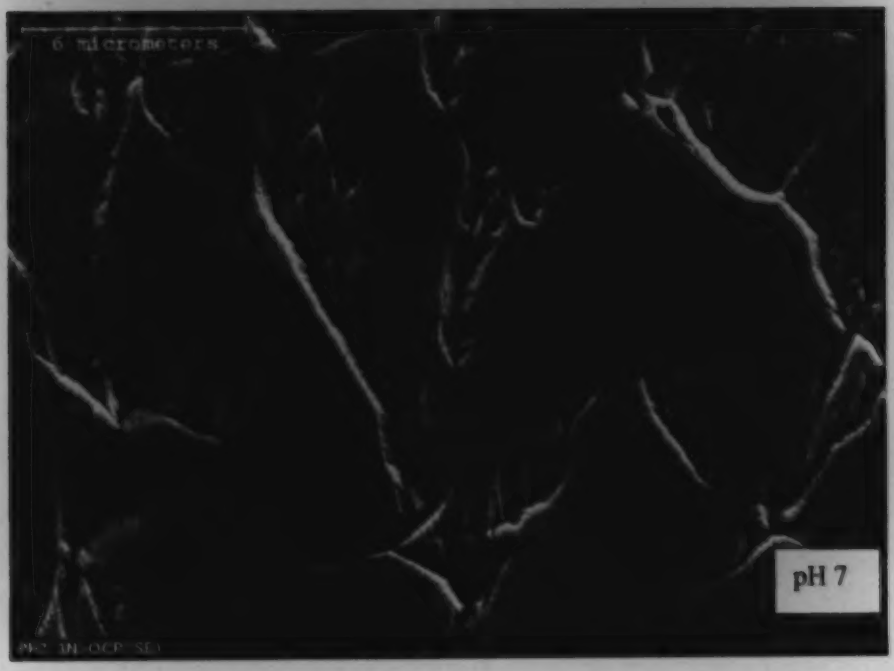
6 micrometers
pH 7

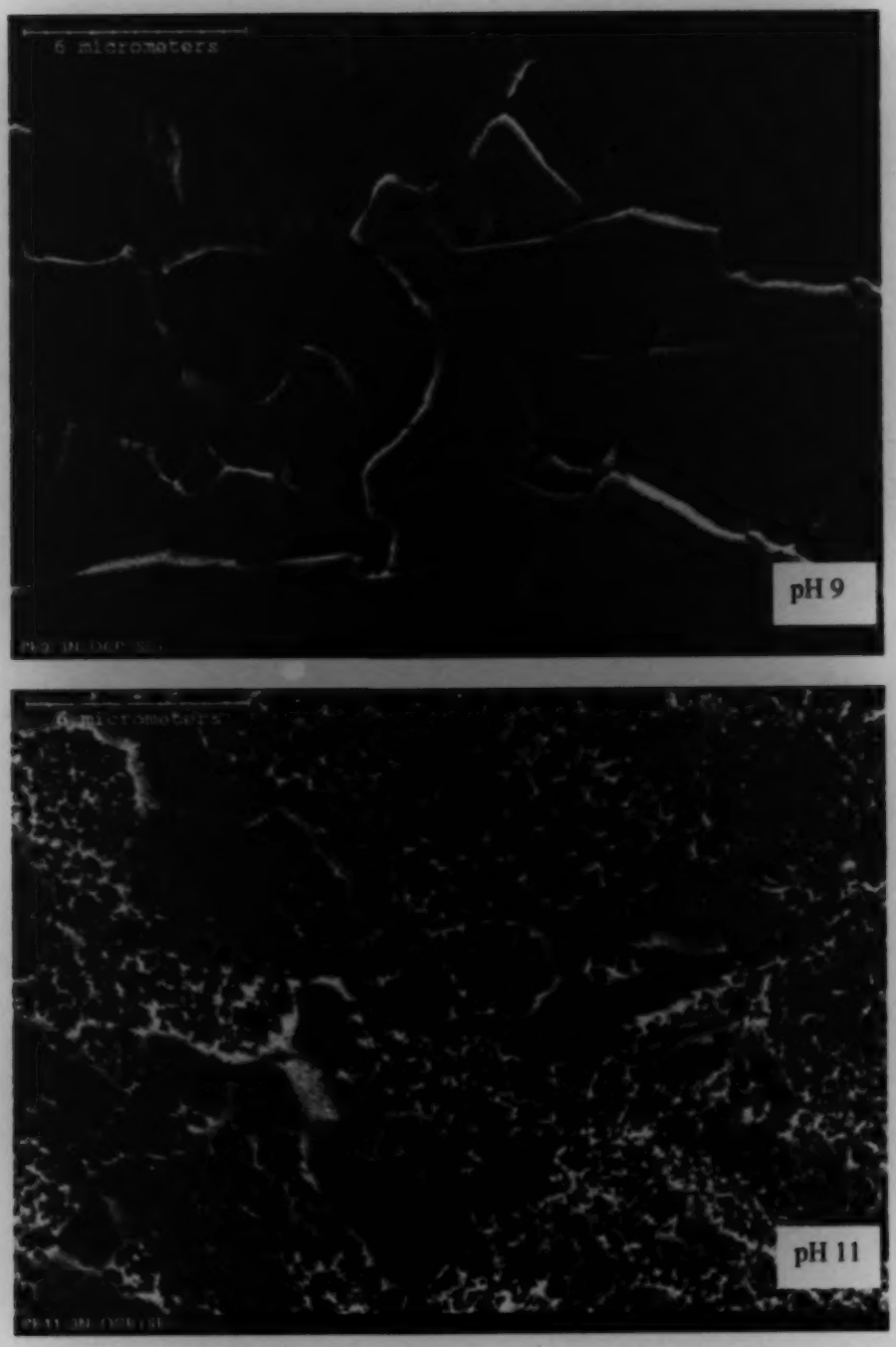


Figure 4-2. SEM micrographs of surface morphology after corrosive wear under OCP at different slurry pH levels under a normal load of 3 N.

6 micrometers
pH 4

6 micrometers
pH 5

6 micrometers
pH 6

6 micrometers
pH 7

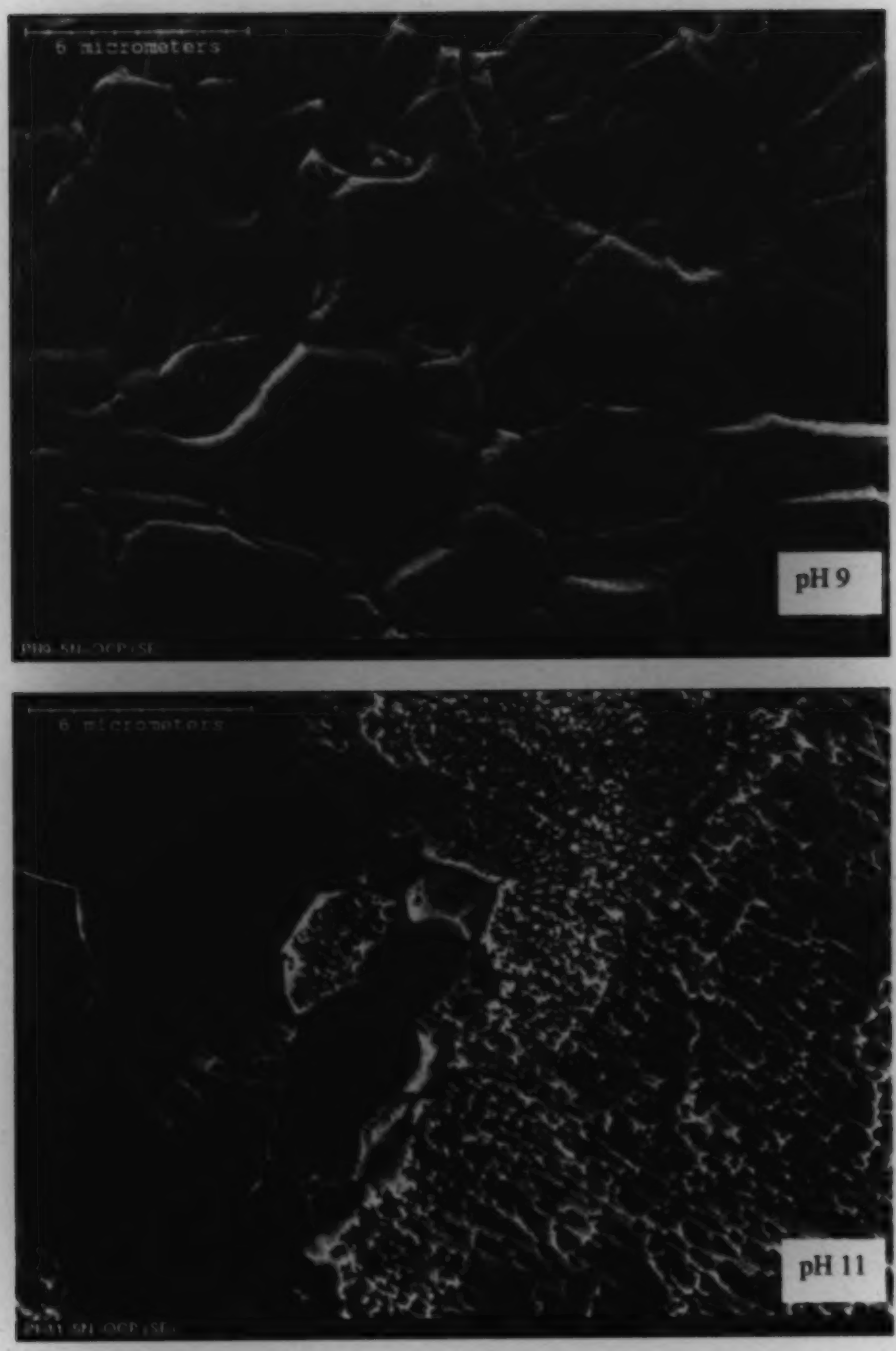


Figure 4-3. SEM micrographs of surface morphology after corrosive wear under OCP at different slurry pH levels under a normal load of 5 N.

6 micrometers
pH 4

6 micrometers
pH 5

6 micrometers
pH 6

6 micrometers
pH 7

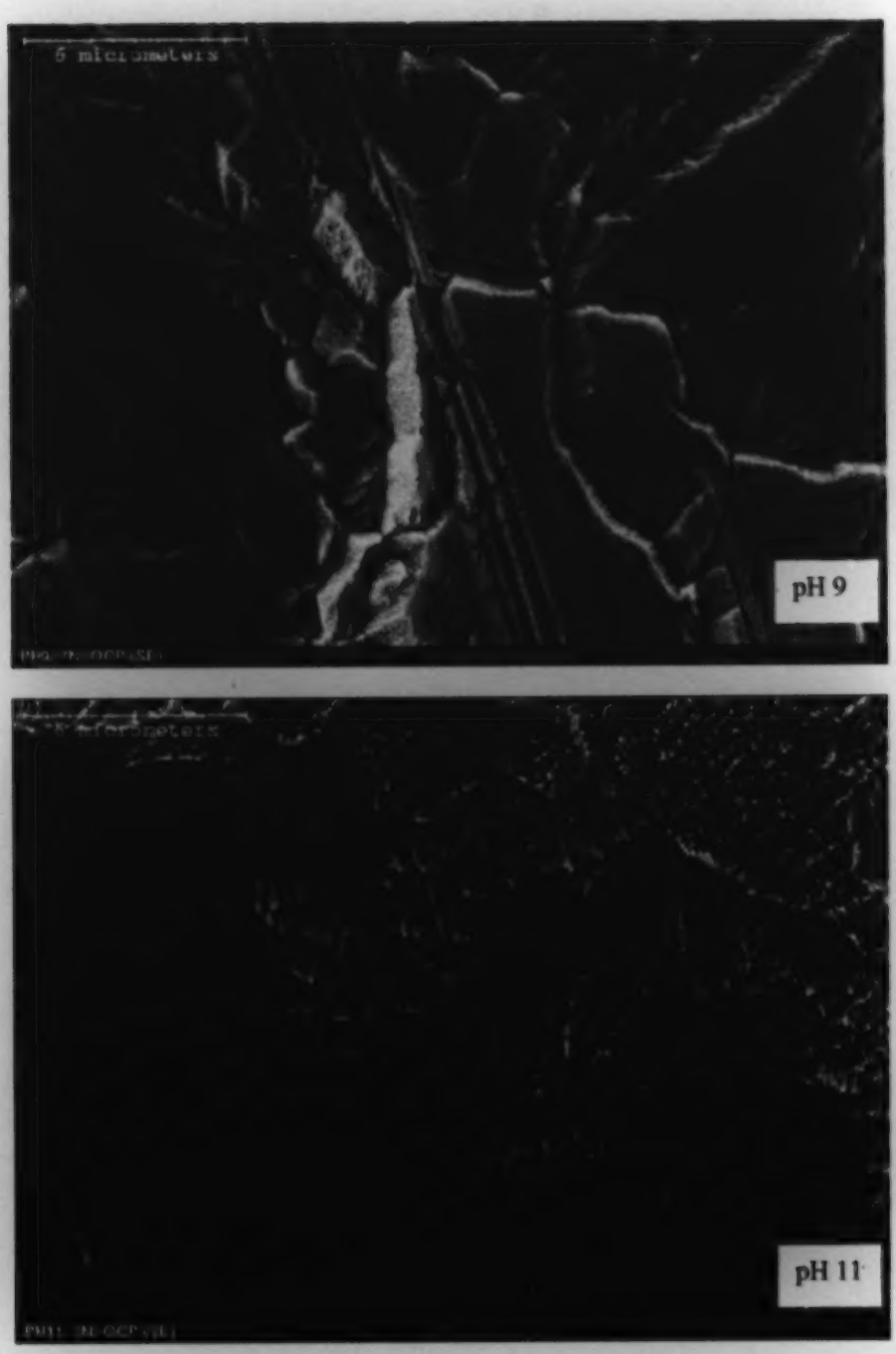


Figure 4-4. SEM micrographs of surface morphology after corrosive wear under OCP at different slurry pH levels under a normal load of 7 N.

Clearly, the observed surface morphologies obtained in low slurry pH as shown in Fig. 4-1 – 4-4 appear to be better than those observed for high slurry pH levels. Therefore, high removal rates at high slurry pH levels, which resulted from the combined action of wear and corrosion (high active dissolution), were not accompanied with desired surface morphologies. Figure 4.5 shows the AFM images of tungsten surface after polishing under a load of 7 N at different slurry pH.

pH 4

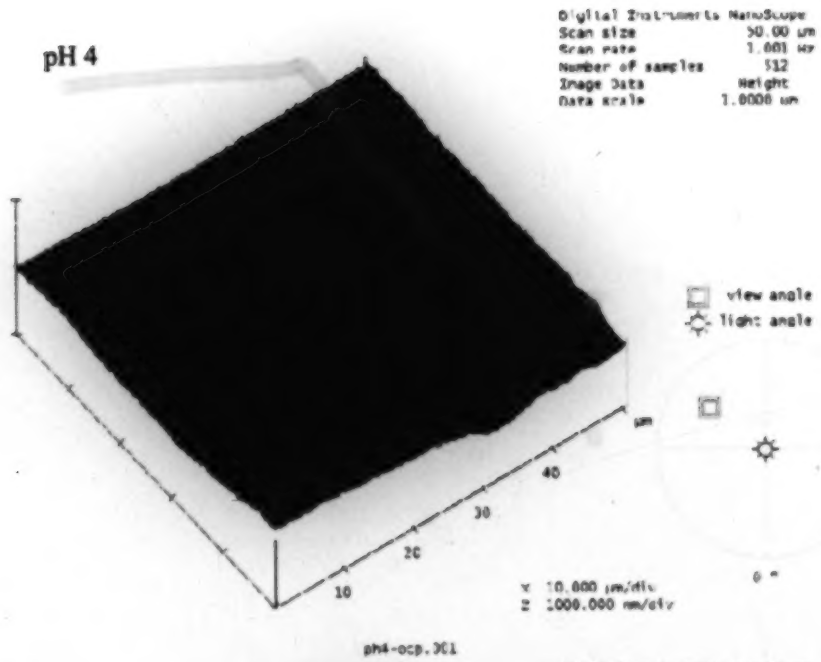
Digital Instruments NanoScope
Scan size 50.00 µm
Scan rate 1.001 Hz
Number of samples 512
Image Data Height
Data scale 1.0000 µm
view angle
light angle
µm
40
30
20
10
0 °
X 10.000 µm/div
Z 1000.000 nm/div
ph4-ocp.001

pH 5

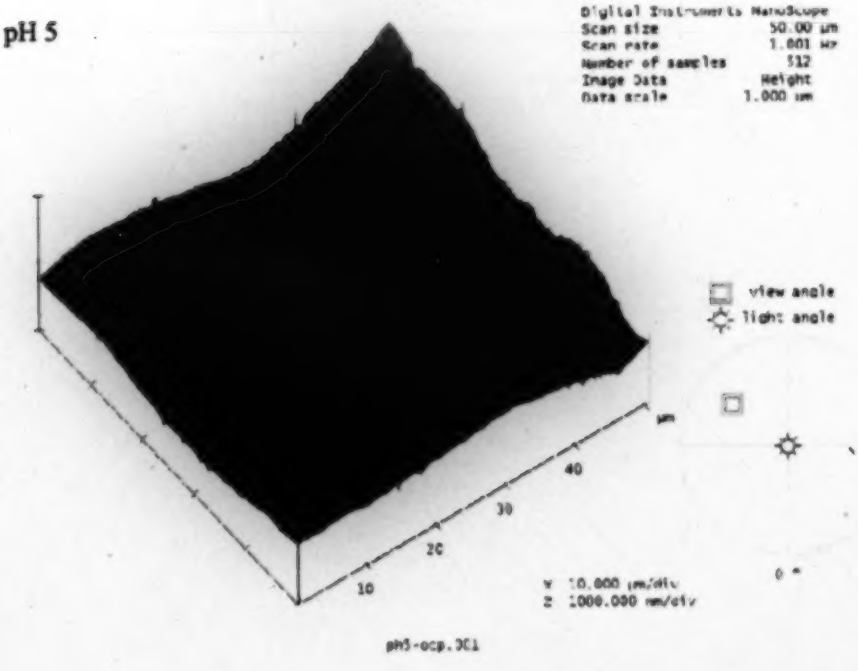
Digital Instruments NanoScope
Scan size 50.00 µm
Scan rate 1.001 Hz
Number of samples 512
Image Data Height
Data scale 1.000 µm
view angle
light angle
µm
40
30
20
10
0 °
X 10.000 µm/div
Z 1000.000 nm/div
ph5-ocp.001

pH 6

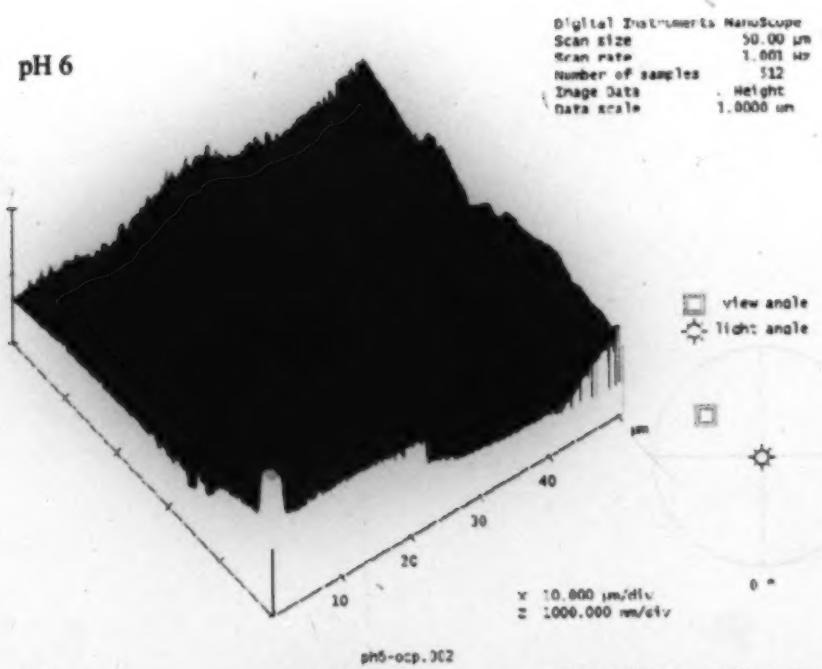


ph6-ocp.002

pH 7

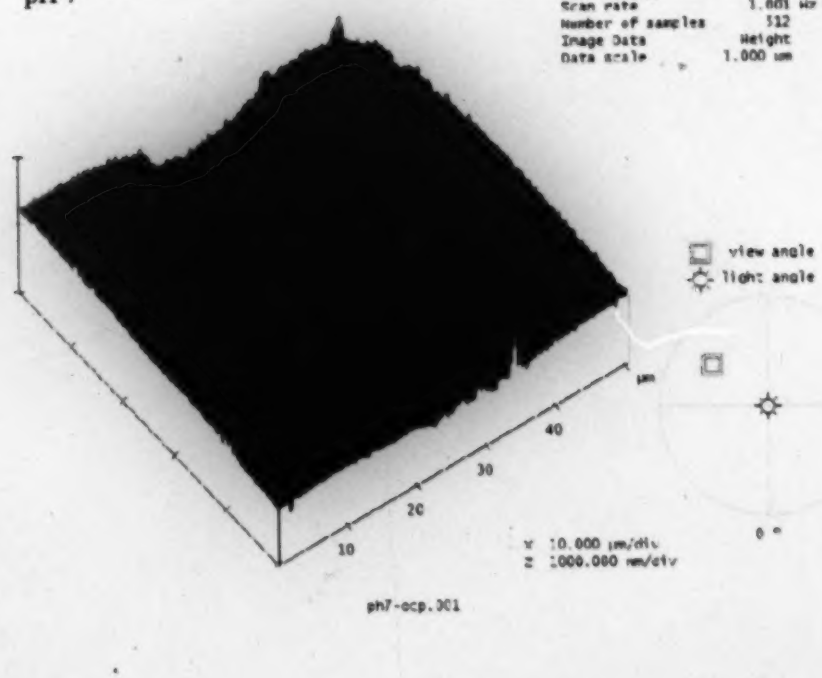


ph7-ocp.001

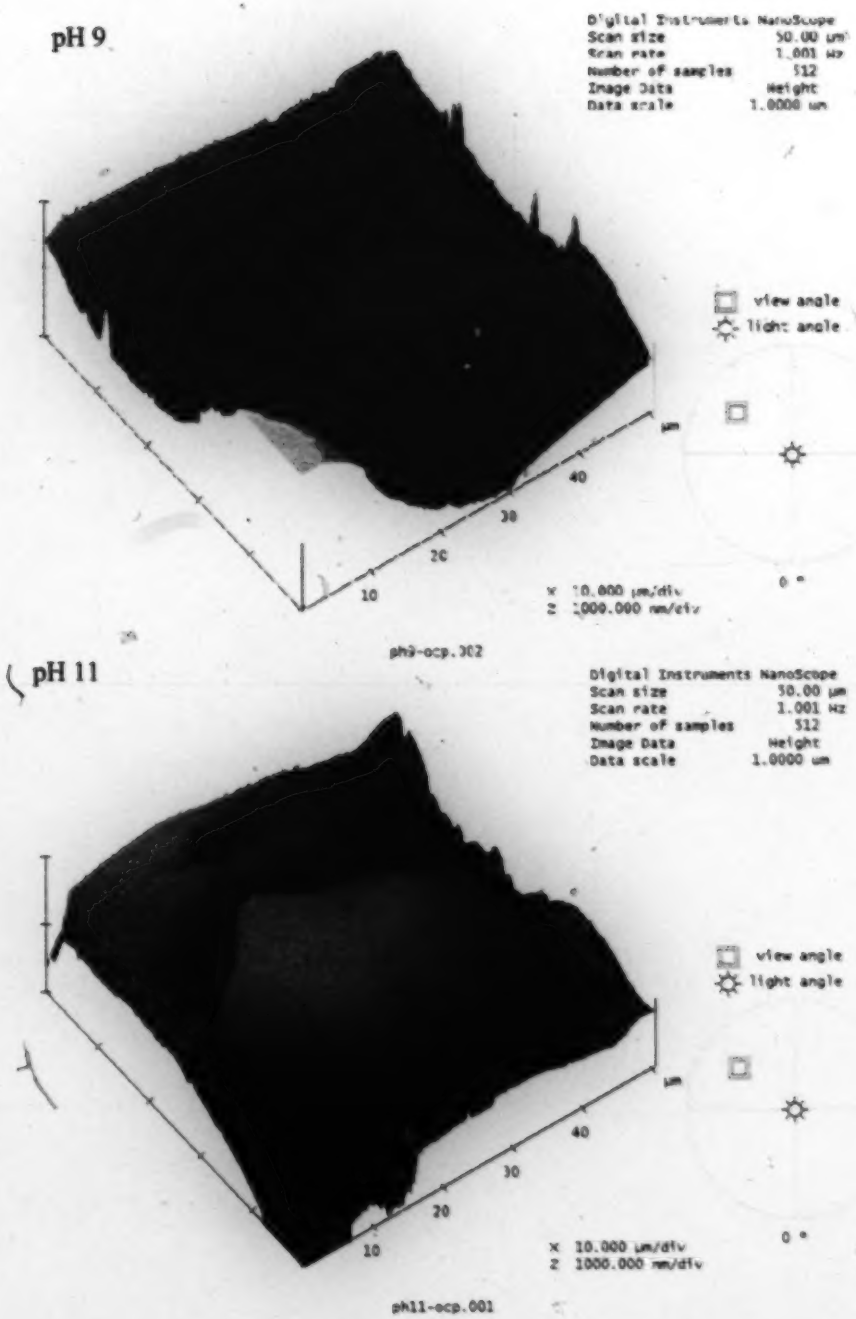


Figure 4-5. AFM images of surface morphology after corrosive wear under OCP at different slurry pH levels under a normal load of 7 N.

## 4.2 Electrochemical Polishing Under an Applied Potential

Electrochemical polishing under an applied potential was carried out in order to determine the effect of electrochemical potential on the removal rate as well as the morphology of the polished tungsten surface. The experimental set-up used in this study was the same as that described in section 3.3 (see Figure 3-7). Because the corrosion potential shifted to less noble potentials with an increase in pH, as shown in figure 2-3, a high potential value was needed to obtain the constant potential-pH dependence of the anodic current in a wide pH range. In this case, a constant potential (potentiostatic) of +1 V was applied prior to and during the polishing process. The tungsten was passivated for 30 minutes prior to the polishing process. The wear rate was determined from the weight loss using equation (3.7).

In addition, the material losses under a potential of +1V for all pH values were larger than those obtained under OCP (see Tables I & III of the Appendix). This result is understandable, since the applied anodic potential controlled the oxidation process. As a result, the removal rate of tungsten could thus be increased as shown in figure 4-6.

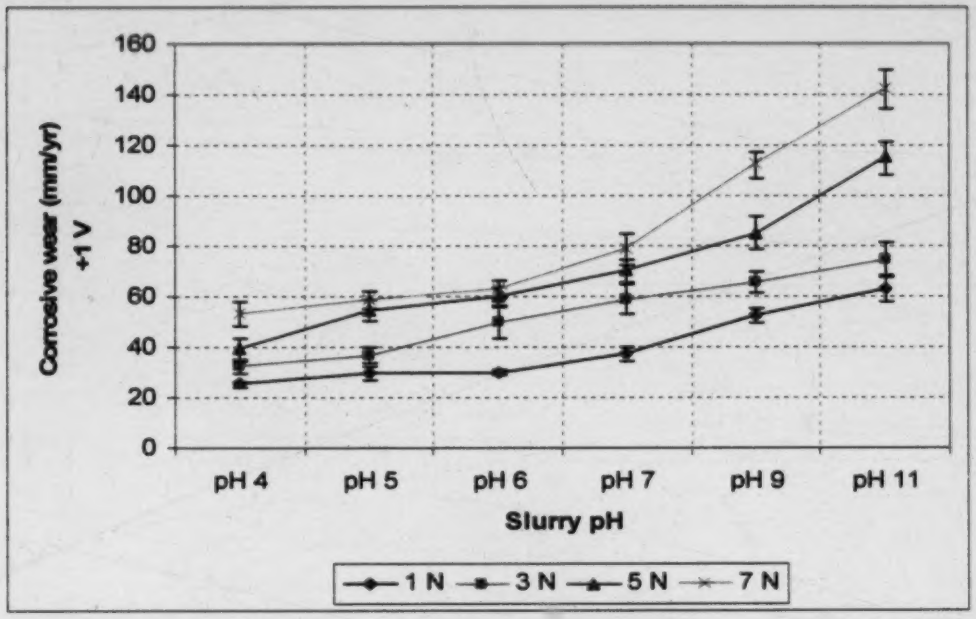


Figure 4 –6. The total wear rate of tungsten under electrochemical potential of +1 V in the $K_3[Fe(CN)_6]$ slurry as function of slurry pH and normal load.

Application of the anodic potential also improved the worn surface quality with smaller roughness as Fig. 4-7 and 4-8 illustrate. Such improvement could be attributed to the accelerated formation of oxide scale with little or no $WO_2$ phase under the applied potential, which may reduce the direct attack on the tungsten substrate. In addition, the stronger interfacial bond of the films formed under anodic potential may also decrease the probability of direct abrasion on the tungsten substrate [109]. As a result, the relatively smoother worn surface could be obtained. In summary, the application of anodic potential appears to be an approach to make the CMP of tungsten more effective in terms of higher removal rate and small surface roughness.

6 micrometers
pH 4

6 micrometers
pH 5

6 micrometers
pH 6

6 micrometers
pH 7

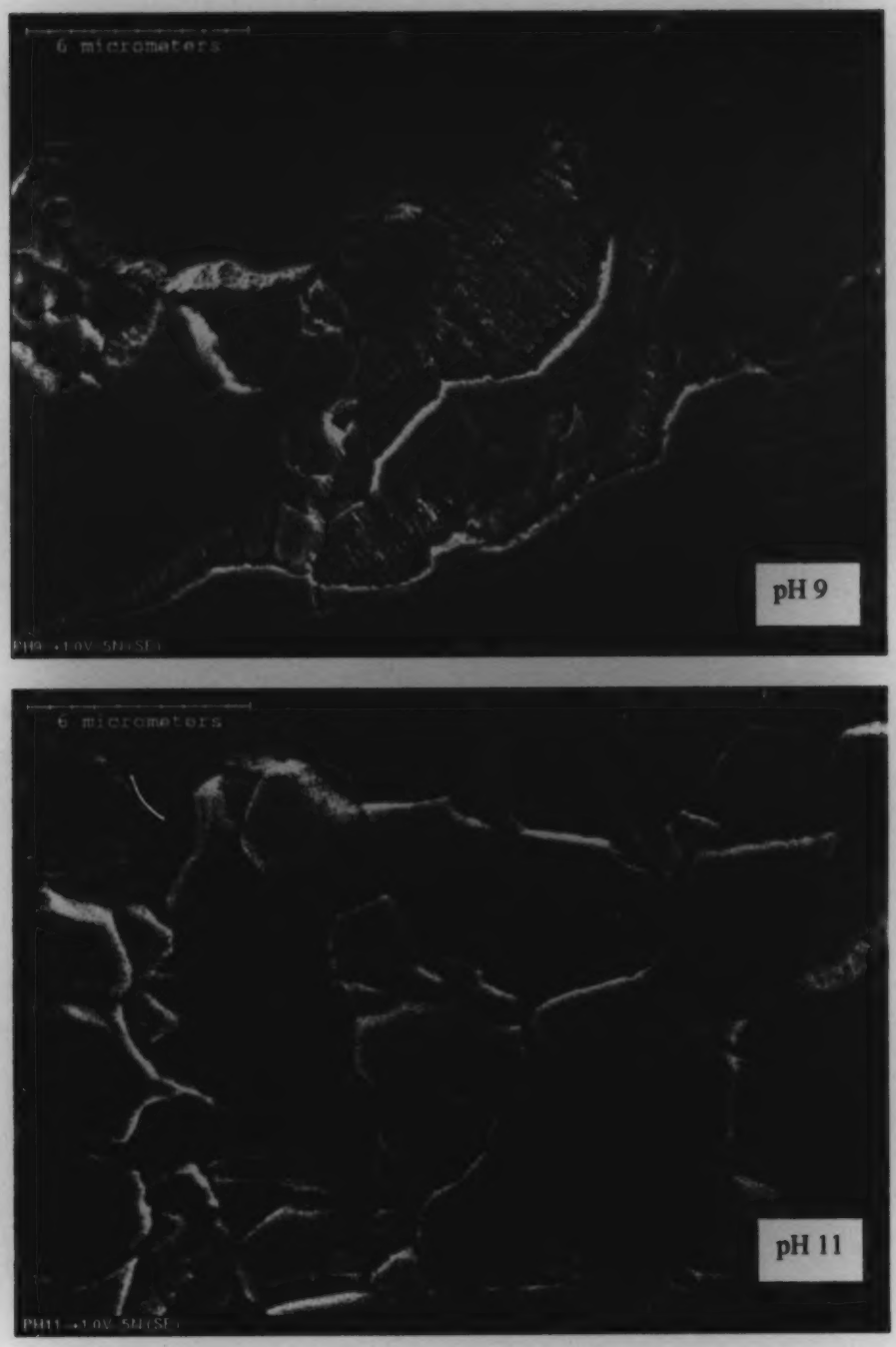


Figure 4-7. SEM micrographs of surfaces after corrosive polishing at different slurry pH levels under a potential of +1 V and a normal wearing load of 5 N.

6 micrometers
pH 4

6 micrometers
pH 5

6 micrometers
pH 6

6 micrometers
pH 7

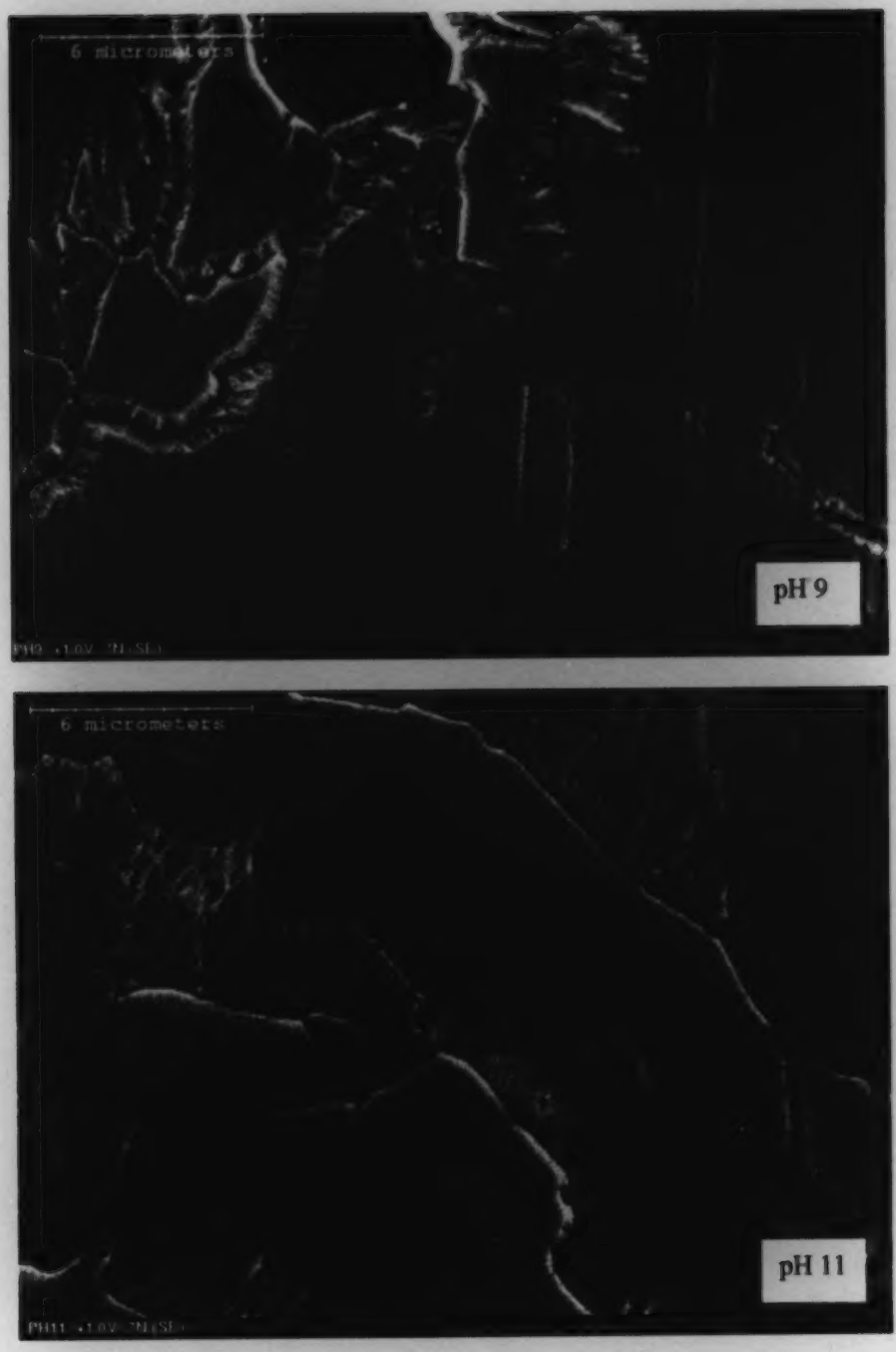


Figure 4-8. SEM micrographs of surfaces after corrosive polishing at different slurry pH under a potential of +1 V and a normal wearing load of 7 N.

## 5.0 Summary and Future Work

In this study, efforts were made to investigate the mechanism of tungsten removal in a $K_3[Fe(CN)_6]$ slurry provided by Intel Corp. It was demonstrated that tungsten passivated beyond the thermodynamic predictions of the Pourbaix diagram within the pH range used in this study. This was mainly attributed to the $K_3[Fe(CN)_6]$ oxidant in the slurry. However, the electrochemical, mechanical and adherence properties of the surface films formed at different slurry pH levels showed that the resistance of the surface film to both mechanical and corrosion damages decreased with an increase in the slurry pH level. The corrosion of the tungsten at relatively high slurry pH was characterized by active dissolution as demonstrated by the SEM images of the films formed at different slurry pH levels.

## 5.1 Summary

As demonstrated in this study, the surface chemistry plays an important role in the removal rate of tungsten in the $K_3[Fe(CN)_6]$ slurry. The following is the summary of the present study:

1. The corrosion rate of tungsten increases with an increase in the slurry pH values. Unlike those formed at higher slurry pH values, the oxide film formed on the surface of tungsten at relatively low pH (4 and 5) appear stronger and adherent to the substrate, thus more effectively reducing further oxidation and dissolution. The interfacial bond between the oxide film and tungsten substrate as well as the

corrosion resistance decreased with an increase in slurry pH; consequently, the resistance to corrosion-wear damage decreased with an increase in the slurry pH.

2. Owing to the variation in surface chemistry at different slurry pH values, the corrosive wear and wear-corrosion synergy changed with the slurry pH and applied wearing load. Of great importance is the fact that all the formed surface oxides were softer than the tungsten substrate, this facilitated tungsten removal by corrosive polishing. The enhancement of corrosion by wear (wear accelerated corrosion) was more pronounced at relatively low pH values and high wearing loads. On the other hand, corrosion accelerated wear facilitated the tungsten removal rate especially at high slurry pH levels owing to higher oxidation and dissolution rates at high pH levels.

3. The total wear rate at OCP increased with an increase in slurry pH and applied load. This was attributed to the increase in oxidation and dissolution rates and enhanced failure of surface oxide scale under larger loads, which became less protective at higher pH values. Corrosion certainly increased the material removal. However, a high removal rate may not necessarily result in the desired surface finish.

4. Application of an anodic potential led to increase in removal rate accompanied with better surface finish. Application of the anodic potential could therefore be a promising approach for effective CMP of tungsten.

## 5.2 Possible Future Work

1. From the XPS analyses of the surface oxides in section 2.4, it was demonstrated the $WO_3/WO_2$ duplex layer contains more $WO_2$ phase as the slurry pH increases. The mechanism responsible for the changes needs to be investigated in order to effectively guide industrial practice.
2. The effect of sliding speed on CMP needs to be investigated, since it may affect the reformation of oxide, material removal, and the quality of a polished surface.

## REFERENCES


[1] R. A. Levy, M. L. Green (1987). "Low-Pressure Chemical Vapor-Deposition of Tungsten and Aluminum for VLSI Applications." Journal of the Electrochemical Society **134**(2): C37-C49.

[2] C. Steinbruchel (1995). "Patterning of Copper for Multilevel Metallization: reactive ion etching and chemical-mechanical polishing." Applied Surface Science **91**: 139-146.

[3] M. Brillouet (1997). "Multilevel Interconnection technologies and Future Requirements for Logic Applications." Microelectronic Engineering **37/38**: 5 – 13.

[4] A.N. Saxena, D. Pramanik (1986). "Planarization Techniques for Multilevel Metallization." Solid State Technology **29**(10): 95-100.

[5] S.P. Murarka (1997). "Advanced Materials for Future Interconnections of the Future Need and Strategy." Microelectronic Engineering **37/38**: 29-37.

[6] J.M. Steigerwald, S. P. Murarka, et al. (1995). "Chemical Processes in the Chemical-Mechanical Polishing of Copper." Materials Chemistry and Physics **41**(3): 217-228.

[7] A.N. Saxena, D. Pramanik (1984). "VLSI Multilevel Metallization." Solid State Technology **27**(12): 93-100.

[8] J. Olsen, F. Moghadam, Planarization Techniques, in Multilevel Metallization for Integrated Circuits, eds. S.R. Wilson, C.J. Tracy, J.L. Freeman, Noyes Publications, Park Ridge, NJ (1993).

[9] W. Kern, G. L. Schnable (1982). "Chemically Vapor-Deposited Borophosphosilicate Glasses for Silicon Device Applications." RCA Review **43**(3): 423-457.

[10] W. Kern (1975). "VLSI Multilevel Metallization." Solid State Technology **25**(12): 25.

[11] I. Avigal (1983). "Inter-Metal Dielectric and Passivation-Related Properties of Plasma BPSG." Solid State Technology **26**(10): 217-224.

[12] A.Takamatsu, M. Shibata, H. Sakai, T. Yoshimi (1984). "Low-Pressure Chemical Vapor-Deposition of Tungsten and Aluminum for VLSI." Journal of the Electrochemical Society **131**: 1865.

[13] E. Baer, J. Lorenz, H. Ryssel (2002). "Simulation of the Influence of via Sidewall Tapering on Step Coverage of Sputter-deposited Barrier Layers" Microelectronic Engineering **64**: 321-328.

[14] J.L. Vossen, G.L. Schnable, W. Kern (1974). "Processes for metallization" Journal of Vacuum Science and Technology **11**(1): 60-70.

[15] N. M. Mazza, A.B. Stambouli (2004). "Submicronc Etching of Borophosphosilicate Glass using $NF_3$ and $NF_3$/He Radio Frequency Glow Discharge" Thin Solid Film **458**: 309-313.

[16] S. Wolf, R.N. Tauber, Silicon processing for the VLSI Era, Vol. 1, Lattice Press, Sunset Beach, CA, 1986, pp. 188.

[17] P. Balk, J.M. Eldridge (1969), Proc. IEEE 57: 1558.

[18] J.M. Eldridge, D. R. Kerr (1971). "Sodium Ion Drift through Phosphosilicate Glass-Sio2 Films." Journal of the Electrochemical Society **118**(6): 986.

[19] J.M. Steigerwald, S.P. Murarka, R.J. Gutmann, Chemical Mechanical Planarization of Microelectronic Materials, John Wliey & Sons,Inc. (1997), pp.26.

[20] N. Nagasima, H. Suzuki, K. Tanaka, S. Nishida. (1974). "Interaction between Phosphosilicate Glass-Films and Water." Journal of the Electrochemical Society **121**(3): 434-438.

[21] R. A. Bowling, G. B. Larrabee (1985). "Deposition and Reflow of Phosphosilicate Glass." Journal of the Electrochemical Society **132**(1): 141-145.

[22] W.M. Paulson, R.W. Kirk (1974). "The Effects of Phophorus-Doped Passivation Glass on the Corrosion of Aluminum". IEEE Proc. Reliability Phys. 172.

[23] L.J. Gallace (1980). "Reliability of Plastic-Packaged Cmos Devices." Solid State Technology **23**(9): 102-108.

[24] Comizzoli, R. B. (1976). "Aluminum Corrosion in Presence of Phosphosilicate Glass and Moisture." RCA Review **37**(4): 483-490.

[25] J.K. Chu, J.S. Multani, S.K. Mittal, J.T. Orton, R. Jecmen, "Spin-On-Glass Dielectrics for Double Metal CMOS Technology". Proc. IEEE VLSI Multilevel Interconnection Conf., 1986: 474-483.

[26] L.B. Vines, S.K. Gupta, "Interlevel Dielectric planarization with Spin-On-Glass Films". Proc. IEEE VLSI Multilevel Interconnection Conf., 1986: 506 – 515.

[27] P. Elkins, K. Reindhart, R. Tang, "A planarization process for double metal CMOS using spin-on-glass as a sacrificial layer". Proc. IEEE VLSI Multilevel Interconnection Conf., 1986: 100 – 106.

[28] D.L.W. Yen, G.K. Rao, "Process Integration with Spin-On-Glass Sandwich as an Intermetal Dielectric Layer for 1.2μm CMOS DLM Process". Proc. IEEE VLSI Multilevel Interconnection Conf., 1988: 85 – 94.

[29] P.L. Pai, "Planarization for 0.5μm CMOS/BiCMOS Technology", Process". Proc. IEEE VLSI Multilevel Interconnection Conf., 1990: 450.

[30] S.N. Chen, Y.C. Chao, J.J. Lin, Y.H. Tsai, F.C. Tseng, "Spin-On-Glass: Characterization and Application", Proc. IEEE VLSI Multilevel Interconnection Conf., 1988: 306 – 312.

[31] C. Chiang, N.V. Lam, J.K. Chu, N. Cox, D. Fraser, J. Bozarth, B. Mumford, "Defects study on spin on glass planarization technology". Proc. IEEE VLSI Multilevel Interconnection Conf., 1987: 404 – 412.

[32] D.E. Bornside (1990). "Mechanism for the Local Planarization of Microscopically Rough Surfaces by Drying Thin-Films of Spin-Coated Polymer Solvent Solutions." Journal of the Electrochemical Society **137**(8): 2589-2595.

[33] G.E. Gimpelson, C.L. Russo, "Plasma Planarization with a Non-Planar Sacrificial Layer", Process". Proc. IEEE VLSI Multilevel Interconnection Conf., 1984: 37.

[34] R.H. Wilson, P. A. Piacente (1986). "Effect of Circuit Structure on Planarization Resist Thickness." Journal of the Electrochemical Society **133**(5): 981-984.

[35] F. Preston (1927), "The theory and design of plate glass polishing machines" J. Soc. Glass Tech. 9, 214-256.

[36] L.M. Cook (1990). "Chemical Processes in Glass Polishing." Journal of Non-Crystalline Solids **120**(1-3): 152-171.

[37] K. Robinson, "Fundamentals of CMP Slurry" Chemical-Mechanical planarization of Semiconductor Materials, M.R. Oliver (ed.)

[38] R. Jairath, M. Desai, M. Stell, R. Tolles, D. Scherber- Brewer (1994), "Consumables for the Chemical-Mechanical Polishing (CMP) of Dielectrics and Conductors". Mat. Res. Soc. Symp. Proc. **337**: 121 – 131.

[39] M. Bielmann, U. Mahajan, et al. (1999). "Effect of particle size during tungsten chemical mechanical polishing." Electrochemical and Solid State Letters **2**(8): 401-403.

[40] D. Devlieger, M. Desai, C. Fruitman, "In Advanced Metallization VLSI Applications in 1994, conf. Proc. ULSI-X, 1995 Mat. Res. Soc., 201 – 205.

[41] J. Luo, D.A. Dornfeld, IEEE Transaction on Semiconductor Manufacturing, **16** (1) 2003.

[42] F.B. Kaufman, D. B. Thompson, et al. (1991). "Chemical-Mechanical Polishing for Fabricating Patterned W Metal Features as Chip Interconnects." Journal of the Electrochemical Society **138**(11): 3460-3465.

[43] H-J. Kim, D-H. Eom, M-S. Kim, J-G. Park (2001), "Physical and chemical characterization of re-used oxide CMP slurry". In Chemical Mechanical Planarization IV, 143-153.

[44] T.R. Dickson, Introduction to chemistry, John Wiley and Sons, NY, !987, 412.

[45] V.S. Chapthapuram, T. Du, K.B. Sundaram, V. Desai (2003), "Role of Oxidizer in the Chemical Mechanical planarization of the Ti/TiN Barrier Layer", Microelectronic Engineering **65**: 478 – 488.

[46] J. Hernandez, P. Wrschka, Y. Hsu, T.-S. kuan, G.S. Oerhrlein, H.J. Sun, D.A. Hansen, J. King, M.A. Fury (1999). "Chemical mechanical polishing of Al and SiO2 thin films: The role of consumables." Journal of the Electrochemical Society **146**(12): 4647-4653.

[47] T-H. Tsao, S-C. Yen (2001). "Electrochemical effects of various slurries on the chemical mechanical polishing of Copper-platted films'. In chemical mechanical planarization IV. 180-190

[48] T. Du, Y. Luo, V. Desai (2004), "The Combinatorial Effect of Compplexing agent and Inhibitor on Chemical-Mechanical Planarization of Copper". Microelctronic Engineering **71**: 90-97.

[49] D.B. James, CMP Polishing Pads, Chemical-Mechanical Planarization of Semiconductor Materials, M.R. Oliver (ed.)

[50] R. Jairath, J. Farkas, C.K. Huang, M. Stell, S-M. Tzeng (1994). "Chemical-Mechanical Polishing – Process Manufacturability." Solid State Technology **37**(7): 71.

[51] P. Renteln, J. Coniff (1994), Mat. Res. Symp. Proc. 337, 105.

[52] M. Forsberg, J. Olsson (2002). "Chemical mechanical polishing for surface smoothing." Physica Scripta **T101**: 200-202.

[53] J. Hernandez, P. Wrschka, G.S. Oehrlein (2001). "Surface chemistry studies of copper chemical mechanical planarization." Journal of the Electrochemical Society **148**(7): G389-G397.

[54] S.P. Murarka, J.M. Steigerwald, R.J. Gutmann (1993), "Inlaid Cu Multilevel Interconnection Using Planarization by CMP". MRS Bulletin **46.**

[55] H. Kim, B. Park, S. Lee, H. Jeong, D.A. Dornfeld (2004), "Self-conditioning fixed abrasive pad in CMP". Journal of electrochemical society, 151 (12): G858 – G862.

[56] P. Jemmely, S. Mischler, et al. (1999). "Tribocorrosion behaviour of Fe-17Cr stainless steel in acid and alkaline solutions." Tribology International **32**(6): 295-303.

[57] S.W. Watson, F. J. Friedersdorf, B.W. Madsen, S.D. Cramer (1995). "Methods of Measuring Wear Corrosion Synergism." Wear **181**: 476-484.

[58] W.J. Schumacher (1993). "Corrosive Wear Principles." Materials Performance **32**(7): 50-53.

[59] W.J. Schumacher (1993) Wear of Materials, ASME, NY, 1985: 538-556 "Corrosive Wear Principles." Materials Performance **32**(7): 50-53.

[60] S.W. Watson, B.W. Madsen, S.D. Cramer (1993). Proc. !2th Int. Corr. Congress, 1353- 1366

[61] Kotlyar, D., C. H. Pitt, et al. (1988). "Simultaneous Corrosion and Abrasion Measurements under Grinding Conditions." Corrosion **44**(4): 221-228.

[62] M. Bielmann, U. Mahajan, R.K. Singh, P. Agarwal, S. Miscler, E. Rosset, D. Landolt (2000). "Tribological Experiments Applied To Tungsten Chemical Mechanical Polishing." Mat. Res. Soc. Symp. Proc. **566**: 97-101.

[63] R.K. Singh, R. Bajaj (2002). "Advances in Chemical-mechanical-Planarization." MRS Bulletin **27**(10): 743 – 751.

[64] Treichel, H., R. Frausto, S. Srivatsan, B. Whithers, T. Meyer, R. Morishige (1999). "Process optimization of dielectrics chemical mechanical planarization processes for ultralarge scale integration multilevel metallization." Journal of Vacuum Science & Technology A **17**(4): 1160-1167.

[65] Ziomek-Moroz, M., A. Miller, et al. (2003). "An overview of corrosion-wear interaction for planarizing metallic thin films." Wear **255**: 869-874.

[66] Sivaram, S., H. Bath, R. Legget, A. Maurry, K. Menning, R. Tolles (1992). "Planarizing Interlevel Dielectrics by Chemical-Mechanical Polishing." Solid State Technology **35**(5): 87-91.

[67] T. Nitta, T. Ohmi, T. Hoshi, S. Sakai, K. Sakaibara, S. Imai, T. Shibata (1993). "Evaluating the Large Electromigration Resistance of Copper Interconnects Employing a Newly Developed Accelerated Life-Test Method." Journal of the Electrochemical Society **140**(4): 1131-1137.

[68] J Edelstein, R. Heindenreich, W. Goldbitt, C. Cote, N. Uzoh, P. Lusting, T. Roper, W. McDevitt, A. Motsiff, J. Simon, R. Dukovic, H. Wachnik, R.

Rathore, L. Schulz, L. Su, L. Luce, J. Slattery (1997), Proceedings of international electron devices meeting (IEDM), IEEE, 77.

[69] Harper, J. M. E., E. G. Colgan, C-K. Hu, J.P. Hummel, L.P. Buchwalter, C.E. Uzoh (1994). "Materials Issues in Copper Interconnections." Mrs Bulletin **19**(8): 23-29.

[70] T. Nitta, T. Ohmi, M. Otsuki, T. Takewaki, T. Shibata (1992). "Electrical-Properties of Giant-Grain Copper Thin-Films Formed by a Low Kinetic-Energy Particle Process." Journal of the Electrochemical Society **139**(3): 922-927.

[71] Steigerwald, J. M., S. P. Murarka, et al. (1995). "Chemical Processes in the Chemical-Mechanical Polishing of Copper." Materials Chemistry and Physics **41**(3): 217-228.

[72] M.M. Mosleshi (1988), "Formation of W thin films for IC applications". In Tungsten and other refractrory metals for VLSI applications III, V.A. Wells (ed), 385-398. Materials Research Society,Penn.

[73] Ghate, P. B., J. C. Blair, et al. (1977). "Metallization in Microelectronics." Thin Solid Films **45**(1): 69-84.

[74] H.B. Michaelson, (1978). "Relation between an Atomic Electronegativity Scale and Work Function." IBM Journal of Research and Development **22**(1): 72-80.

[75] J. Li, T.E. Seidel, J.W. Mayer (1994), "Copper-Based metallization in ULSI structures. 2. Is copper ahead of its time as on-chip interconnect material". MRS Bulletin **19** (8): 15 – 18.

[76] S.M. Sze, Physics of Semiconductor Devices, John Wiley & Sons, Inc., NY, 1981

[77] Mcbrayer, J. D., R. M. Swanson, T.W. Sigmon (1986). "Diffusion of Metals in Silicon Dioxide." Journal of the Electrochemical Society **133**(6): 1242-1246.

[78] Blewer, R. S. (1986). "Progress in LPCVD Tungsten for Advanced Microelectronics Applications." Solid State Technology **29**(11): 117-126.

[79] Kaufman, F. B., D. B. Thompson, et al. (1991). "Chemical-Mechanical Polishing for Fabricating Patterned W Metal Features as Chip Interconnects." Journal of the Electrochemical Society **138**(11): 3460-3465.

[80] M. Pourbaix, "Atlas of Electrochemical Equilibria in Aqueous Solutions." NACE, Houston, TX 1974.

[81] Shankoff, T. A. and E. A. Chandross (1975). "High-Resolution Tungsten Patterning Using Buffered, Mildly Basic Etching Solutions." Journal of the Electrochemical Society **122**(2): 294-298.

[82] Kneer, E. A., C. Raghunath, et al. (1996). "Electrochemistry of chemical vapor deposited tungsten films with relevance to chemical mechanical polishing." Journal of the Electrochemical Society **143**(12): 4095-4100.

[83] Perry, S. S., H. C. Galloway, et al. (2001). "The influence of chemical treatments on tungsten films found in integrated circuits." Applied Surface Science **180**(1-2): 6-13.

[84] Kneer, E. A., C. Raghunath, et al. (1997). "Electrochemical measurements during the chemical mechanical polishing of tungsten thin films." Journal of the Electrochemical Society **144**(9): 3041-3049.

[85] Stein, D. J., D. Hetherington, et al. (1998). "In situ electrochemical investigation of tungsten electrochemical behavior during chemical mechanical polishing." Journal of the Electrochemical Society **145**(9): 3190-3196.

[86] P.L. Pai, C.H. Ting (1989), IEEE Electron Devices Lett., 10 : 423.

[87] A.N. Saxena, D. Pramanik, "Manufacturing issues and emerging trends in VLSI multilevel metallizations". International IEEE VLSI multilevel interconnection conference, 1986, 9 – 42.

[88] T. Ohba (1995), "Adavanced multilevel metallization technology". Applied surface science 91: 1-11.

[89] H. Treichel, G. Ruhl, P. Ansmann, R. Wurl, Ch. Muller, M. Dietlmeier (1998), "Low dielectric constant materials for interlayer diecelctric". Microelectronic engineering 40: 1-19.

[90] Kondo, S., N. Sakuma, et al. (2000). "Abrasive-free polishing for copper damascene interconnection." Journal of the Electrochemical Society **147**(10): 3907-3913.

[91] Bing-Hung Chen, H. Zhang, S.Y.M. Chooi, L. Chan, Y. Xu, J.H. Ye, corrosive behavior of tungsten in post dry-etch residue remover, Ind. Eng. Chem. Res. 42 (2003) 6096-6103.

[92] Astha, S., R. Balasubramaniam, et al. (1999). "On the passivation of iron aluminides by addition of tungsten." Journal of Materials Science Letters **18**(19): 1555-1556.

[93] Universal Micro-Tribometer Operation Manual, Center for Tribology Inc.

[94] T. Du, V. Desai (2003), "Chemical mechanical planarization of copper: pH effect". Journal of Materials Science Letters 22: 1623 – 1625.

[95] B.W. Madsen, Standard guide for determining amount of synergy between wear and corrosion. 1994 Annual book of ASTM Standards: ASTM international,PA, 03.02 ASTM G 119-93: 494-499.

[96] J. Dones, Principles and Prevention of Corrosion, 2nd edition, 1996. pp 144.

[97] J.R. Scully, Corrosion methods for laboratory corrosion testing. In corrosion testing and evaluation, R. Baboin, S.W. Dean (eds.), ASTM, PA, 1990.

[98] M. Anik, K. Osseo-Asare (2002), "Effect of pH on the anodic behavior of tungsten". Journal of electrochemical society 149(6): B224-B233.

[99] S.M. El-Raghy, H. Abd-El-Kader, M.E. Abou-El-Hassan (1984), "Electrochemistry of abrasion corrosion of low alloy steel in 1% NaCl solution"., Corrosion 40: 60 – 61.

[100] M-H. Hong, Su-Il Pyun (1991), "Corrosive wear behavior of 304-L stainless steel in 1 N $H_2SO_4$ solution, Part 1: effect of applied potential". Wear 147: 59-67.

[101] W.J. Tomlinson, M.G. Talks (1991), "Erossion and corrosion of cast iron under cavitation conditions". Tribology international 24 (2): 67 – 69.

[102] C.H. Pitt, Y.M. Chang (1986), "Jet slurry corrosive wear of high-chromium cast iron and high-carbon steel grinding ball". Corrosion 42: 312-317.

[103] Y. Huang, X. Jiang, S. Li (2000), "pure mechanical wear loss in corrosive wear". Bulletin of Materials Science **23** (6): 539 – 542.

[104] Hong, M. H. and S. I. Pyun (1991). "Corrosive Wear Behavior of 304-L Stainless-Steel in 1-N H2so4 Solution .1. Effect of Applied Potential." Wear **147**(1): 59-67.

[105] Assi, F. and H. Bohni (1999). "Study of wear-corrosion synergy with a new microelectrochemical technique." WEAR **235**: 505-514.

[106] Y. Huang, X. Jiang, S. Li (2000), "Pure mechanical wear loss measurement in corrosive wear", Bull. Mater. Sci. **23** : 539 – 542.

[107] Pitt, C. H. and Y. M. Chang (1986). "Jet Slurry Corrosive Wear of High-Chromium Cast-Iron and High-Carbon Steel Grinding Ball Alloys." Corrosion **42**(6): 312-317.

[108] Friedersdorf, F. J. and G. R. Holcomb (1998). "Pin-on-disk corrosion-wear test." Journal of Testing and Evaluation **26**(4): 352-357.

[109] Akonko, S.B., Li, D.Y., M. Ziomek-Moroz, Hawk, J., Miller, A and Cadien, K (2005). "Effects of $K_3[Fe(CN)_6]$ slurry's pH value and applied potential on tungsten removal rate for chemical–mechanical planarization application". WEAR 259: 1299-1307

# Appendix

Table I. Total wear rate, T (mm/yr), of tungsten in the $K_3[Fe(CN)_6]$ slurry under open circuit potential as a function of slurry pH and normal load.

| Load (N) / pH | 1 | 3 | 5 | 7 |
|---|---|---|---|---|
| 4 | 19.29 | 24.46 | 29.03 | 36.58 |
| 5 | 25.97 | 28.86 | 36.83 | 48.78 |
| 6 | 26.60 | 31.50 | 40.22 | 53.01 |
| 7 | 29.76 | 36.19 | 55.98 | 70.84 |
| 9 | 32.15 | 39.59 | 71.05 | 86.11 |
| 11 | 34.79 | 49.17 | 89.99 | 114.44 |

Table II. Pure wear rate, $W_O$ (mm/yr) of bulk tungsten in the $K_3[Fe(CN)_6]$ slurry under a cathodic potential of –0.5 V as a function of slurry pH and normal load.

| Load (N) / pH | 1 | 3 | 5 | 7 |
|---|---|---|---|---|
| 4 | 16.52 | 20.34 | 24.96 | 29.79 |
| 5 | 22.19 | 25.85 | 31.79 | 36.81 |
| 6 | 23.70 | 27.61 | 32.65 | 40.12 |
| 7 | 25.59 | 31.73 | 37.95 | 52.18 |
| 9 | 26.35 | 35.08 | 44.92 | 58.52 |
| 11 | 27.99 | 40.36 | 54.80 | 68.46 |

Table III. The total wear rate (mm/yr) of tungsten under electrochemical potential of +1 V in the $K_3[Fe(CN)_6]$ slurry as function of slurry pH and normal load.

| Load (N) / pH | 1 | 3 | 5 | 7 |
|---|---|---|---|---|
| 4 | 25.22 | 32.09 | 39.59 | 53.22 |
| 5 | 29.57 | 36.81 | 54.40 | 58.65 |
| 6 | 29.88 | 49.54 | 59.69 | 62.68 |
| 7 | 37.47 | 58.93 | 70.21 | 78.67 |
| 9 | 52.22 | 65.49 | 85.10 | 112.26 |
| 11 | 62.93 | 74.56 | 115.03 | 142.10 |